Title

RESONANCE RAMAN SPECTROSCOPY OF MANGANESE (III) ETIOPORPHYRIN I, CHROMIUM (III) TETRAPHENYLPORPHIN AND HEMOGLOBIN: THE DEPENDENCE OF RESONANCE ENHANCEMENT ON THE RESONANT ELECTRONIC TRANSITION

Author

Asher, Sanford Abraham.

Publication Date

1976-10-01

LBL-5375
c.1

RESONANCE RAMAN SPECTROSCOPY OF MANGANESE (III) ETIOPORPHYRIN I, CHROMIUM (III) TETRAPHENYLPORPHIN AND HEMOGLOBIN: THE DEPENDENCE OF RESONANCE ENHANCEMENT ON THE RESONANT ELECTRONIC TRANSITION

Sanford Abraham Asher
(Ph. D. thesis)

October 1976

Prepared for the U. S. Energy Research and Development Administration under Contract W-7405-ENG-48

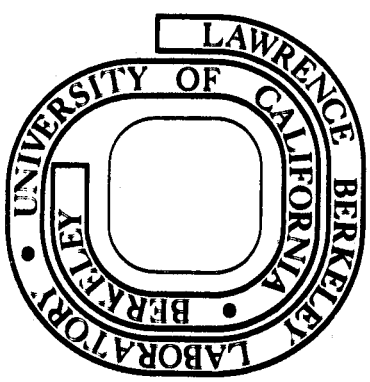

LBL-5375
c.1

DISCLAIMER

RESONANCE RAMAN SPECTROSCOPY
OF MANGANESE (III) ETIOPORPHYRIN I,
CHROMIUM (III) TETRAPHENYLPORPHIN AND
HEMOGLOBIN: The Dependence of Resonance
Enhancement on the Resonant Electronic Transition

Table of Contents

Resonance Raman Spectroscopy of Manganese (III) Etioporphyrin I, Chromium (III) Tetraphenylporphin and Hemoglobin: The Dependence of Resonance Enhancement on the Resonant Electronic Transition

Sanford Abraham Asher

Department of Chemistry
and Laboratory of Chemical Biodynamics
Lawrence Radiation Laboratory
University of California
Berkeley, California

October 1976

Abstract

A combination of resonance Raman spectroscopy (RRS) and magnetic circular dichroism (MCD) is used to study the electronic transitions of manganese (III) etioporphyrin I (MnETP). The data supports the assignment of the strong band of Mn (III) porphyrins between 460-490 nm to a charge transfer transition. The two bands occurring between 540-600 nm are assigned to vibronic components of a $\pi \rightarrow \pi^*$ transition. The band in the near UV appears to contain a number of components. It is suggested that this band has both $\pi \rightarrow \pi^*$ and charge transfer character.

Dramatic differences are found in the RR spectra of MnETP upon excitation within different absorption bands. The RR spectra of MnETP - X (X = F^-, Cl^-, Br^-, I^- or butanol) excited in the charge transfer band show large differences in the low frequency region (100-500 cm^{-1}), depending on the axial ligand. Pure Mn-halide vibrations are assigned. An explanation is proposed to account for the differences between the RR

spectra excited in the Q bands and the charge transfer band. Some of the vibrational Raman bands in the low frequency region may serve as probes for the degree of out-of-plane distortion of the metal from the porphyrin plane. The resonance Raman spectra of Cr (III) tetraphenylporphin (CrTPP) indicate that the three absorption bands of CrTPP occurring between 420-600 nm result from $\pi \rightarrow \pi^*$ transitions. The resonance Raman spectra of F^-, N_3^- and OH^- complexes of methemoglobin are studied by excitation in the charge transfer bands, which occur between 590-650 nm. A selective enhancement of vibrations of the axial ligand against the iron is observed.

The addition of inositol hexaphosphate results in no changes in the resonance Raman spectra. The lack of a shift in the energy of the Fe-F^- vibration is interpreted to indicate that there is no movement of the iron relative to the porphyrin plane. The significance of these results with respect to the Perutz model is discussed.

The Raman spectrometer constructed for these measurements is described. The exciting source is a pulsed dye laser, tunable from 265 to 363 nm in the UV and from 435-730 nm in the visible spectral region.

Dedication

To my lovely, inspiring wife, Nancy and my children, David and Dianne.

Acknowledgments

I am deeply indebted to the many people who have guided me in the years leading up to this thesis. In the forefront is Professor Kenneth Sauer, my research director, who with infinite patience impressed upon me the qualities necessary for productive research. I appreciate the scientific independence he allowed me and thank him for the support he gave me in difficult times.

I would also like to thank my good friend, Paul Hartig for the support we shared in our graduate student careers.

I would like to thank all of my fellow graduate students for their friendship. However, the list would form a chapter in itself. Thus, I mention only a few and hope that the majority who are not mentioned do not feel slighted: Douglas Vaughan, Bruce Henkin, and Lynn Austin. I would like to thank Bruce Johnson and Professor Richard Mathies for their friendship and for the many helpful discussions on Raman theory. I am grateful to Professor Martin Gouterman for the helpful conversations on the spectroscopy of porphyrins and the generous gifts of metalloporphyrins. I would like to thank Dr. Larry Vickery for many helpful discussions and for collaborating in the hemoglobin experiments. I am indebted to Marlyn Amann for the illustrations. I would also like to thank Karla Kirkegaard, who attempted to teach me punctuation and patiently helped me reword this thesis into a more coherent form. I am especially indebted to my wife Nancy, for her patience and love during the creation of this thesis.

This work was done with support from the U. S. Energy Research and Development Administration.

Introduction

Resonance Raman spectroscopy is a technique for the study of the vibrational spectrum of a dilute molecular species. Excitation within an absorption band of a molecule induces an enhancement of the intensity of the Raman scattered light. The ability to enhance one particular component selectively from a multi-component system makes resonance Raman spectroscopy useful for the study of biological chromophores. One particular chromophore, heme, an iron porphyrin is found in such biologically important molecules as hemoglobin and the cytochromes.

This thesis describes the study of the resonance Raman spectrum of manganese (III) etioporphyrin I (MnETP), chromium (III) tetraphenylporphin (CrTPP) and Methemoglobin (MetHb). The dependence of the resonantly enhanced vibrations on the nature of the electronic transitions of metalloporphyrins is detailed.

Each of the chapters in the thesis contains an introduction, therefore a lengthy introduction will not be given here. However, a map of the structure of the thesis will be presented to aid the reader.

Chapter I describes the Raman spectrometer which was constructed to obtain many of the measurements discussed in Chapters IV and V. Chapter I also includes many of the experimental details involved in the measurements described in subsequent chapters. Chapter II discusses Raman and resonance Raman theory.

Chapter III presents a review of the absorption and magnetic circular dichroism (MCD) spectra of porphyrins. The electronic structure of porphyrins is discussed and absorption and MCD spectroscopy is used to

assign the electronic transitions of manganese (III) etioporphyrin I (MnETP).

Chapter IV is a study of the dependence of the resonance Raman spectra of MnETP and CrTPP on the resonant electronic transition. The conclusion is that excitation in a charge transfer band enhances vibrational modes about the metal. In particular, it is shown that axial ligand modes are enhanced. Chapter V is the culmination of the model studies reported in Chapter IV. The resonance Raman spectra of various complexes of Methemoglobin are examined by excitation in charge transfer bands. The enhanced Raman peaks contain information about the structure and molecular dynamics of MetHb.

CHAPTER I

EXPERIMENTAL

This thesis includes absorption, MCD and Raman spectral studies of various metalloporphyrins and derivatives of hemoglobin. The experimental techniques used for the preparation and measurements of the various samples have been collected in this chapter. Also included is a description of the Raman spectrometer constructed for the studies in Chapters IV and V.

Materials and Methods

Samples of manganese etioporphyrin I acetate (MnETP) were kindly supplied by Dr. M. Calvin. The visible, UV, and near IR absorption spectra correspond to those in the literature (Boucher, 1972). Thin layer chromatography performed on the MnETP using a 1:1 pyridine-water solution on a cellulose plate demonstrated the presence of only one component.

The halogen salts of MnETP were prepared from a methanol solution of MnETP containing the sodium salt of the halide. Water was added dropwise with stirring. The resulting precipitate was washed repeatedly with water and centrifuged. The halide salts were dried under vacuum, and their absorption spectra were subsequently monitored (Table I). An elemental analysis of MnETP-Cl^- indicated: 64.22%, C; 6.09%; H; and 9.6% N. The expected percentages were: 65.7%, C; 6.60%, H; and 9.6%, N assuming H_2O as the sixth ligand.

The absorption spectra of all of the halides of MnETP except for the fluoride agreed with those in the literature (Boucher, 1972). The absorption peaks of the fluoride complex in chloroform were 2-6 nm to higher energy from the values reported by Boucher (Boucher, 1972). The intensity ratio of band V/VI [R in Boucher's nomenclature (Boucher, 1972) was also 80% higher. It should be noted that there is a large variation in the value of R as the axial ligand is changed from I^- to Br^- to Cl^- (Boucher, 1972). The change that Boucher observes in going to F^- is surprisingly low. In addition, the chloroform solutions

TABLE I

Absorption maxima (nm) of MnETPX in $CHCl_3$ compared with values reported in the literature (Boucher, 1972)

X^-	F^-		Cl^-		Br^-		I^-	
Band	this study	Lit.	this study	Lit.	this study	Lit.	this study	Lit.
III	582	585	592	592				
IV	550	552	560	559	562	562	568	568
V	450	452	474	474	479	478	492	493
Va			428	427	432	431		
VI	350	356	357	356	361	361	368	368
R	1.30	.72	0.69	.69	.46	.42	.27	.24

$$R = \frac{\text{Abs. peak V}}{\text{Abs. peak VI}}$$

of MnETP-F were labile. With time our samples exhibited absorption changes toward the values reported by Boucher. The liability of the fluoride complex of MnETP in $CHCl_3$ is similar to the lability of the phenoxide complex of Cr^{3+} octaethylporphyrin (CrOEP) in $CHCl_3$ solution (Gouterman et al., 1975). Presumably, Cl^- produced by a gradual photodissociation of the solvent replaces phenoxide as the axial ligand of the Cr in CrOEP (Gouterman et al., 1975). Apparently a similar phenomenon occurs with MnETP in $CHCl_3$. In addition, the MnETP-F salt that we have prepared gives the characteristic spectrum of MnETP complexes in coordinating solvents such as methanol and pyridine, indicating that no alteration of the MnETP moiety occurred during the preparation of the F^- salt.

The $Na^{35}Cl$(99.35%) and $Na^{37}Cl$(90.36%) were obtained from Oak Ridge National Laboratories.

The samples of Cr^{3+} tetraphenylporphin chloride (CrTPP–Cl) were kindly supplied by Professor Martin Gouterman. An absorption spectrum in BuOH indicated the presence of impurities with a peak appearing at 420 nm, possibly indicating the presence of the free base.

The CrTPP–Cl^- was chromatographed on a neutral aluminum oxide column, grade 1. In contrast to a recent report in the literature (Gouterman et al., 1975) the CrTPPCl would not elute from the aluminum oxide column with CH_2Cl_2. The eluting solvent used was 10% n-butanol, 90% CH_2Cl_2 V/V. The Cr^{3+}TPP eluted as a narrow band. However, following this band was a very diffuse band. Absorption spectra of the CrTPP–Cl in BuOH and fresh $CHCl_3$ agreed with previously reported absorption spectra (Gouterman et al., 1975).

Human hemoglobin A_0, purified by the method of Williams and Tsay (Williams and Tsay, 1973) was generously provided by Professor Todd M. Schuster (University of Connecticut, Storrs). Met-hemoglobin was prepared by Dr. Larry Vickery (Department of Chemistry, University of California, Berkeley) by oxidation of oxyhemoglobin with excess potassium ferricyanide, followed by extensive dialysis against 0.1 M HEPES, 1 mM EDTA, pH 7.0; liganded complexes were formed by the addition of salts directly to the capillary tube to be used for Raman excitation. Absorption spectra were measured for 200-fold dilutions of the stock (ca 0.6 M solution). In addition, absorption spectra were measured for each of the Raman-illuminated samples to insure that sample degradation had not occurred. The absorption spectra were measured for thin films of the material spread on a microscope slide and held in place by a cover slip.

All of the solvents used for the Raman measurements were freshly distilled. The room temperature absorption spectra were measured on a Cary 14 recording spectrophotometer. The low temperature absorption spectra were measured on a Cary 118 recording spectrophotometer equipped with a dewar to allow variable temperature absorption measurements. This dewar was also used in the MCD measurements. The MCD instrument has been described previously (Sutherland et al., 1974).

The Raman spectra recorded with excitation at 568.2 and 530.9 nm and the Raman spectrum of MnETP acetate in butanol with excitation at 457.9 nm were measured through the courtesy of Dr. J. Scherer at Western Regional Laboratories, USDA, Albany, Ca. (Bailey and Horvat, 1970). Excitation at 568.2 and 530.9 were obtained from a Spectra Physics Model 165-01 Kr^+ laser.

Excitation at 457.9 nm was obtained from a Coherent Radiation Model 52 Ar^+ laser. The spectra of the halide complexes of MnETP were measured using an instrument belonging to Dr. H. Strauss at the University of California, Berkeley, Department of Chemistry. A Coherent Radiation model CR2 Ar^+ laser was coupled to a Spex 1401 double monochromator. The incident laser beam was chopped, and the scattered light was amplified with synchronous detection.

Raman Spectrometer

Optical Path

The remaining Raman spectra were obtained on an instrument that was constructed as outlined in Fig. 1.

The exciting source is a CMX-4 Xenon flashlamp excited, pulsed dye laser produced by Chromatix Corp. of Mountain View, California. The laser produces 1 μsec (halfwidth at half maximum intensity) pulses at 5, 10, 15, 20 or 30 Hz. The laser is tunable from 430-730 nm in the visible spectral region and 265-365 nm by second harmonic generation using ADP crystals. Fig. 2 shows the tunability curves specified by Chromatix Corp. Included in the figure is a list of currently available dyes that enable tunability through each of the wavelength intervals numbered in Fig. 2. The dashed curves indicate only peak power. Oxazine 170 in methanol, which is tunable from 675-730 and 335-366 nm doubled shows poor intensity stability from pulse to pulse unless the repetition rate is limited to 10 Hz. Coumarin 2 which covers the wavelength region from 445 nm to 482 nm shows a rapid photochemical decomposition of the dye. To obtain Raman spectra using these two dyes the repetition rate of the laser must

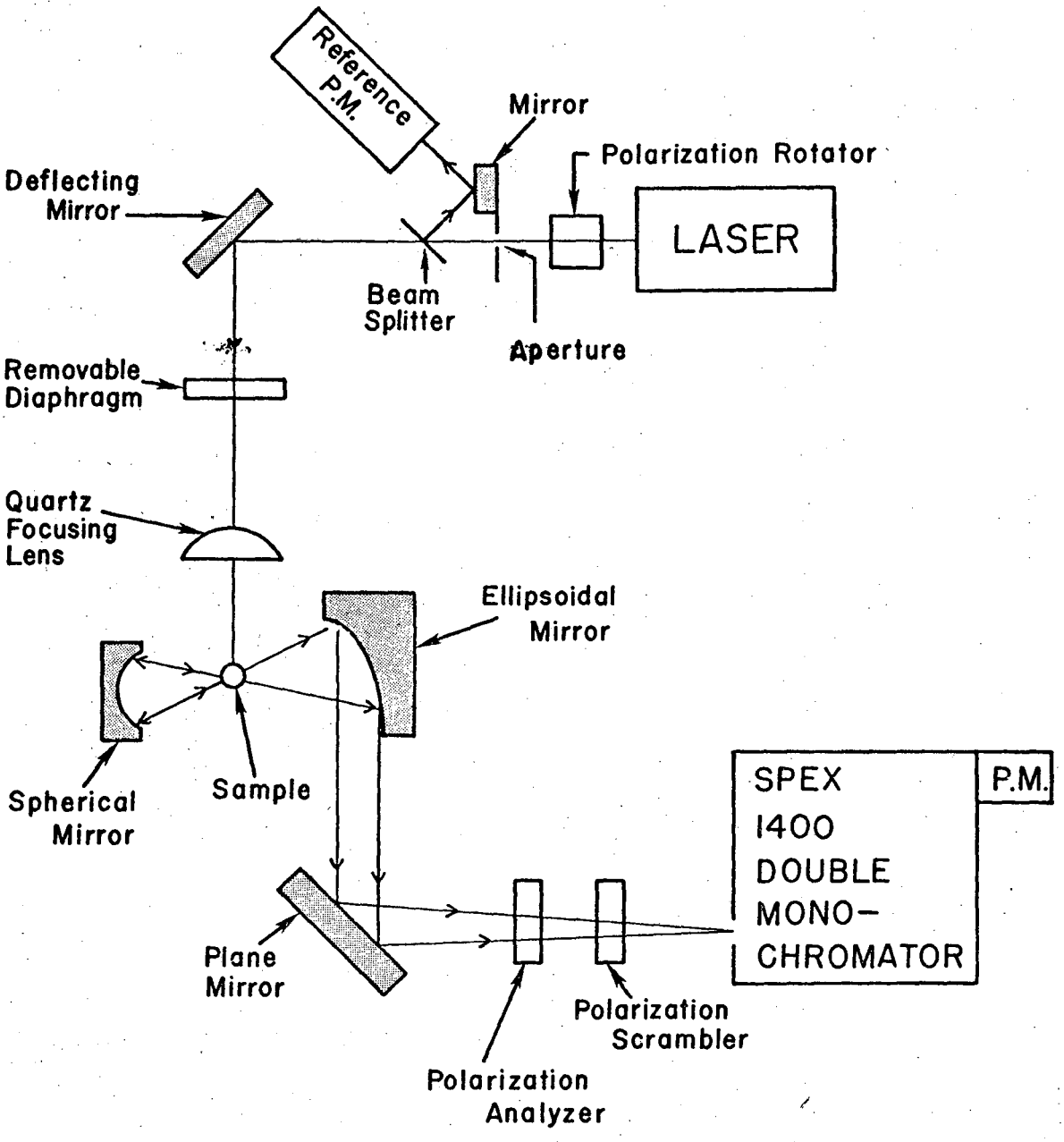

Fig. I-1. Optical schematic of Raman spectrometer.

Fig. I-2. Dye ranges and power curves (from CMX-4 laser manual).

Curve	Dye	Tuning Range (nm)	Peak Gain Wavelength (nm)
1	Coumarin 120	435-455	442
2	Coumarin 2	445-482	460
3	Coumarin 102	476-518	490
4	Coumarin 30	493-540	512
5	Coumarin 6	521-558	540
6	Sodium Fluorescein	542-577	558
7	Rhodamine 575 (1:1 water/ Methanol)	566-610	590
8	Rhodamine 6G (1:1 water/ Methanol)	577-625	598
9	Rhodamine 6G (4% Ammonyx LO)	585-633	610
10	Kitton Red S	622-665	642
11	Cresyl Violet	655-700	673
12	Oxazine 170	675-730	705

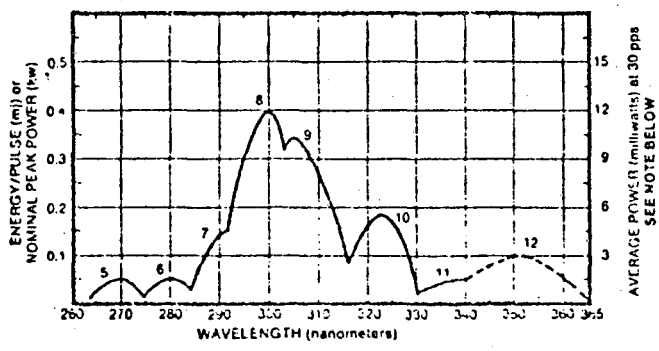

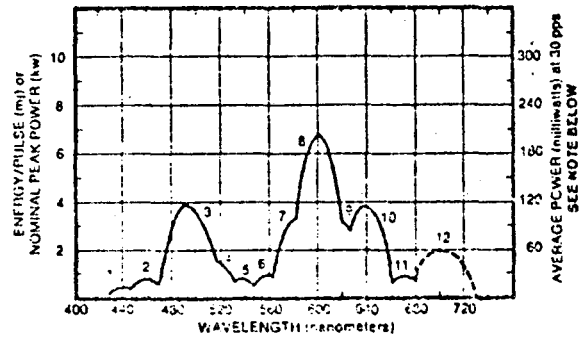

NOTE: Dashed curves are for peak powers and energy per pulse only, not average power.

be limited to 10 Hz. The compositions of the dye solutions used to excite the Raman spectra reported in this thesis are detailed in Table II.

The light emerging from the laser is polarized vertically with respect to the laser for the doubled UV radiation and is polarized horizontally for the fundamental visible radiation. In order that the laser light incident on the sample is polarized transversely to the plane defined by the laser beam axis and the viewing axis, a polarization rotator (Spectra-physics model 310-21 Broadband Polarization Rotator, Spectra-Physics Corp., Mountain View, California) is used to rotate the visible light (Fig. 1). The polarization rotator is removed for measurements in the ultraviolet wavelength region.

The laser beam is 3 mm in cross section as it emerges from the laser output mirror. In addition to the primary laser beam two secondary non-coincident beams of much lower intensity are emitted from the output mirror. An aperture consisting of a blackened aluminum plate with a 3mm hole serves to remove the secondary lasing beams and any nonlasing light from the flashlamp. The aperture also serves to define the position of the incident beam.

For laser output in the UV, the fundamental laser light is frequency doubled by ADP crystals placed inside the laser cavity. A fused quartz block replaces the doubling crystals for visible operation without changing the laser cavity configuration. The refractive indices of both the doubling crystals and the quartz block depend on wavelength. Thus, the laser beam which energes from the doubling crystals or the quartz block shifts position with respect to the center of the laser output mirror when the wavelength of the laser beam is changed. After aligning the optical path of the Raman instrument for one excitation wavelength the aperture is introduced to define a

TABLE II

Dye solutions used for Raman spectra reported in this thesis

Dye	tuning range (nm)	dye concentration (mg/ℓ)	solvents and additives	dye supplier
Coumarin 2	445-482	42.5	600 mℓ water 400 mℓ methanol 12.5 mℓ DMA[a]	Exciton Chemical Co. Dayton, Ohio
Fluoral 7 GA[b]	540-590	130.0	970 mℓ water 30 mℓ Ammonyx[c] 0.2 mℓ conc. HCℓ 0.5 mℓ COT[d]	GAF Corporation Melrose Park, Ill.
Rhodamine 6 G	566-610	62.5	500 mℓ water 500 mℓ methanol	Eastman Kodak Rochester, New York
Rhodamine 6 G	585-633	62.5	960 mℓ water 40 mℓ Ammonyx[c]	Eastman Kodak Rochester, New York
Kiton Red S	622-665	62.5	960 mℓ water 40 mℓ Ammonyx[c]	Exiton Chemical Dayton, Ohio
Rhodamine 640	630-685	67.5	500 mℓ water 500 mℓ methanol 0.2 mℓ conc. HCℓ	Exiton Chemical Dayton, Ohio
Oxazine 170 perchlorate	675-730	32.5	300 mℓ water 700 mℓ methanol 0.5 mℓ conc. HCℓ	Eastman Kodak Rochester, New York

[a] DMA - Dimethyl acetamide

[b] Fluorol 7 GA must be recrystallized from ethanol (Lambropoulos, 1975)

[c] Ammonyx purchased from Onyx Chemical Corporation, Jersey City, New Jersey

[d] COT - cyclooctatetraene

cross section through which the laser beam must be incident. To maintain the alignment of the laser beam with respect to the sample and to the scattered light collection optics the laser is repositioned for each new exciting wavelength so that the beam again traverses the aperture.

Following the aperture the beam is split into two beams by a quartz plate beam splitter. To maximize the power incident on the sample, the quartz beam splitter is antireflection coated with MgF_2. Since antireflection coatings in the visible enhance reflection in the UV two separate antireflection coated beam splitters are utilized, one for visible operation and the other for the UV.

The beam which is reflected by the beam splitter represents approximately 1% of the incident radiation and is reflected by a mirror mounted to the side of the aperture into the reference photomultiplier. The reference beam is diffused by a ground quartz plate on the front of the photomultiplier housing. The diffused light is then attenuated by a number of neutral density filters prior to the photocathode of the EMI 9558 QB photomultiplier. For operation in the UV a UV pass filter (Kodak 18A or Corning 7-54) is introduced to remove the fundamental visible light which is colinear with the UV beam.

The light transmitted through the beam splitter, the sample beam, is deflected into the sampling compartment by a deflecting mirror and through a removable diaphragm which helps to define the optical path. The beam is focused onto the sample by a movable 5 cm quartz lens. The light scattered from the sample is imaged by an off axis ellipsoidal mirror (Perkin-Elmer Corp., Irvine, California, mirror #186-0110).

The advantage of an ellipsoidal mirror is that it is free of chromatic and spherical aberrations. To image non-monochromatic light from any light source, the imaging element or elements must show no dispersion of the refractive index with respect to frequency. In the visible spectral region, lenses using different types of glass may be combined such that the array is nearly achromatic. However the technical problems of producing such a lens in the UV are severe. Thus a reflecting imaging system is utilized.

An ellipsoidal mirror (Fig. 3) has the property that any ray originating from one of the two foci is reflected through the other focus. When a spherical mirror is used to image an object anywhere but at the radius of curvature of the mirror, the spherical surface is being used as an approximation to an ellipsoidal surface. The quality of the focused image is degraded by spherical aberrations. These occur because different annular rings of the spherical mirror focus the image at different distances from center of the mirror. A large loss in light collection thus occurs when imaging a point light source into the entrance slits of the monochromator.

The scattered light focused by the ellipsoidal mirror is reflected by a plane mirror onto the entrance slit of a Spex 1400 double monochromator. The object is magnified by a factor of 6.

A spherical mirror, used to collect light scattered opposite the ellipsoidal mirror, is positioned such that the sample is at its radius of curvature. The collected scattered light is re-imaged through the sample and is collected by the ellipsoidal mirror.

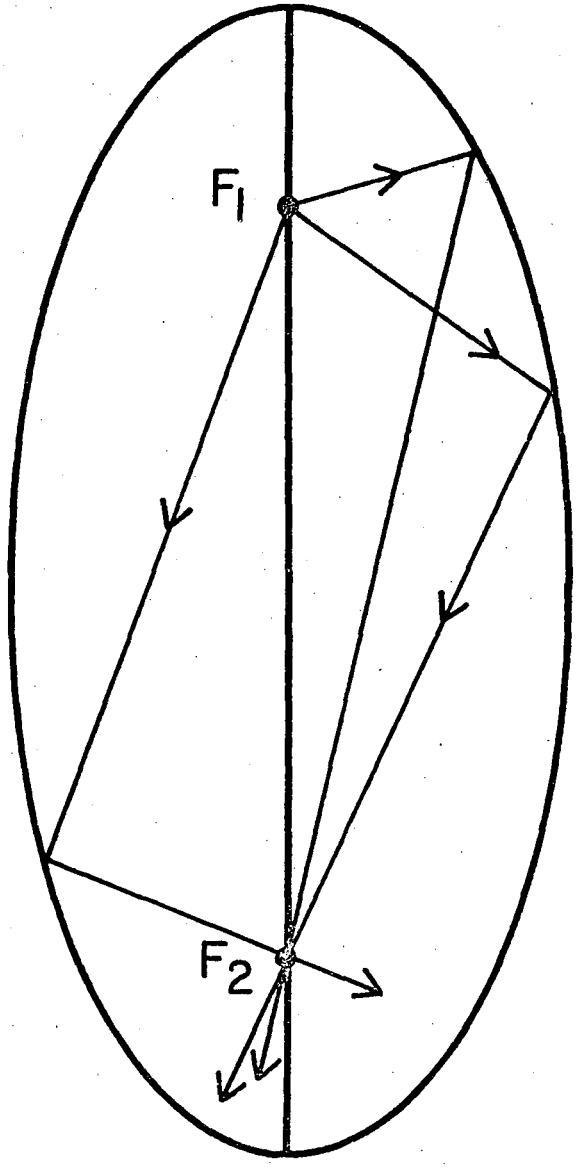

XBL 768-6096

Fig. I-3. Ray tracing of light reflection by an ellipsoidal mirror of a point light source at F_1.

Grating monochromators are known to have different transmittances for light polarized parallel and perpendicular to the entrance slits (Bailey and Scherer, 1969). To avoid intensity artifacts resulting from the polarization bias of the monochromator, a polarization scrambler consisting of a quartz wedge (Lambda Optica, Berkeley Heights, New Jersey, Number S-114) is introduced into the imaged beam prior to the entrance slit of the monochromator. An air spaced UV transmitting polarizing prism is used for analysing the polarization of the scattered light. The monochromator is a Spex 1400 double monochromator. The two 4" square gratings are aluminized and blazed at 7500 Å with 1200 grooves per millimeter resulting in a dispersion of 5 Å/mm. The photomultiplier used is an EMI 9558 QB which has a flat end window.

Electronics

A block diagram of the electronic detection system is shown in Fig. 4. Both the reference and sampling photomultipliers are powered by a single high voltage power supply. The high voltage to the reference photomultiplier is attenuated by a voltage divider between the photomultiplier and the high voltage power supply.

The photomultiplier bases are wired without a load resistor but with coupling capacitors between the last three dynodes. Because the laser is pulsed, a large current is drawn from the photomultipliers at each laser pulse. The purpose of the coupling capacitors is to avoid draining the dynode resistor chain during the laser pulse which would result in a non-linear response of the photomultiplier. To discriminate against dark noise from the photomultiplier and to amplify the signal from the photomultipliers a dual channel boxcar

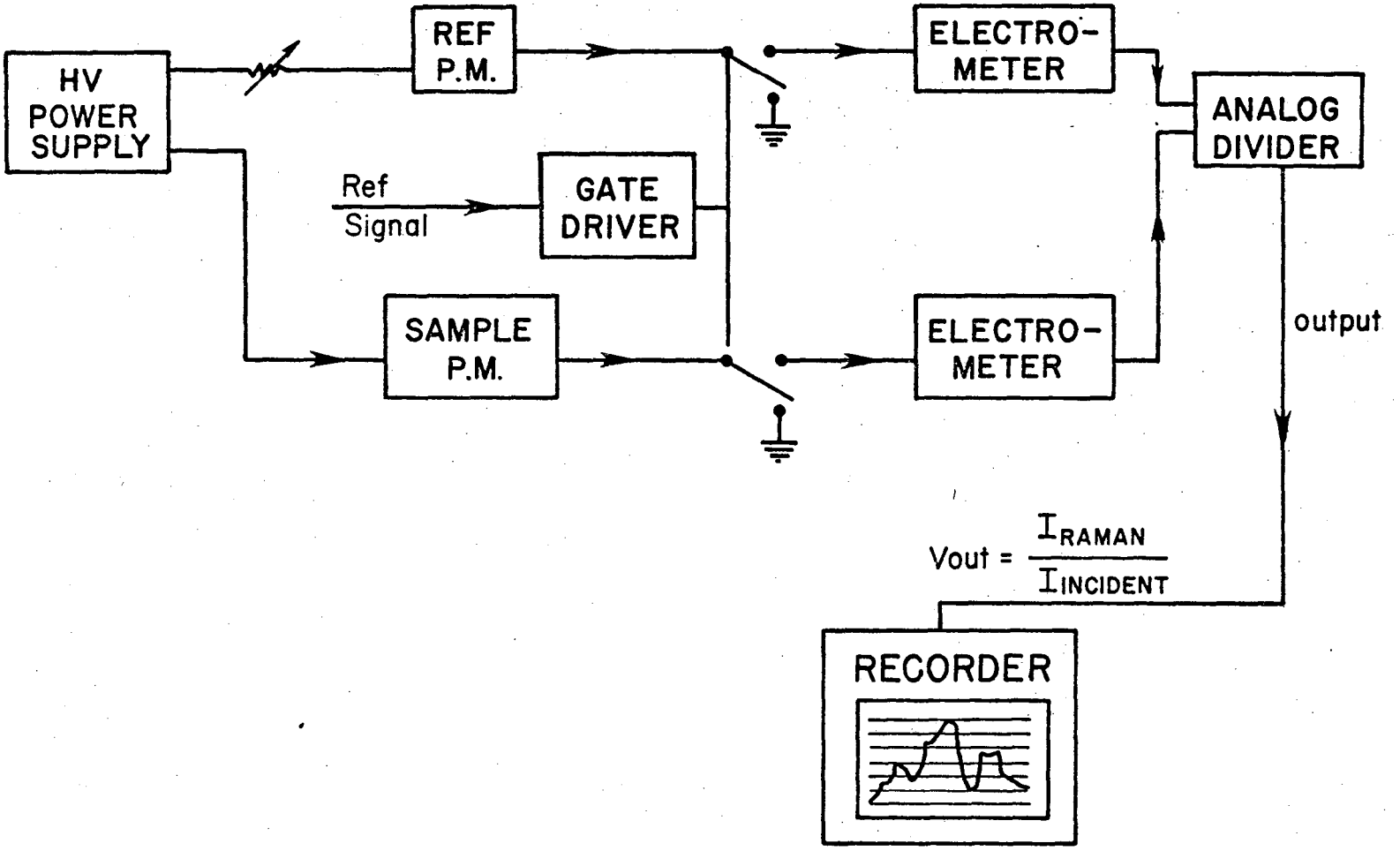

Fig. I-4. Block diagram of the electronic detection system of the Raman spectrometer.

XBL 768-6097

integrator was utilized to amplify the outputs of the photomultipliers. The dual channel boxcar integrator used in the Raman spectrometer was designed by the electronics shop of the Physics Department (University of California, Berkeley). The design was modified and the unit was built by the electronics shop of the Chemistry Department (University of California, Berkeley). The gate circuit was further modified by Bojan Turko and Branko Leskovar of Lawrence Berkeley Laboratories.

To discriminate against dark noise from the photomultiplier the integrating circuit is gated and is driven by an electronic reference pulse from the laser. The reference pulse arrives about 2 microseconds prior to the light pulse. The electronic reference signal activates the gate driver which operates a gate between the electrometers and ground. Between light pulses the output of the photomultiplier is grounded. Just prior to the light pulse, the gate connects the photomultiplier output to the electrometers. Immediately after the microsecond laser pulse the gate disconnects the photomultiplier outputs from the electrometers and reconnects them to ground. With this gating circuit, it was not necessary to cool the two photomultipliers to reduce dark current noise.

Two fluctuations occur in the output light intensity of the laser. The first is the short term fluctuation from pulse to pulse. This variation in laser intensity can be as much as ± 20%. The second variation, usually a slow decrease of laser intensity with time, results from two factors: dye decay and temperature expansion of the optical components of the laser cavity. Both the variation in pulse-to-pulse intensity and the variation in average output power must be compensated

for. The output of the electrometer is proportional to the average incident light intensity on the photomultipliers. The electrometers are wired in an integrating mode. The resistor and capacitor placed across the electrometers provide a two-second time constant. The electrometers integrate the current pulses from the photomultipliers at each pulse, but between pulses a small exponential decay of the charge on the capacitor occurs due to the two-second time constant. A stationary level is reached when the exponential decay between pulses is equal to the additional charge introduced by each pulse.

The number of pulses averaged is a function of the time constant of 2 seconds. To reach an output within 1% of the stationary level requires 5 time constants. At a repetition rate of 30 Hz, 300 pulses are averaged. However, the 300 pulses averaged are not weighted equally. The most recent pulse has more influence on the output level than the one preceding it, which has more influence than the one preceding it and so forth. Thus, after reaching a stationary level of V_1 from photomultiplier pulses of charge q_1, if subsequent pulses were of charge $q_2 = 0.5\ q$, the output level would not be the average of 299 pulses of q_1 and one pulse of $0.5\ q_1$. The voltage out would exponentially decrease to V_2 with a time constant of 2 seconds.

The stationary level reached is linearly proportional to the average photon intensity. The integration averages out the short term pulse-to-pulse fluctuations in laser intensity, but the circuit still responds to changes in the average photon flux reaching the photomultiplier.

The longer term decay in average laser power intensity is compensated by an analog divider which divides the sample channel by the reference channel. The output voltage of the divider is thus a voltage proportional to the number of incident photons reaching the sampling photomultiplier, but the output is normalized to the intensity of the laser pulse. Varying the high voltage to the reference photomultiplier thus changes the apparent signal level of the Raman spectrum.

Each of the electrometers responds to an average current. Thus, the electrometers can be calibrated for photoelectron sensitivity with a high impedence constant current source and by gating the electrometers with a pulse generator.

The output voltage per (photoelectron $\cdot$ sec^{-1}) can then be calculated from:

$$O = \frac{VG}{IwRe}$$

where O is the output voltage per (photoelectron $\cdot$ sec^{-1}), V is the output voltage measured, G is the gain of the photomultiplier and I is the input current. w is the gate width. R is the repetition rate and e is the number of electrons per coulomb.

Thus for an input current of 10^{-6} amps, a gatewidth of 5 μsec and repetition rate of 30 Hz, the output was measured to be 3.55 V. For a photomultiplier with a gain of 10^{6} the output voltage is approximately 3 mV per (photoelectron $\cdot$ sec^{-1}). For a photomultiplier with a quantum efficiency of 10% and a laser repetition rate of 10 Hz a 3 mV output occurs if each laser pulse results in one photon impinging on the photocathode of the photomultiplier.

The linearity of the electrometer output as a function of the average input current and repetition rate was measured for input currents ranging from the equivalent of 1 photoelectron per second (one photon per 30 laser pulses) to the equivalent of 3000 photoelectrons per second (100 photons per laser pulse) at 30 Hz. The proportionality between the output voltage and the input current appears constant to within 2%. The proportionality between the output voltage and repetition rate for a given input current was also measured and was found to be constant to within 5% for repetition rates from 5 to 100 Hz.

Raman spectra were collected on a chart recorder. Peak height measurements were used to determine Raman intensities.

Monochromator Calibration

The monochromator was calibrated with respect to wavelength with low pressure Hg, Ar, Kr and Xe discharge lamps. The reflectivity of the mirrors, monochromator efficiency and photomultiplier efficiency is a function of the wavelength of the incident light. Thus, for an accurate determination of relative intensities of Raman lines, the observed spectrum must be normalized against an efficiency profile of the spectrometer.

The spectral response of the spectrometer was measured using an Epply Laboratory, Inc. standard intensity incandescent lamp. The lamp illuminated (Fig. 5) two mirrors placed at 45° to a plate coated with MgO. The mirrors were positioned such that they formed a small slit opening through which light scattered from the MgO plate could pass for collection by the ellipsoidal mirror and for imaging into the monochromator.

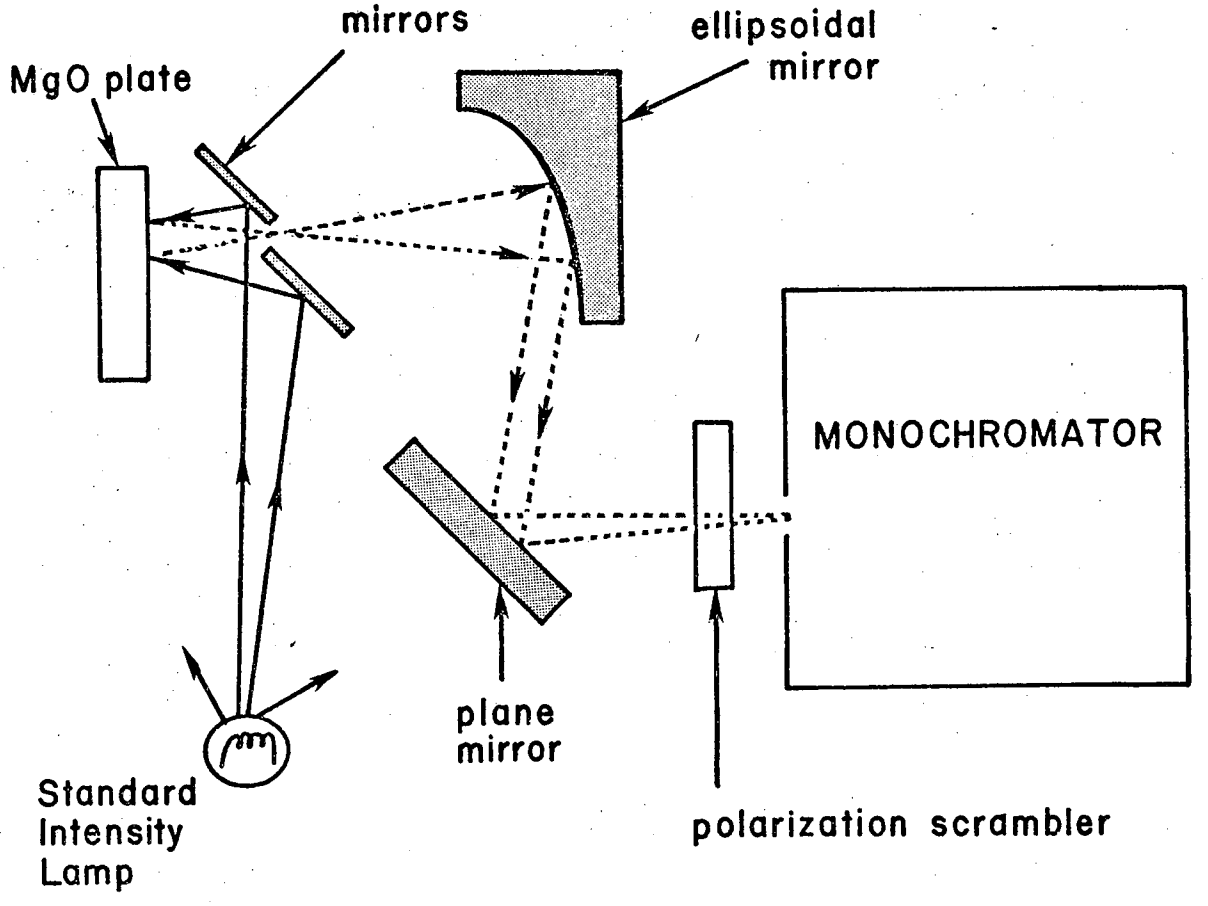

Fig.I-5. Experimental configuration used for the efficiency calibration of the Raman spectrometer.

90° scattering from the MgO plate is essential in order that the frequency distribution of the scattered light be identical to that of the standard intensity incandescent lamp (Scherer, 1975).

Figure 6 shows the relative efficiency curve of the spectrometer. The relative spectrometer efficiency, E_λ at wavelength λ, is defined as:

$$E_\lambda = \frac{i_\lambda}{I_\lambda \, E_{\lambda_{max}}}$$

where i_λ is the output current of the photomultiplier at λ. I_λ is the intensity of the standard intensity incandescent lamp at λ and $E_{\lambda_{max}}$ is the maximum value of E_λ at λ_{max}. The low efficiency below 500 nm results from the monochromator gratings, which are blazed at 750 nm. The decline in efficiency above 600 nm is due to the loss in quantum efficiency of the photomultiplier.

All of the spectra used in the excitation profiles obtained with excitation wavelengths above 400 nm were normalized to the efficiency curve of the spectrometer. Spectra obtained with excitation in the ultraviolet were not corrected for spectrometer efficiency.

The monochromator was used in second and third order for all of the Raman spectra measured with ultraviolet excitation, to stay as close to the blaze angle as possible. To measure the spectral response of the spectrometer with the monochromator used in a higher order, all of the visible light from the standard intensity incandescent lamp must be excluded. This is a formidable undertaking.

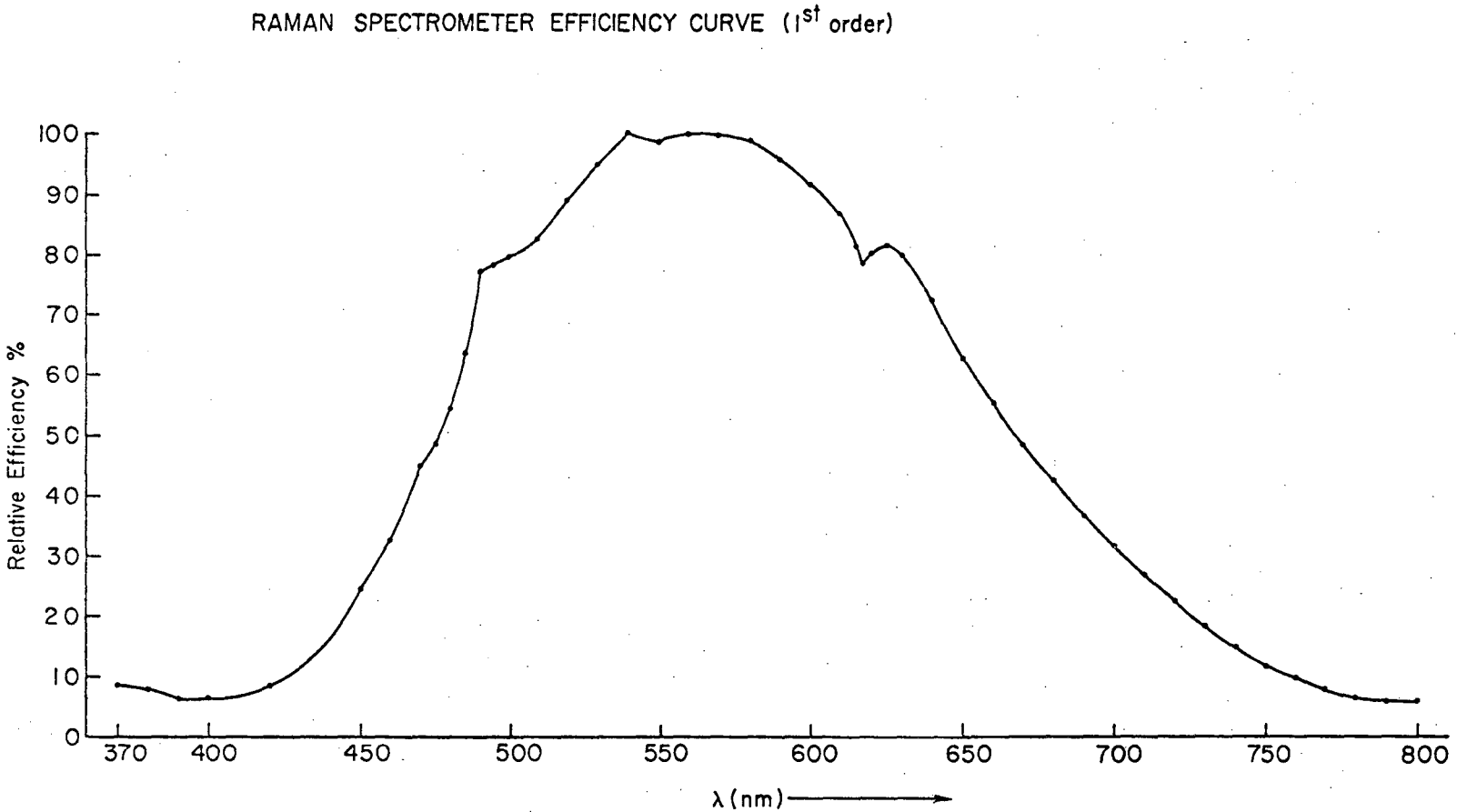

Fig. I-6. Raman spectrometer efficiency curve in first order.

XBL 768-9500

The Raman spectra obtained with excitation in the UV were not corrected for the variation in spectrometer efficiency with wavelength. To evaluate the intensity error that might result in a typical Raman spectrum covering 1500 cm^{-1} requires an estimate of the variation with wavelength of the reflectivity of the mirrors, the efficiency of the gratings and the quantum efficiency of the photomultiplier. The variation in the reflectivity of a typical first surface UV enhanced Al mirror is less than 1% for any wavelength interval spanned by a 1500 cm^{-1} Raman spectral scan in the UV.

The efficiency of a grating is wavelength dependent and is highest in first order at the blaze wavelength. A grating blazed at λ_b in first order is also blazed at λ_b/n for order n. The efficiency of a grating decreases away from the blaze wavelength. However, the rate of change of the efficiency with respect to wavelength is smallest near the blaze wavelength.

All of the UV Raman spectra were obtained in second and third order in order to stay as close to the blaze wavelength as possible. The variation in efficiency for a typical 1200 groove grating blazed at 7500 Å in first order over a 1500 cm^{-1}. UV Raman spectrum measured in second and third order is less than 10% (Landau and Mitteldorf, 1972).

The photomultiplier quantum efficiency is wavelength dependent. However, the quantum efficiency of a typical EMI 9558 QB photomultiplier is relatively flat with respect to wavelength below 4500 Å. Within a 1500 cm^{-1} Raman spectrum excited in the UV, the variation in quantum efficiency is expected to be less than 5%. Thus, the maximum

error expected from intensity measurements in a 1500 cm^{-1} Raman spectrum excited in the UV due to variations in the efficiency of the spectrometer is less than 16%.

Sample Handling

Resonance Raman spectra obtained in the visible spectral region were measured with the samples enclosed in melting point capillaries of ca 1 mm inside diameter. Excitation was transverse to the long axis of the capillary and scattering was viewed at 90° to the plane defined by the axis of the incident laser beam and the long axis of the capillary. The position of the capillary with respect to the laser beam was adjusted to minimize self absorption by exciting close to the capillary wall. Resonance Raman spectra in the UV were obtained by 75° scattering from a 1.0 mm pathlength quartz (Spectrosil) absorption cuvette (Lightpath cells, Inc., St. Louis, Mo, catalog number 1-Q-1).

Raman spectroscopy in the ultraviolet is especially plagued by fluorescence, both from the sample and the sample container. For example, every solvent used for samples excited with ultraviolet light required careful distillation. The fluorescence from typical commercially available solvents was so intense that a blue emission could be visually observed along the path of the laser beam through the solvent. Distilled H_2O was redistilled in glass prior to use. An impurity which is at very low concentration can give rise to a background which obscures the Raman spectra of the sample. For example, a 0.001%

impurity which has a quantum yield of fluorescence of 10^{-1} will give a fluorescence background comparable to the Raman peaks if the Raman cross section of the sample is 10^{-7}.

Because the monochromator is used in second and third order, fluorescence in the visible spectral region is also passed by the monochromator and contributes to the background observed in the Raman spectra. A UV pass filter (Kodak 18A or Corning7-54) was inserted prior to the entrance slit of the monochromator for the Raman spectra measured with UV excitation. The use of a solar blind photomultiplier should eliminate interference from visible fluorescence.

Fluorescence from the sample container is also a serious problem. Only very pure spectrosil quartz (Thermal American Fuzed Quartz, Montville, NJ) is suitable as a sample container. Natural fuzed Quartz shows a very intense fluorescence, presumably from impurities in the quartz. Another problem is the Raman spectra shown by the quartz. The Raman spectrum of quartz is broad and gives an intense background below 450 cm^{-1}. Other materials such as sapphire may be more suitable as sample containers for Raman spectroscopy excited in the UV.

REFERENCES

Bailey, G. F., and Horvat, R. J., J. Am. Oil Chemists Soc. 49, 494 (1970).

Bailey, G. F., and Scherer, J. R., Spectrosc. Lett. 2, 261 (1969).

Boucher, L. J., Coord. Chem. Rev. 7, 289 (1972).

Gouterman, M., Hanson, L. K., Khalil, G-E, Leenstra, W. R., and Buchler, J. W., J. Chem. Phys. 62, 2343 (1975).

Lambropoulous, M., Opt. Comm. 15, 35 (1975).

Landau, D. O., and Mitteldorf, A. J., Spex Speaker 17(1) (1972).

Scherer, J., (1975), private communication.

Sutherland, J. C., Vickery, L. E., and Klein, M. P., Rev. Sci. Instr. 45, 1089 (1974).

Williams, Jr., R. C., and Tsay, K-Y, Anal. Biochem. 54, 137 (1973).

Ellipsoidal Mirrors, Technical Bulletin, Perkin Elmer Corp., Norwalk, Conn. (1963).

CHAPTER II

RAMAN THEORY

Introduction

The Raman effect is a consequence of inelastic scattering of light by a material substance. The difference in energy between the incident and Raman scattered photon corresponds to the energy difference between the initial and final states of the scattering media. Although the effect is named after Sir C.V. Raman who observed inelastic light scattering from liquids in 1928 (Krishnan, 1971; Konigstein, 1972), the Raman effect was observed almost simultaneously by Landsberg and Mandelstam in the U.S.S.R. in their studies of light scattering from quartz (Krishnan, 1971; Sushchinskii, 1972). However the possibility of inelastic light scattering was envisioned earlier in 1923 by Smekal (Krishnan, 1971).

For vibrational Raman scattering the difference between the energy of the incident and scattered photon corresponds to the energy of a vibrational transition of the molecule. The energy and polarization differences between the Raman scattered and incident photons depend on the internal forces of the molecule. Thus, studies of the Raman spectra of molecules give information on the vibrational modes, electronic structure and chemical environment of the molecule. The physical interpretation of Raman spectra requires an understanding of the interactions of the incident photon with the electronic and vibrational states of the molecule.

Physical Description

A simple physical picture of the Raman effect is visualized in Fig. 1. An electromagnetic wave of frequency ν_o is incident on a molecule. The oscillating electromagnetic field drives the molecule at the incident frequency ν_o with an amplitude that is a function of the molecular polarizability. Since the polarizability is a function of the nuclear coordinates, nuclear vibrations modulate the polarizability with a frequency ν_v, the frequency of vibration of the nuclei. The oscillating electron cloud of the molecule is manifested as an oscillating dipole moment which radiates light with frequency ν_o, (Rayleigh scattered light), $\nu_o + \nu_v$ (Anti-Stokes Raman scattered light) and $\nu_o - \nu_v$ (Stokes Raman scattered light). This picture can be visualized more quantitatively by examining the dipole moment induced in a molecule by an electromagnetic field (Chantry, 1967).

$$\hat{\mu} = \alpha \hat{E}_o \cos 2\pi \nu_o t \qquad (1)$$

where $\hat{\mu}$, the induced dipole moment, is proportional to the polarizability of the molecule, α, and to the amplitude of the electric field, $\hat{E}_o$, which oscillates with frequency ν_o. The polarizability varies with the configuration of the nuclei such that for a vibrational mode of frequency ν_v the polarizability may be expanded as a Taylor series based on the equilibrium internuclear configuration,

$$\alpha = \alpha_o + \left(\frac{\partial \alpha_o}{\partial Q}\right)_o \Delta Q + \ldots . \qquad (2)$$

where Q is the normal coordinate of the vibration.

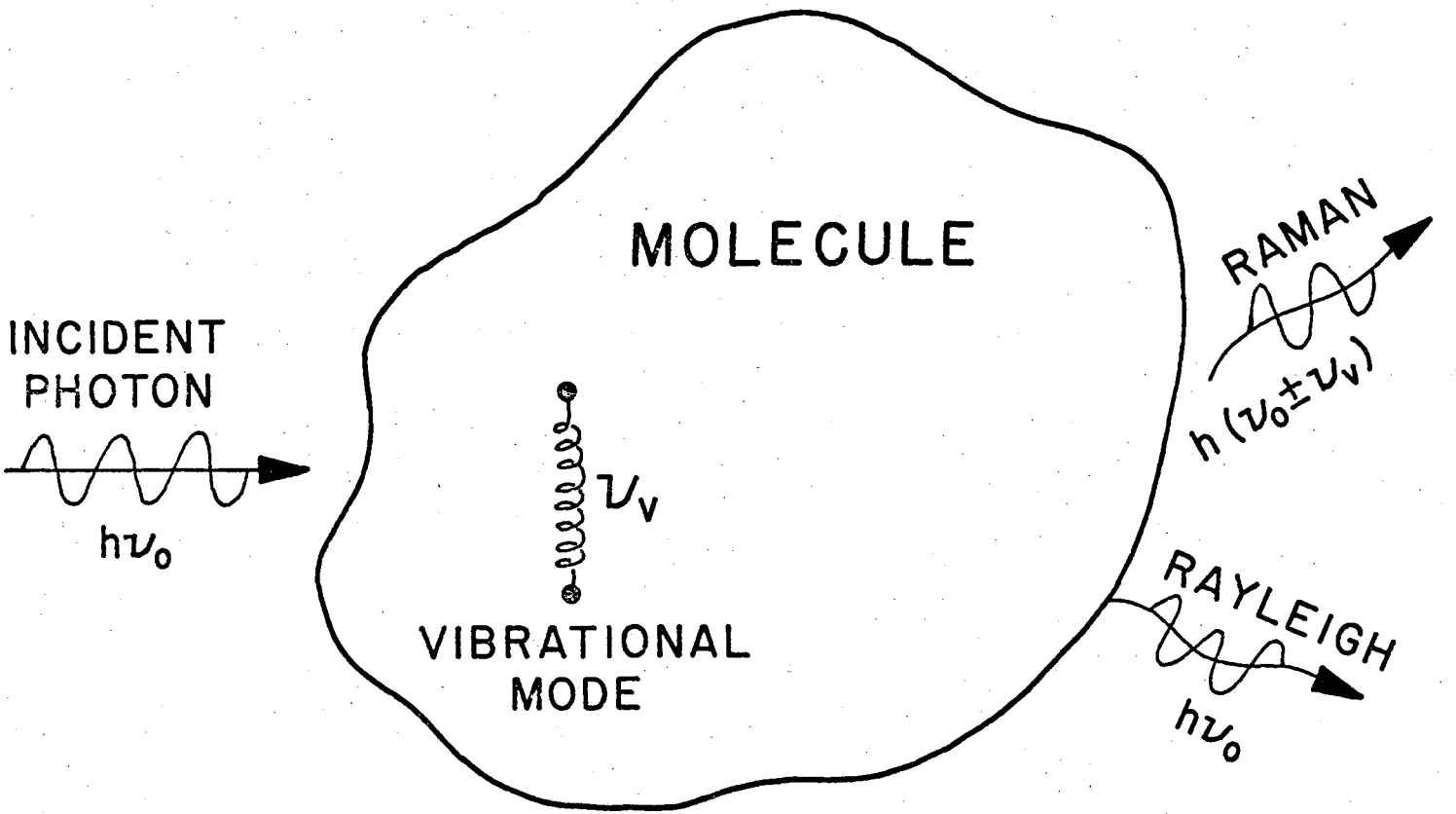

Fig. II-1. Polarizability picture of Rayleigh and Raman light scattering.

XBL 768-9544

For a diatomic molecule

$$\Delta Q_o = A \cos 2\pi \nu_v t$$

where A is the amplitude of vibration. Defining $A \left(\frac{\partial \alpha_o}{\partial Q}\right)_o$ as α_1 and substituting in Eq. (1).

$$\hat{\mu} = \alpha_o \hat{E}_o \cos 2\pi \nu_o t + \alpha_1 \hat{E}_o \cos 2\pi \nu_o t \cos 2\pi \nu_v t \quad (3)$$

An oscillating dipole moment radiates power at a rate (Konigstein, 1972; Dushman, 1938; Chantry, 1967).

$$I = \frac{16\pi^2 \nu^4}{3c^2} (\mu)^2 \quad (4)$$

Substituting Eq. (3) into Eq. (4) and using a trigonometric identity yields:

$$\begin{aligned} I = \frac{16\pi^2}{3c^3} [& \nu_o^4 \alpha_o^2 E_o^2 \cos^2 2\pi \nu_o t + \\ & (\nu_o+\nu_v)^4 \alpha_1^2 E_o^2 \cos 2\pi (\nu_o+\nu_v) t + \\ & (\nu_o-\nu_v)^4 \alpha_1^2 E_o^2 \cos 2\pi (\nu_o-\nu_v) t \\ & + \text{cross terms}] . \end{aligned} \quad (5)$$

A number of features are clear from Eq. (5). The intensity, I, is proportional to the fourth power of the radiated frequency. Thus, the higher the frequency of the incident light the greater the intensity of scattering. For example, the scattering efficiency for 300 nm light is 16 times as high as for 600 nm light.

The first term in Eq. (5) represents elastic (i.e., Rayleigh) scattering, because the frequency radiated is ν_o. The second and third terms are responsible for Anti-Stokes and Stokes Raman scattering, because the frequency radiated is $\nu_o + \nu_v$ and $\nu_o - \nu_v$, respectively. The cross terms can be neglected since the power they propagate integrates to zero (Chantry, 1967).

Although the classical description of Raman scattering is useful for a physical insight into the Raman phenomenon, the magnitudes of α_0 and α_1 and, more important, the interaction of the electronic and vibrational states of the molecule are not detailed. An understanding of the interaction of the incident light with the molecule requires an explicit description of the polarizability tensor, α. A quantum mechanical approach is necessary to describe the states of the molecule, the interactions between the vibrational and electronic states and the interaction between the photon and the molecule.

Polarizability Tensor

Equation (5) gives a simplified description of Raman scattering from an oscillating dipole moment induced by a linearly polarized electromagnetic field incident on a one dimensional oriented molecule. For a real molecule fixed in space the polarizability is three dimensional and Eq. (5) should read (Albrecht, 1961):

$$I_{ij} = \frac{2^7 \pi^5}{3^2 c^4} I_o \, (\nu_o - \nu_{ij})^4 \sum_{\rho,\sigma} |(\alpha_{\rho\sigma})_{ij}|^2 \, . \qquad (6)$$

I_o is the intensity of the incident light and I_{ij} is the intensity of Raman scattered light for the vibrational transition $i \rightarrow j$, where i is the initial vibrational sublevel of the ground electronic state and j is the final vibrational sublevel of the ground electronic state. The process described by Eq. (6) is shown in Fig. 2. The molecule starts in the i'th vibrational sublevel of one particular vibrational mode in the ground electronic state. The outgoing photon carries off an energy of $h\nu_o - (E_j - E_i)$. The final state of the system is the j'th vibrational level of one normal mode of the ground electronic state. The polarizability is expressed as $\alpha_{\rho\sigma}$, where ρ and σ are coordinates in the reference frame of the molecule.

Whenever the polarizability of the molecule is anisotropic the polarizability must be expressed as a second order tensor (Konigstein, 1972; Wilson et al., 1955) in which the elements are labelled by ρ and σ. The polarizability tensor determines the orientation of the dipole moment of the molecule, induced by the incident electromagnetic field, and is expressed as

$$\hat{\alpha} = \begin{vmatrix} \alpha_{xx} & \alpha_{xy} & \alpha_{xz} \\ \alpha_{yx} & \alpha_{yy} & \alpha_{yz} \\ \alpha_{zx} & \alpha_{zy} & \alpha_{zz} \end{vmatrix}, \qquad (7)$$

where the subscripts x, y, z labeling the polarizability matrix elements are defined in the laboratory coordinate system. The induced dipole moment is a vector and is:

$$\hat{\mu} = \hat{\alpha}\,\hat{E} \qquad (8)$$

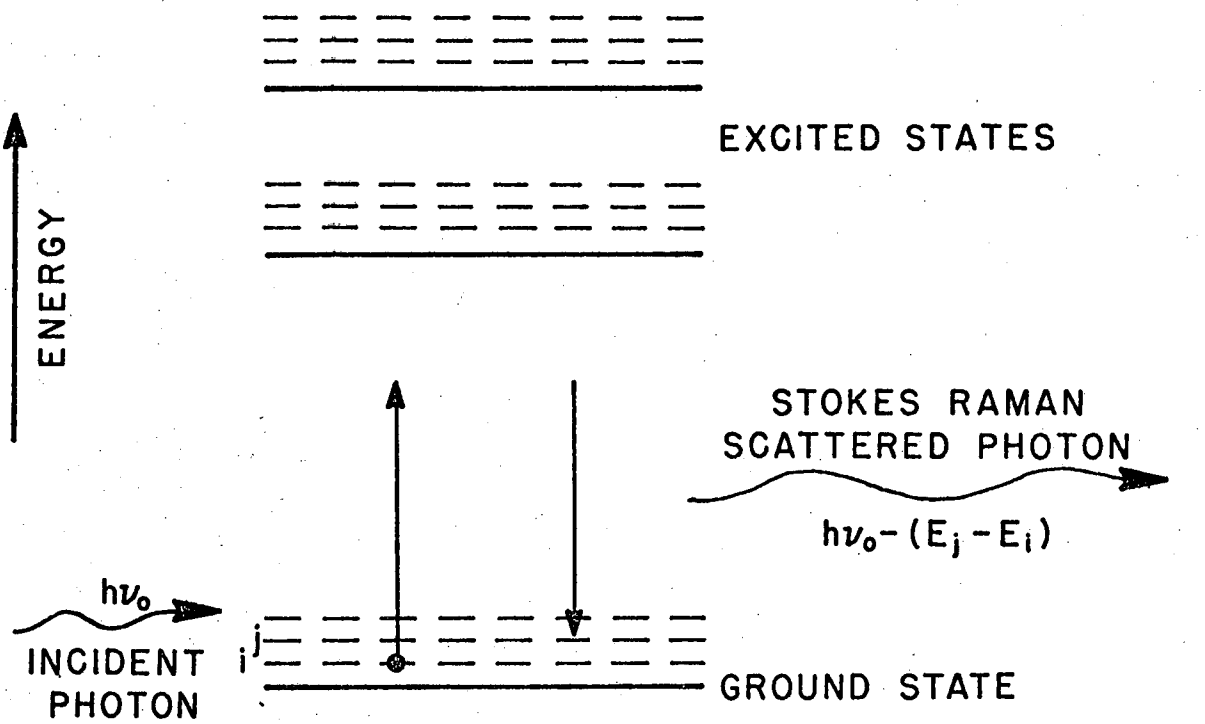

XBL 768-9542

Fig. II-2. Energy level diagram for Raman scattering.

where $\hat{E}$, the electric field can be described by a column vector

$$\hat{E} = \begin{vmatrix} E_x \\ E_y \\ E_z \end{vmatrix} \quad . \tag{9}$$

For a molecule fixed in space, at the origin of a laboratory defined coordinate system the dipole moment induced by the electromagnetic field is:

$$\hat{\mu} = \mu_x \hat{i}_x + \mu_y \hat{i}_y + \mu_z \hat{i}_z =$$
$$(\hat{\alpha}_{xx} \hat{E}_x + \hat{\alpha}_{xy} \hat{E}_y + \hat{\alpha}_{xz} \hat{E}_z) +$$
$$(\hat{\alpha}_{yx} \hat{E}_x + \hat{\alpha}_{yy} \hat{E}_y + \hat{\alpha}_{yz} \hat{E}_z) +$$
$$(\hat{\alpha}_{zx} \hat{E}_x + \hat{\alpha}_{zy} \hat{E}_y + \hat{\alpha}_{zz} \hat{E}_z)$$

where $\hat{i}_x$, $\hat{i}_y$ and $\hat{i}_z$ are unit vectors in the laboratory coordinate system. For example, for light polarized along the x direction the induced dipole moment along the y direction is:

$$\hat{\mu}_y = \hat{\alpha}_{yx} \hat{E}_x$$

However, for a collection of molecules in solution which can assume all possible orientations of the principal axes of the molecules to the laboratory coordinate frame, orientational averaging is necessary. The result is expressible in terms of three quantities associated with the polarizability tensor, which are called the isotropic, $\bar{\alpha}^2$, symmetric, γ_s^2, and antisymmetric, γ_{as}^2 invariants of the polarizability tensor (Konigstein, 1972; Wilson et al., 1955) and are defined as:

$$\bar{\alpha}^2 = \frac{1}{9}(\alpha_{xx} + \alpha_{yy} + \alpha_{zz})^2 \tag{11a}$$

$$\gamma_s^2 = \frac{1}{2}[(\alpha_{xx}-\alpha_{yy})^2 + (\alpha_{yy}-\alpha_{zz})^2 + (\alpha_{zz}-\alpha_{xx})^2] + \frac{3}{4}[(\alpha_{xy}+\alpha_{yx})^2 + (\alpha_{zx}+\alpha_{xz})^2 + (\alpha_{yz}+\alpha_{zy})^2] \tag{11b}$$

$$\gamma_{as}^2 = \frac{3}{4}[(\alpha_{xy}-\alpha_{yx})^2 + (\alpha_{xz}-\alpha_{zx})^2 + (\alpha_{yz}-\alpha_{zy})^2] \tag{11c}$$

These tensor invariants are independent of the orientation of the molecules to the laboratory coordinate frame. The effect of orientation averaging is to relate the polarizabilities along the principal axes of the molecule to the polarizability observed for an unoriented collection of molecules in the laboratory frame.

Depolarization Ratio

The depolarization ratio, ρ, of Raman scattering using a 90° collection geometry is defined as $\rho = \frac{I_\perp}{I_\parallel}$, where $I_\perp$ and $I_\parallel$ are the observed scattered intensities for a polarization analyzer oriented perpendicular and parallel to the incident polarization direction (Fig. 3). For the oriented molecule pictured in Fig. 3 with the light incident along the z axis, polarized along the x axis and with the scattered light measured along the y axis:

$$\rho = \frac{I_\perp}{I_\parallel} = \frac{(\alpha_{zx})^2}{(\alpha_{xx})^2} \quad .$$

However, for a collection of molecules which are free to rotate and which can assume any orientation with respect to the laboratory reference frame, the depolarization ratio must be written in terms of the invariants of the polarizability tensor (Eqs. 11a, b and c)

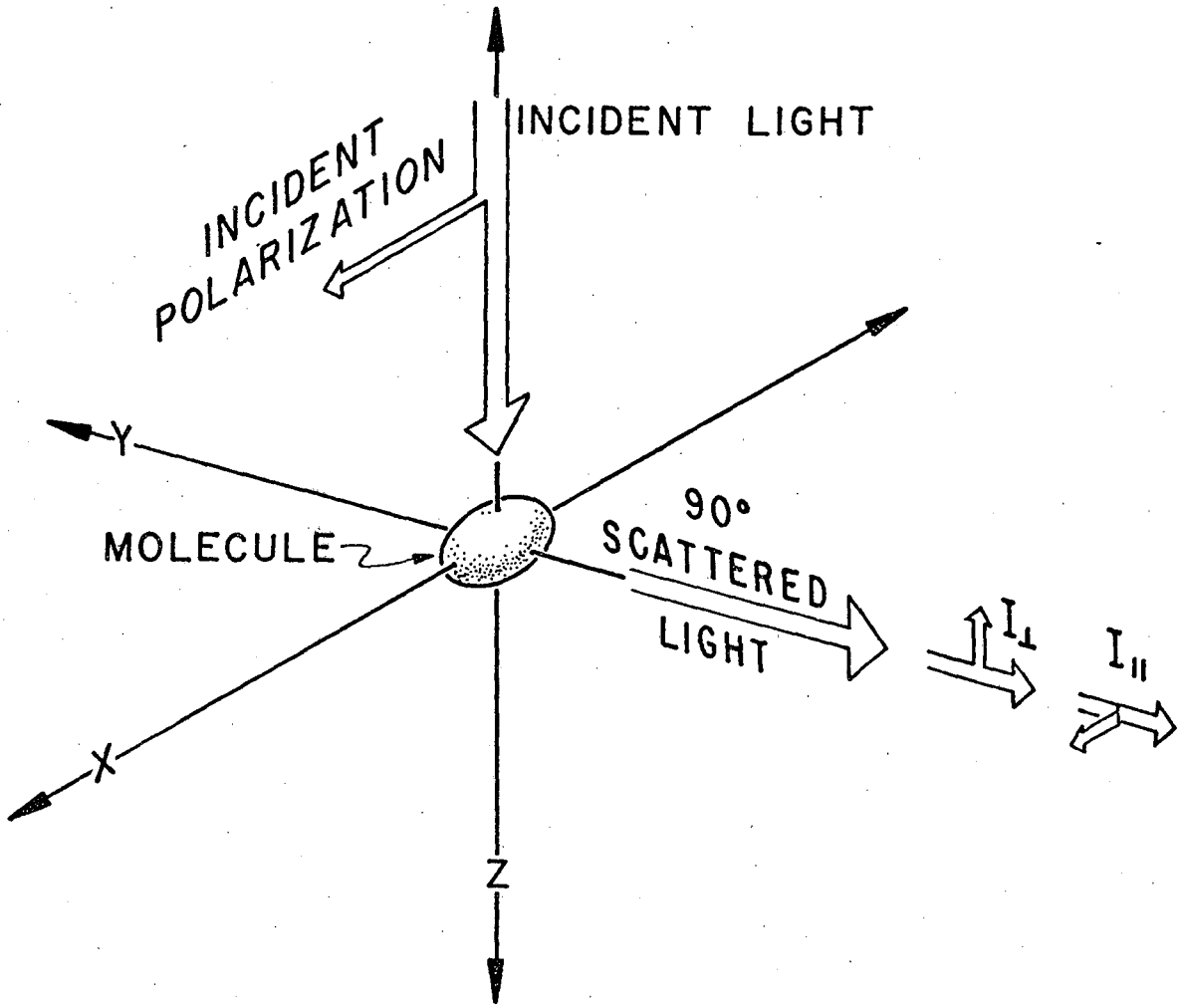

Fig. II-3. Scattering geometry for depolarization ratio measurements.

(Konigstein, 1972; Wilson et al., 1955). The depolarization ratio for linearly polarized light is:

$$\rho = \frac{3\gamma_s^2 + 5\gamma_{as}^2}{45\bar{\alpha}^2 + 4\gamma_s^2} \quad . \tag{12}$$

By examining the point group of the molecule and the symmetry properties of the vibrational modes (Wilson et al., 1955; Cotton, 1963), the depolarization ratios can be predicted for vibrations of different symmetries.

The polarizability tensor patterns for different point groups have been calculated and listed by McClain (McClain, 1971). Table I lists the tensor elements for vibrations of A_1, A_2, B_1 and B_2 symmetry in the C_{4v}, D_4, D_{2d} and D_{4h} point groups. Each of the entries in the matrices for the vibrations of symmetries A_1, A_2, B_1 and B_2 corresponds to an element of the polarizability tensor. The tensor elements are calculated from group theoretical arguments which can predict which tensor elements vanish.

For a molecule of D_{4h} or C_{4v} symmetry such as a metalloporphyrin, the depolarization ratios can be calculated from the matrices in Table I. For a vibration of A_1 symmetry, Eqs. 11a, b and c, and Table I yield:

$$\bar{\alpha}^2 = \frac{1}{9}(2S_1+S_2)^2$$

$$\gamma_s^2 = (S_1-S_2)^2$$

$$\gamma_{as}^2 = 0$$

Table I. Scattering tensor patterns for the point groups C_{4v}, D_4, D_{2d} and D_{4h} (McClain, 1971)

$$A_1 = \begin{vmatrix} S_1 & 0 & 0 \\ 0 & S_1 & 0 \\ 0 & 0 & S_2 \end{vmatrix} \qquad A_2 = \begin{vmatrix} 0 & S_3 & 0 \\ -S_3 & 0 & 0 \\ 0 & 0 & 0 \end{vmatrix}$$

$$B_1 = \begin{vmatrix} S_4 & 0 & 0 \\ 0 & -S_4 & 0 \\ 0 & 0 & 0 \end{vmatrix} \qquad B_2 = \begin{vmatrix} 0 & S_5 & 0 \\ S_5 & 0 & 0 \\ 0 & 0 & 0 \end{vmatrix}$$

Whether an element of the polarizability tensor is identically equal to zero can be calculated by group theoretical arguments (McClain, 1971). However an element of the tensor which is not formally equal to zero may be found to be very small when the properties of the molecule are considered. It will be shown subsequently that each of the elements of the polarizability tensor depends on the electronic transitions of the molecule. For a porphyrin, in which the most intense electronic transitions are x, y polarized, $S_1 >> S_2$ (the z components of the polarizability tensor are small) (Nestor and Spiro, 1973) and

$$\bar{\alpha}^2 = \frac{4}{9} S_1^2$$

$$\gamma_s^2 = S_1^2$$

$$\gamma_{as}^2 = 0 \quad .$$

Using Eq. (12), the depolarization ratio for a vibration of A_1 symmetry in a porphyrin is predicted to be 0.125. (Raman bands with $\rho < 0.75$ are called polarized.) For vibrations of B_1 symmetry

$$\bar{\alpha}^2 = 0$$

$$\gamma_s^2 = 3 S_4^2$$

$$\gamma_{as}^2 = 0 \quad .$$

Thus $\rho_1 = 0.75$ for vibrations of B_1 symmetry and the Raman scattered light is called depolarized. Vibrations of B_2 symmetry have:

$$\bar{\alpha}^2 = 0$$

$$\gamma_s^2 = 3 S_5^2$$

$$\gamma_{as}^2 = 0$$

$$\rho = 0.75 \quad .$$

Vibrations of A_2 symmetry have:

$$\overline{\alpha}^2 = 0$$

$$\gamma_s^2 = 0$$

$$\gamma_{as}^2 = 3\, S_3^2$$

$$\rho = \infty \quad ,$$

indicating that the scattered light is polarized 90° from the direction of polarization of the incident light. The scattered light is called inversely polarized.

Although inverse polarization had been predicted by Placzek over 40 years ago (Placzek, 1934) it was first observed in 1972 by Spiro and Strekas from resonance Raman scattering from heme proteins (Spiro and Strekas, 1972). Thus a measurement of the depolarization ratio will differentiate modes of symmetry A_1, A_2 and the set B_1, B_2 from each other. Unfortunately vibrations of both B_1 and B_2 symmetry show depolarized Raman scattering and cannot be differentiated by a depolarization measurement.

Quantum Mechanical Description

The interaction between the photon and the electronic and vibrational states of the molecule is contained in the elements of the polarizability tensor. Using time-dependent perturbation theory of the interaction of radiation and matter, the polarizability can be shown to be (Konigstein, 1972; Davydov, 1963; Placzek, 1934):

$$(\alpha_{\rho\sigma})_{mn} = \sum_e \left[\frac{\langle n|R_\rho|e\rangle\langle e|R_\sigma|m\rangle}{E_e - E_m - E_o} + \frac{\langle m|R_\sigma|e\rangle\langle e|R_\rho|n\rangle}{E_e - E_n + E_o} \right] . \qquad (13)$$

where the summation is over all of the vibronic states $|e\rangle$ of the molecule, R_σ and R_ρ are the dipole moment operators along σ and ρ. E_e, E_m and E_n are the energies of the states $|e\rangle$, $|m\rangle$ and $|n\rangle$ and E_o is the energy of the incident photon. The states of the molecule are specified using the Born-Oppenheimer approximation (Albrecht, 1961).

$$\Psi_g = \Theta_g(\xi,Q)\ \Phi_i^g(Q) = |g\rangle\ |i\rangle$$

$$\Psi_e = \Theta_e(\xi,Q)\ \Phi_v^e(Q) = |e\rangle\ |v\rangle$$

where $\Theta_g(\xi,Q)$ is the electronic wave function for the state $|g\rangle$ and is a function of the electronic coordinates, ξ, and nuclear coordinates Q. $\Phi_i^g(Q) = |i\rangle$ is the i'th vibrational state wave function of the ground electronic state and is a function of the nuclear coordinates. $|e\rangle$ is an excited electronic state and $|v\rangle$ is v'th vibrational state wave function of the excited electronic state $|e\rangle$.

Eq. (13) may be rewritten:

$$(\alpha_{\rho\sigma})_{gi,gj} = \sum_{ev} \left[\frac{\langle j\| (g|R_\rho|e)\| v\rangle\langle v\| (e|R_\sigma|g)\| i\rangle}{E_{ev} - E_{gi} - E_o} + \frac{\langle i\| (g|R_\sigma|e)\| v\rangle\langle v\| (e|R_\rho|g)\| j\rangle}{E_{ev} - E_{gj} + E_o} \right], \tag{15}$$

where each of the matrix elements $(g|R_\sigma|e)$ represent the electronic transition moment at a particular nuclear configuration Q, and $|j\rangle$ is a vibrational state function of the ground electronic state. Eq. (15) is an expression for the Raman tensor for the vibrational transition $i \to j$. For incident light of energy E_o the energy of the Raman scattered light is $E_o - (E_{gj} - E_{gi})$.

However, the Born-Oppenheimer stationary electronic states of the system are perturbed by vibrations of the nuclei. The perturbation operator is (Albrecht, 1961):

$$h_a = \left(\frac{\partial \mathcal{H}}{\partial Q_a}\right)^o \Delta Q_a \qquad (16)$$

where $\mathcal{H}$ is the electronic Hamiltonian, and ΔQ_a is the displacement of the normal mode, a. The superscript o indicates that the expression is evaluated at the equilibrium nuclear configuration. Using first order perturbation theory for the effect of vibrational motion on the Born-Oppenheimer excited state, $|e\rangle$ and ground state, $|g\rangle$:

$$|e) = |e^o) + \sum_a \sum_{s \neq e} \frac{(s^o|h_a|e^o)\ \Delta Q_a}{E_e^o - E_s^o}\ |s^o) \qquad (16a)$$

$$|g) = |g^o) + \sum_a \sum_{t \neq g} \frac{(t^o|h_a|g^o)\ \Delta Q_a}{E_g^o - E_t^o}\ |t^o)\ , \qquad (16b)$$

in which the summations are over all of the vibrational modes, a. The effect of the vibrational perturbation operator is to create a new basis set of wavefunctions which are linear combinations of the original Born-Oppenheimer states. The summation over electronic states is labeled by s in Eq. (16a) and labeled by t in Eq. (16b). The summations over s and t each span the entire basis set except for the diagonal components $\Big(|s) \neq |e)$ and $|t) \neq |g) \Big)$.

The superscript o indicates wave functions and energies evaluated at the equilibrium nuclear configuration in the ground electronic state (Albrecht, 1960).

Combining Eqs. (14) and (15) and assuming the wave functions are real yields to first order in Q_a (Tang and Albrecht, 1970):

$$(\alpha_{\rho\sigma})_{gi,gj} = A + B + C$$

$$A = \sum_{e\neq g} \sum_{v} \left[\frac{(g^o|R_\sigma|e^o)(e^o|R_\rho|g^o)}{E_{ev} - E_{gi} - E_o} + \frac{(g^o|R_\rho|e^o)(e^o|R_\sigma|g^o)}{E_{ev} - E_{gj} + E_o} \right] \langle i\| v\rangle\langle v\| j\rangle$$

$$B = \sum_{e\neq g}{}' \sum_{v} \sum_{s\neq e}{}' \sum_{a}$$

$$\times \left[\frac{(g^o|R_\sigma|e^o)(e^o|h_a|s^o)(s^o|R_\rho|g^o)}{E_{ev} - E_{gi} - E_o} + \frac{(g^o|R_\rho|e^o)(e^o|h_a|s^o)(s^o|R_\sigma|g^o)}{E_{ev} - E_{gj} + E_o} \right]$$

$$\times \langle i\| v\rangle\langle v\| Q_a\| j\rangle/(E_e^o - E_s^o)$$

$$+ \left[\frac{(g^o|R_\sigma|s^o)(s^o|h_a|e^o)(e^o|R_\rho|g^o)}{E_{ev} - E_{gi} - E_o} + \frac{(g^o|R_\rho|s^o)(s^o|h_a|e^o)(e^o|R_\sigma|g^o)}{E_{ev} - E_{gj} + E_o} \right]$$

$$\times \langle i\| Q_a\| v\rangle\langle v\| j\rangle/(E_e^o - E_s^o) \qquad (17)$$

$$C = \sum_{e\neq g}{}' \sum_{t\neq g}{}' \sum_{v} \sum_{a}$$

$$\times \left[\left\{ \frac{(g^o|h_a|t^o)(t^o|R_\sigma|e^o)(e^o|R_\rho|g^o)}{E_{ev} - E_{gi} - E_o} + \frac{(g^o|h_a|t^o)(t^o|R_\rho|e^o)(e^o|R_\sigma|g^o)}{E_{ev} - E_{gj} + E_o} \right\} \right.$$

$$\times \left. \frac{\langle i\| v\rangle\langle v\| Q_a\| j\rangle}{E_g^o - E_t^o} \right.$$

$$+\left\{\frac{(g^o|R_\sigma|e^o)(e^o|R_\rho|t^o)(t^o|h_a|g^o)}{E_{ev}-E_{gi}-E_o}+\frac{(g^o|R_\rho|e^o)(e^o|R_\sigma|t^o)(t^o|h_a|g^o)}{E_{ev}-E_{gj}+E_o}\right\}$$

$$\times\left.\frac{\langle i\|Q_a\|v\rangle\langle v\|j\rangle}{E_g^o-E_t^o}\right] \qquad (17)$$

where $|i\rangle$ indicates the initial vibrational state, $|j\rangle$ the final vibrational state and $|v\rangle$ labels the vibrational sublevels of the intermediate electronic state.

Equation (17) expresses one of the theoretical formulations for Raman intensity. It describes the intensity of Raman scattering when the energy of the incident photon is far from an electronic transition of the molecule (i.e., far from resonance).

A number of important features are evident from Eq. (16). Term A is responsible for Rayleigh scattering because of the Franck-Condon overlap factors $\sum_v \langle i|v\rangle\langle v|j\rangle = \delta_{ij}$. Thus, there are no allowed vibrational transitions. However, a further expansion of the A term may lead to Raman intensity (vide infra). Terms B and C give rise to Raman scattering via the vibrational terms

$$\sum_v \langle i|v\rangle\langle v|Q|j\rangle = \langle i|Q_a|j\rangle = \delta_{i,j\pm1}$$

Thus, the selection rule is $j = i \pm 1$.

The C term results from the mixing of the ground state with excited electronic states of the molecule. In general, the difference in energy between the ground state and any excited state is greater than the difference in energy between adjacent excited states. As a result, the ratio of Raman intensities of the C term to the B term is

$$\frac{I_C}{I_B} \cong \left(\frac{E_e^o - E_g^o}{E_t^o - E_g^o}\right)^2 << 1 .$$

Thus the C term is in general less important in Raman scattering than the B term (Albrecht, 1961) (see, however, Johnson and Peticolas, 1976a).

If E_o is far from an electronic transition, $E_{ev} - E_{gi} \approx E_{ev} - E_{gj} \approx E_e^o - E_g^o$ and by combining and rearranging terms, the B term in Eq. (17) simplifies to (Tang and Albrecht, 1970)

$$B' = - \sum_e \sum_{s \neq e} \sum_a \left[(g^o|R_\rho|e^o)(e^o|h_a|s^o)(s^o|R_\sigma|g^o) + (g^o|R_\sigma|e^o)(e^o|h_a|s^o)(s^o|R_\rho|g^o)\right] \times \frac{[(E_e^o - E_g^o)(E_s^o - E_g^o) + E_o^2] \langle i|Q_a|j\rangle}{[(E_e^o - E_g^o)^2 - E_o^2][(E_s^o - E_g^o)^2 - E_o^2]} \Bigg] . \quad (18)$$

The summation occurs twice over all of the excited states. However the diagonal component is excluded, $e \neq s$.

The diagonal components of the B term, $|e\rangle = |s\rangle$, result from an expansion of the energy denominator of the A term in Eq. (17) in a power series and the expansion of electronic integrals in terms of ΔQ_a (Tang and Albrecht, 1970). The final result for non-resonant Raman scattering is:

$$(\alpha_{\rho\sigma})_{gi,gj} = A + B''$$

$$A = \sum_{e \neq g}{}' \sum_v \left[\frac{(g^o|R_\sigma|e^o)(e^o|R_\rho|g^o)}{E_{ev} - E_{gi} - E_o} + \frac{(g^o|R_\rho|e^o)(e^o|R_\sigma|g^o)}{E_{ev} - E_{gj} + E_o} \right] \langle i|| v\rangle\langle v||j\rangle \quad (19)$$

$$B'' = -\sum_e \sum_s \sum_a [(g^o|R_\rho|e^o)(e^o|h_a|s^o)(s^o|R_\sigma|g^o) + (g^o|R_\sigma|e^o)(e^o|h_a|s^o)(s^o|R_\rho|g^o)] \times \frac{(E_e^o - E_g^o)(E_s^o - E_g^o) + E_o^2}{[(E_e^o - E_g^o)^2 - E_o^2][(E_s^o - E_g^o)^2 - E_o^2]} \langle i\|Q_a\|j\rangle \quad . \tag{19}$$

In general, the A term is, as in Eq. (17), responsible for Rayleigh scattering. The second term resembles the B term of Eq. (18), but now contains the diagonal part where $|s\rangle = |e\rangle$.

Selection Rules

For a vibration to show intensity in Raman spectroscopy the matrix elements $\langle g|R_\sigma|e\rangle$, $\langle e|h_a|s\rangle$ and $\langle s|R_\rho|g\rangle$ must not vanish. For a totally symmetric ground state with $\Gamma_{A_{1g}}$, for $\langle g|R_\sigma|e\rangle$ not to vanish $\Gamma_g \times \Gamma_{R_\sigma} \times \Gamma_e = \Gamma_{R_\sigma} \times \Gamma_e$ must contain $\Gamma_{A_{1g}}$ (Cotton, 1963). For a non-degenerate excited state $\Gamma_e = \Gamma_{R_\sigma}$. Therefore Γ_e must transform as does Γ_x, Γ_y, Γ_z under the point group of the molecule. Similarly the representation of $|s\rangle$ must be Γ_x, Γ_y, Γ_z. Therefore for $\langle e|h_a|s\rangle$ not to vanish $\Gamma_e \times \Gamma_s \times \Gamma_{h_a}$ must contain $\Gamma_{A_{1g}}$. Therefore Γ_{h_a} must transform as the product of coordinates x, y, z under the molecular point group (i.e., Γ_{x^2}, Γ_{y^2}, Γ_{z^2}, Γ_{xy}, Γ_{xz}, Γ_{yz}). The representation of the normal mode of the vibration is identical to the representation of h_a (Albrecht, 1961). Thus the symmetry representation of the normal mode must have the representation of the product of coordinates.

Raman intensity is also proportional to the transition moment of the electronic states. Thus the greater the oscillator strength of an electronic transition, the more it contributes to Raman intensity. There is also a selection of the nearest electronic transitions for mixing by the vibrational perturbation h_a, via the energy denominators $[(E_s - E_g)^2 - E_o^2]$ in Eq. (19).

A physical picture of Eq. (19) is shown in Fig. 4. Incident light of frequency ν_o drives the electron cloud of the molecule. The electronic transitions $\langle g|R_\sigma|e\rangle$, $\langle g|R_\rho|s\rangle$ of energies E_e and E_s are represented as tightly coiled springs (harmonic oscillators). When we are far from resonance each of the electronic transitions is being driven away from its characteristic frequency. As driven oscillators they radiate light of frequency ν_o. However, a nuclear vibration illustrated by a loosely coiled spring couples the two electronic oscillators causing a modulation in the frequency of oscillation and Raman scattered light of $h\nu_o \pm E_v$ is radiated. The coupling of the oscillators in Fig. 4 bears an analogy to the mixing of the adiabatic wave functions by the vibrational perturbation in Eq. (19).

Resonance Raman Theory

As the energy of the incident photons approach an electronic transition, the denominator in Eq. (19) becomes smaller and Eq. (19) predicts an increase of Raman and Rayleigh scattering. However, Eq. (19) predicts that the intensity will increase without limit when the resonance condition exists. This is neither physically reasonable

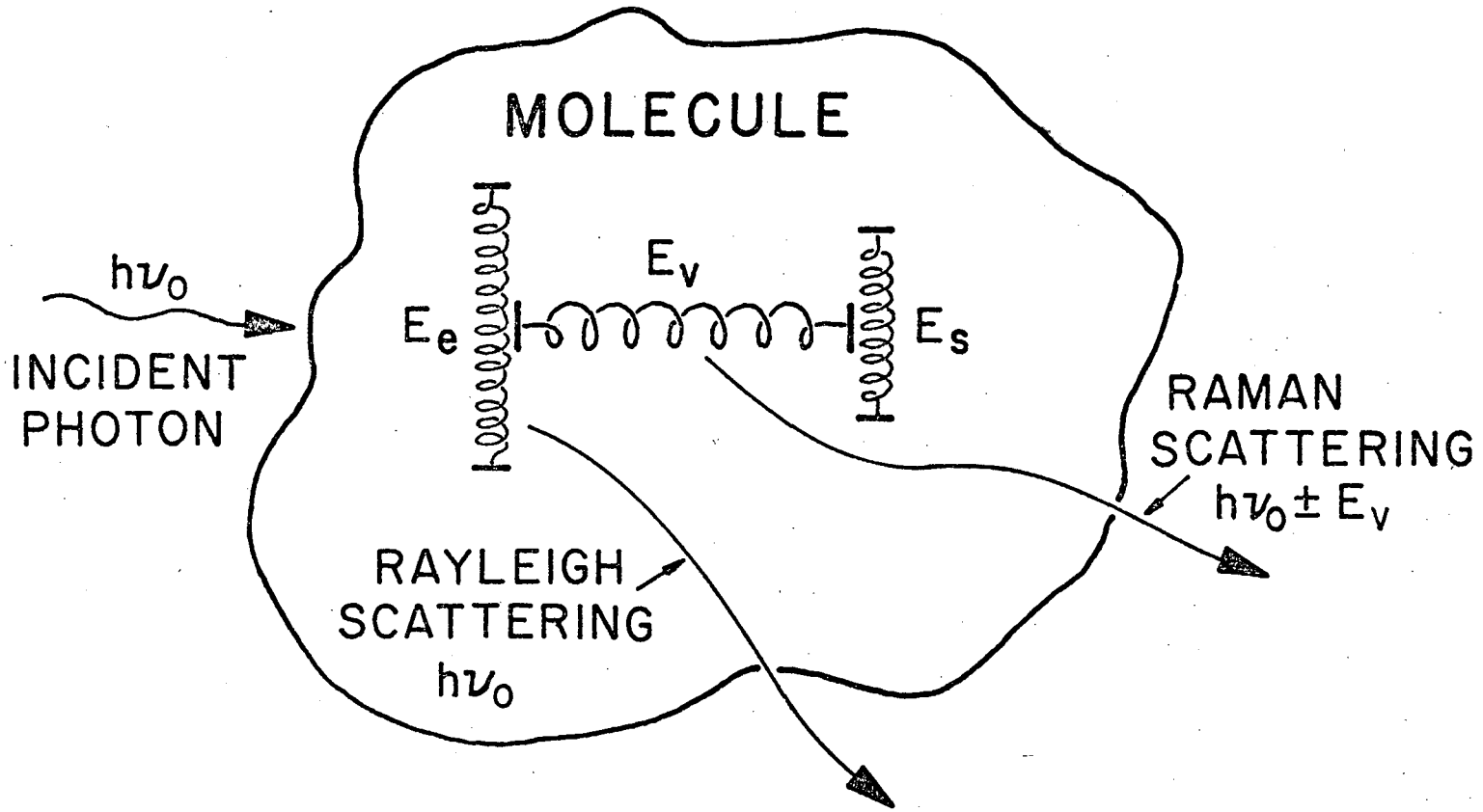

Fig. II-4. Physical picture of the vibrational mixing between electronic states.

XBL 768-9543

nor experimentally observed (Behringer, 1967). This failure of Raman theory in the resonance case results from the inability of perturbation theory to deal with such large perturbations (Konigstein, 1972).

This dilemma is resolved phenomenologically by the addition of a damping correction, $i\Gamma$, to the energy denominators in Eq. (19). The result is (Albrecht and Hutley, 1971):

$$(\alpha_{\rho\sigma})_{gi,gj} = A'' + B'''$$

$$A'' = \sum_{v} \frac{(g^o|R_\rho|e^o)(e^o|R_\sigma|g^o)}{E_e^o - E_g^o - E_o^o + i\Gamma} \langle i|v\rangle\langle v|j\rangle$$

$$B''' = -\sum_{s}\sum_{a} [(g^o|R_\rho|e^o)(e^o|h_a|s^o)(s^o|R_\sigma|g^o) \qquad (20)$$

$$+ (g^o|R_\sigma|e^o)(e^o|h_a|s^o)(s^o|R_\rho|g^o)]$$

$$\times \frac{(E_e^o - E_g^o)(E_s^o - E_g^o) + E_o^2 \cdot}{[(E_e^o - E_g^o)^2 - E_o^2 + i\Gamma][(E_s^o - E_g^o)^2 - E_o^2]} \langle i|Q_a|j\rangle$$

The physical interpretation of the damping constant, $i\Gamma$ in the denominator is at present not well understood. However, it has been proposed to be associated with the lifetime of the resonant excited state (Konigstein, 1972; Adar et al., 1976). One of the simplifications in Eq. (20) over (19) is in the neglect of the second term of the A term, where the energy of the incident photon is added in the denominator. The second term must be much smaller than the first term when $E_e^o - E_g^o = E_o^o$. The second simplification occurs by the removal of the summation over e, because the resonant condition results in the selection of one particular excited state $|e\rangle$.

For an electronic transition that is localized in a molecule, the vibrationally induced mixing enhances vibrations that couple (see Fig. 4) the resonant electronic transition with other electronic transitions. This leads to a selectivity of resonance enhanced vibrations. For example, in the resonance Raman spectra of hemoglobin excited in the visible electronic transitions of the heme, only the porphyrin macrocycle modes are enhanced. The electronic transitions of the protein are sufficiently removed both in energy and spatially that they do not appear in the spectrum (Spiro, 1975). The vibrations of peripheral aliphatic substituents around the porphyrin ring are spatially isolated from the resonant $\pi \rightarrow \pi^*$ electronic transition. Thus, they do not appear with any intensity. However, a vinyl substituent on the ring has an electronic transition sufficiently close spatially that the vibration of the substituent successfully mixes the electronic transitions of the vinyl group and the porphyrin macrocycle, analogously to the vibration in Fig. 4.

Another mechanism for Raman intensity is via the first term in Eq. (20). In general $\sum_v \langle i|v\rangle \langle v|j\rangle = \delta_{ij}$. However, if a displacement occurs in the internuclear distances for the excited state versus the ground state, the vibrational wave functions for the excited state are solutions to a Hamiltonian different from the Hamiltonian of the ground state. Thus, the vibrational wave functions in the excited state are not orthonormal to the vibrational wave functions of the ground state and $\sum_v \langle i|v\rangle \langle v|j\rangle \neq \delta_{ij}$. Thus the first term of Eq. (20) may also be

responsible for Raman intensity. Additionally, overtones and combination bands may derive intensity from the first term of Eq. (20) because there are no formal selection rules for the Franck-Condon overlap factors.

The enhancement shown in Raman scattering by resonance excitation can be very large. For example, β carotene shows a resonance enhancement of ~ 10^6 (Behringer, 1967). Thus, the Raman spectrum of β carotene has been observed to concentrations as low as 10^{-7}M. Resonance enhancement for other molecules is smaller, in general. However, resonance Raman spectra of porphyrins are typically observed in 10^{-5}M solutions (Spiro, 1975). The intensities of the porphyrin vibrations are comparable to the intensities of the solvent, though the porphyrins are ~ 10^{-6} of the concentration of the solvent.

Resonance Raman theory is presently in a developmental stage. A large number of workers are studying the theory and presenting various formulations (Peticolas, et al., 1970; Mingardi and Siebrand, 1975; Garrozzo and Galluzzi, 1976; Johnson et al., 1976). The formulation used in this thesis contains the basic elements found in all of the other formulations of Raman theory. However, other formulations include additional terms in the polarizability expression which result from inclusion of the nuclear kinetic energy operator (non-adiabatic coupling) (Mingardi and Siebrand, 1975). Although the resulting expressions for Raman intensity may be quantitatively more correct, they make the equations much more complicated and make a physical interpretation of the Raman expressions more difficult.

Since it is not clear at this point which formulation gives the most useful expression for Raman intensity, the simplest and most concise formulation was chosen.

References

Adar, F, Gouterman, M., and Aronwitz, S., J. Phys. Chem., in press (1976).

Albrecht, A.C., J. Chem. Phys. 33, 156 (1960).

Albrecht, A.C., J. Chem. Phys. 34, 1476 (1961).

Albrecht, A.C., and Hutley, M.C., J. Chem. Phys. 55, 4438 (1971).

Behringer, J., Raman Spectroscopy Vol. I, Ed. H.A. Szymanski, Plenum Press, N.Y. (1967).

Chantry, G.W., The Raman Effect Vol. I, Ed. A. Anderson, M. Dekker, Inc., N.Y. (1971).

Cotton, F.A., Chemical Applications of Group Theory, Wiley, N.Y. (1963).

Davydov, A.S., Quantum Mechanics, N.E.D. Press, Ann Arbor, Mich. (1963).

Dushman, S., The Elements of Quantum Mechanics, Wiley, N.Y. (1938).

Garrozzo, M. and Galluzzi, F., J. Chem. Phys., in press (1976).

Johnson, B.B. and Peticolas, W.L., Ann. Rev. Phys. Chem. 27 (in press) (1976a).

Johnson, B.B., Nafie, L.A., and Peticolas, W.L., Chem. Phys. (in press) (1976b).

Konigstein, J.A., Introduction to the Theory of the Raman Effect, Reidal Publishing Co., Dordrecht-Holland (1972).

Krishnan, R.S., The Raman Effect Vol. I, Ed. A. Anderson, Dekker, Inc., N.Y. (1971).

McClain, W.M., J. Chem. Phys. 55, 2789 (1971).

Mingardi, M. and Siebrand, W., J. Chem. Phys. 62, 1074 (1974).

Nestor, J. and Spiro, T.G., J. Raman Spectrosc. 1, 539 (1973).

Peticolas, W.L., Nafie, L., Stein, P., and Fanconi, B., J. Chem. Phys. 52, 1576 (1970).

Placzek, G., Rayleigh and Raman Scattering, UCRL Trans. No. 526L from Handbuch der Radiologie, ed. E. Marz, Leipzig, Akademische Verlagsgesellschaft VI, 209-374 (1934). Available from Natl. Tech. Info. SRVC., U.S. Dept. of Commerce, Springfield, VA.

Spiro, T.G. and Strekas, T.C., Proc. Natl. Acad. Sci. USA 69, 2622 (1972).

Spiro, T.G., Biochem. Biophys. Acta 416, 169 (1975).

Sushchinskii, M.M., Raman Spectra of Molecules and Crystals, Israel Program for Scientific translations, N.Y. (1972).

Tang, J. and Albrecht, A.C. in Raman Spectroscopy Vol. II, ed. H.A. Szymanski (Plenum Press, N.Y.) (1970).

Wilson, E.G., Decius, J.C., and Cross, P.C., Molecular Vibrations, McGraw-Hill, N.Y. (1955).

CHAPTER III

ELECTRONIC STRUCTURE OF PORPHYRINS

Introduction

The basic porphyrin skeleton consists of four pyrrole groups linked together by methine bridges into a single, planar conjugated ring. The simplest porphyrin, porphin (Fig. 1) is substituted about the ring and methine carbons with H atoms. Figure 1 shows the structure of the free-base form of porphin in which two of the pyrrole nitrogens are protonated. The protons are on opposite sides of the ring, giving the ring D_{2h} symmetry (Gouterman, 1961; Gurinovich, et al., 1963; Platt, 1956). The axes of the ring are labeled with the x axis through the pyrrole nitrogens containing the free-base protons.

A variety of peripheral substituents are found in naturally occuring porphyrins, such as heme and chlorophyll (Gurinovich, 1963). A much larger variety of substituents is possible for synthetic porphyrins. Figure 1 illustrates the labeling scheme for the porphyrin skeleton (Falk, 1964) and Table I lists the structures for the porphyrins which will be discussed in this thesis. In addition to peripheral substituents, a variety of metals can be complexed into the center of the porphyrin. The metal may bind additional ligands arranged perpendicular to the porphyrin plane (axial ligands).

The porphyrin is an aromatic, highly conjugated molecule containing eleven double bonds. However, two of the double bonds in the porphyrin are not well conjugated into the macrocyclic ring system and are called "semi-isolated" double bonds (Gurinovich, 1963; Simpson, 1949). Thus, there are 18 π electrons in the conjugated macrocycle, which satisfies

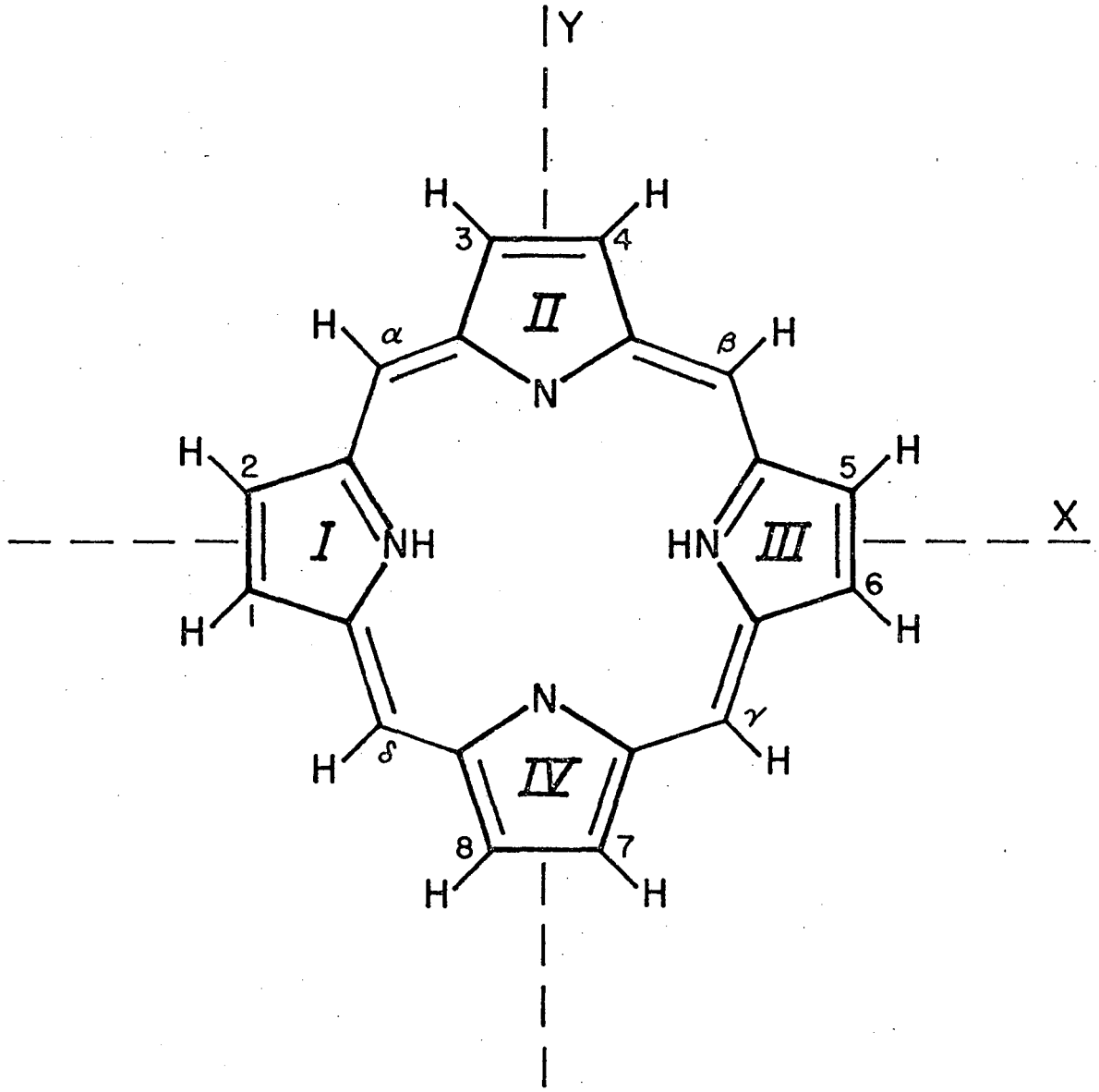

XBL 769-9645

Fig. III-1. Structure of porphin showing the numbering scheme for the atoms and rings.

Table I. Structure of Porphyrins.

(Substituent position labels are defined in Fig. 1.)

Substituent Position	α	β	γ	δ	1	2	3	4	5	6	7	8
Etioporphyrin I	H	H	H	H	M	E	M	E	M	E	M	E
Tetraphenyl Porphin	ϕ	ϕ	ϕ	ϕ	H	H	H	H	H	H	H	H
Protoporphyrin IX	H	H	H	H	M	V	M	V	M	P	P	M

side-chain abbreviations: H, hydrogen; ϕ, phenyl;

V, vinyl; M, methyl; P, $-CH_2CH_2COOH$; E, ethyl.

the 4n + 2 rule for aromaticity.

Absorption Spectra

The absorption spectra of free-base porphyrins show four weak bands in the visible and a very intense absorption band in the near UV called the Soret band. Although some variations occur both in the energies and in the relative intensities of the absorption bands, the spectra of all of the free-base porphyrins are qualitatively similar.

A simplification occurs in the absorption spectrum of the dianion, dication and for many metal complexes of free-base porphyrins (Gouterman, 1961, 1959; Gurinovich, et al., 1963, 1968; Caughey, et al., 1965). Upon metallation or production of the dianion or dication, the symmetry of the porphyrin ring changes from D_{2h} to D_{4h} symmetry and the absorption spectrum shows two weak bands called α and β in the visible and a narrower Soret band in the UV. The 4 absorption bands in the visible spectral region of the free base, some of which appear to result from the inequivalency of the x and y direction (induced by the free-base protons), merge into 2 bands that result from doubly degenerate transitions (Gurinovich, et al., 1963, 1968; Platt, 1956).

Electron-in-a-Ring Model

A simple free electron model which treats the porphyrin π electrons as if they are free to circulate in a ring (Simpson, 1949) explains the absorption spectra of porphyrins surprisingly well. The approach concentrates on the 18 π electrons of the porphyrin macrocycle which are confined to the ring. Figure 2 shows the energy level diagram and the orbital occupancy for the electronic orbitals of an electron-in-a-ring system containing 18 electrons. The energy levels are labeled by their angular momentum, l.

the 4n + 2 rule for aromaticity.

Absorption Spectra

The absorption spectra of free-base porphyrins show four weak bands in the visible and a very intense absorption band in the near UV called the Soret band. Although some variations occur both in the energies and in the relative intensities of the absorption bands, the spectra of all of the free-base porphyrins are qualitatively similar.

A simplification occurs in the absorption spectrum of the dianion, dication and for many metal complexes of free-base porphyrins (Gouterman, 1961, 1959; Gurinovich, et al., 1963, 1968; Caughey, et al., 1965). Upon metallation or production of the dianion or dication, the symmetry of the porphyrin ring changes from D_{2h} to D_{4h} symmetry and the absorption spectrum shows two weak bands called α and β in the visible and a narrower Soret band in the UV. The 4 absorption bands in the visible spectral region of the free base, some of which appear to result from the inequivalency of the x and y direction (induced by the free-base protons), merge into 2 bands that result from doubly degenerate transitions (Gurinovich, et al., 1963, 1968; Platt, 1956).

Electron-in-a-Ring Model

A simple free electron model which treats the porphyrin π electrons as if they are free to circulate in a ring (Simpson, 1949) explains the absorption spectra of porphyrins surprisingly well. The approach concentrates on the 18 π electrons of the porphyrin macrocycle which are confined to the ring. Figure 2 shows the energy level diagram and the orbital occupancy for the electronic orbitals of an electron-in-a-ring system containing 18 electrons. The energy levels are labeled by their angular momentum, l.

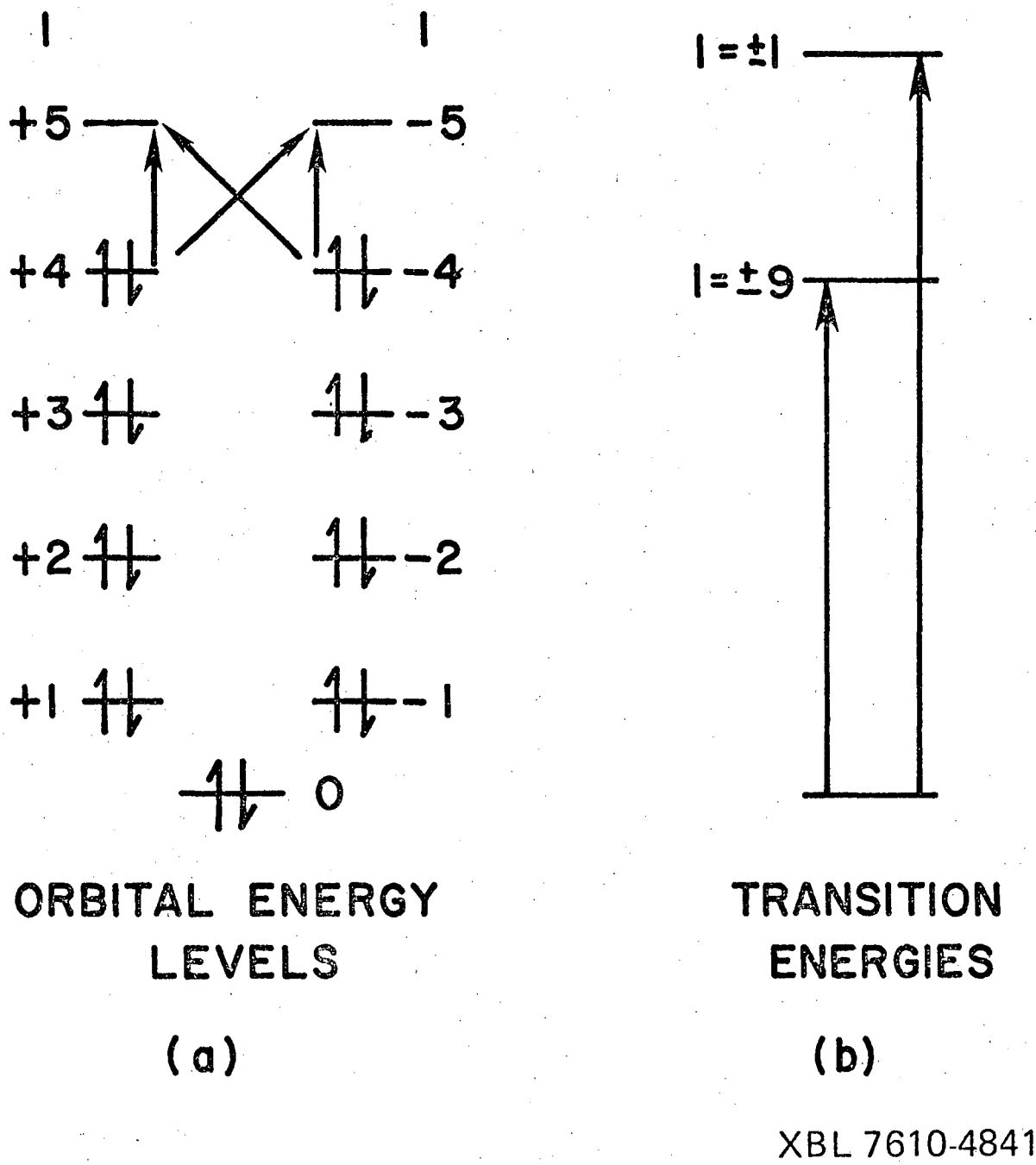

XBL 7610-4841

Fig. III-2. a) Energy levels and electron populations for the electron-in-a-ring model of porphyrins.

b) Electronic transitions for the electron-in-a-ring model.

There are two sets of doubly degenerate electronic transitions possible from the two highest occupied degenerate orbitals, where $1 = \pm 4$ to the two lowest unoccupied orbitals which have $1 = \pm 5$. As Fig. 2b indicates, these transitions correspond to changes in angular momentum of ± 9 and ± 1. Hund's rule indicates that, for a given multiplicity, the lowest energy states have the greatest angular momentum. Thus, the transition with $1 = \pm 9$ is placed lower in energy than the transition with $1 = \pm 1$. The model predicts a two banded absorption spectrum for porphyrins with a very intense allowed electronic transition at higher energy than a forbidden electronic transition.

Four Orbital Model

The visible and near UV spectra of porphyrins can be interpreted more quantitatively using the 4-orbital model proposed by Gouterman (Gouterman, 1961, 1973). This model proposes that the electronic transitions that give rise to the characteristic spectra of metal porphyrins [α, β (Q bands) and Soret (B band)] result from excitation from the two highest filled orbitals of a_{1u} and a_{2u} symmetry under the D_{4h} point group to the lowest empty orbitals of e_g symmetry (Fig. 3). The two highest occupied orbitals are nearly degenerate in energy. Thus, the two doubly degenerate excited states that result are of identical symmetry and are nearly degenerate in energy. Consequently, they are mixed by configuration interaction to give two new doubly degenerate states resulting from addition or subtraction of the transition dipoles. This leads to a very intense absorption band at high energy, the Soret band, and a less intense band at lower energy,

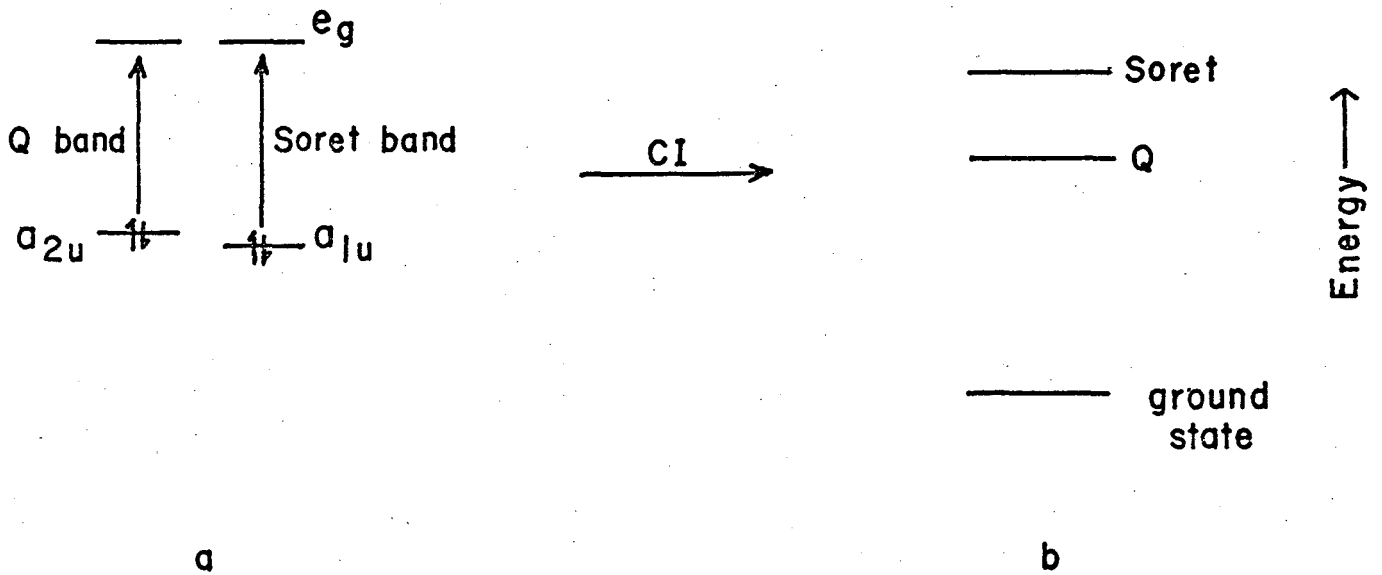

XBL 753-5114B

Fig. III-3. Four orbital model for the electronic transitions of metalloporphyrins.
a) orbital transitions.
b) electronic states after configuration interaction.

the α band (Gouterman, 1961, 1973). In addition, the 0-1 vibronic overtone (β band) is also active and appears as an additional peak on the high energy side of the 0-0 transition (α band).

The visible and UV spectra of most metalloporphyrins and of the dianion and dication of the free-base porphyrins are remarkably similar (Gouterman, 1959; Weiss, et al., 1965; Gurinovich, et al., 1968), indicating little metal porphyrin interaction. Substitution of a wide variety of metals such as Zn, Co, Cu, Ni, Pd, Ag, Mg and V (Caughey, et al., 1965) results in relatively small changes in the absorption spectrum. However, a few metalloporphyrins such as Fe^{3+} and Mn^{3+} porphyrins, for example, show a much more complicated absorption spectrum (Gouterman, 1973).

Through an extended Hückel calculation Gouterman and his coworkers (Zerner and Gouterman, 1966) have shown that the energies of the porphyrin π orbitals and the metal d orbitals are sufficiently different for most metalloporphyrins that little mixing occurs.

MCD Spectra of Porphyrins

Introduction to MCD

Magnetic Circular Dichroism (MCD) measures the difference between the absorption of left (lcp) and right (rcp) circularly polarized light ($\Delta A = A_{lcp} - A_{rcp}$) induced by a magnetic field (McCaffery, 1971; Schatz and McCaffery, 1969; Sutherland, 1976; Dratz, 1966). The effect of the magnetic field is to split degenerate electronic states into their non-degenerate Zeeman levels which differ in energy by $\Delta E = 2\ \beta\ H\ M_z$, where ΔE is the energy splitting.

β is the Bohr magneton, H is the intensity of the magnetic field and M_z is the z component of the angular momentum of the excited state, where the z direction is along the magnetic field. Another effect of the magnetic field is to induce mixing between the initial stationary states of the molecule. The preparation of new states from degeneracy-splitting and the mixing of states induced by the magnetic field results in new electronic transitions which preferentially absorb right or left circularly polarized light. Three types of line shapes may be observed in MCD spectroscopy. These are designated A, B and C terms. The terminology A, B and C derives from the quantum mechanical formulation of MCD which results in three different possible interactions between the molecule and the magnetic field (Stephens, et al., 1966).

The A term results from degeneracies in the ground or excited state. For a molecule in a magnetic field the degeneracy is split into its Zeeman components. Circularly polarized light has an associated angular momentum (McCaffery, 1971), with rcp and lcp having angular momenta of $M_z = -1$ and $M_z = +1$, respectively. Figure 4a shows an energy level diagram for a molecule with a non-degenerate ground state and a doubly degenerate excited state. When the magnetic field along the z direction is turned on, the degeneracy is split into two non-degenerate Zeeman levels with $M_z = \pm 1$. Since angular momentum must be conserved, transitions to $M_z = +1$ and $M_z = -1$ are allowed only for lcp and rcp, respectively.

Figure 4b shows the absorption spectrum of a molecule in the absence of a magnetic field. When the field is turned on, the absorption spectra for rcp and lcp are shifted oppositely in energy, but symmetrically with respect to the maximum of the absorption spectrum in the absence of the field. The resultant MCD spectrum appears with the shape of the derivative of the absorption band.

The C term (Fig. 5) results from degeneracies in the ground state. The degeneracy is lifted by the magnetic field and transitions are allowed from $M_z = +1$ and $M_z = -1$ to the non-degenerate excited state by lcp and rcp, respectively. However, the population of the $M_z = +1$ and $M_z = -1$ states is governed by a Boltzmann distribution. Thus, $A_{rcp} \neq A_{lcp}$ and the C term has a shape similar to the absorption spectrum. The intensity of the C term is inversely proportional to the absolute temperature.

The Faraday B term results from the mixing of states by the magnetic field and has the shape of the absorption band. For electronic transitions in which neither the ground nor excited state is degenerate, the B term is the only contribution to the MCD spectrum. Neither the A nor the B term has any temperature dependence other than the usual changes in absorption lineshape.

MCD Spectra of Porphyrins

The MCD spectra of free-base porphyrins show MCD B terms (Sutherland, 1976; Gale, et al., 1972) for the visible absorption bands, indicating that the electronic transitions responsible for the absorption bands do not involve degenerate electronic states. The

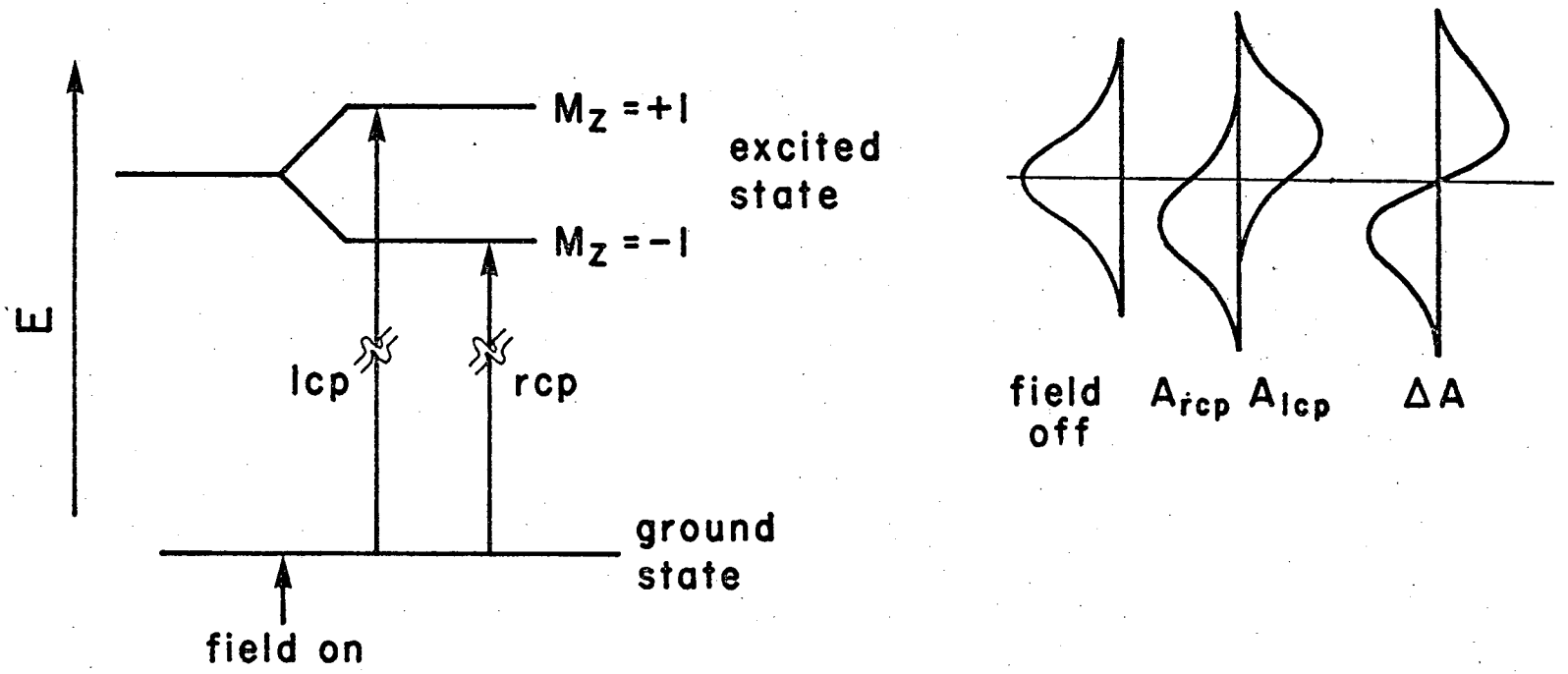

XBL 760-9638

Fig. III-4. a) Effect of a magnetic field on a degenerate excited state and the selection rules for lcp and rcp.
b) Resultant MCD A term.

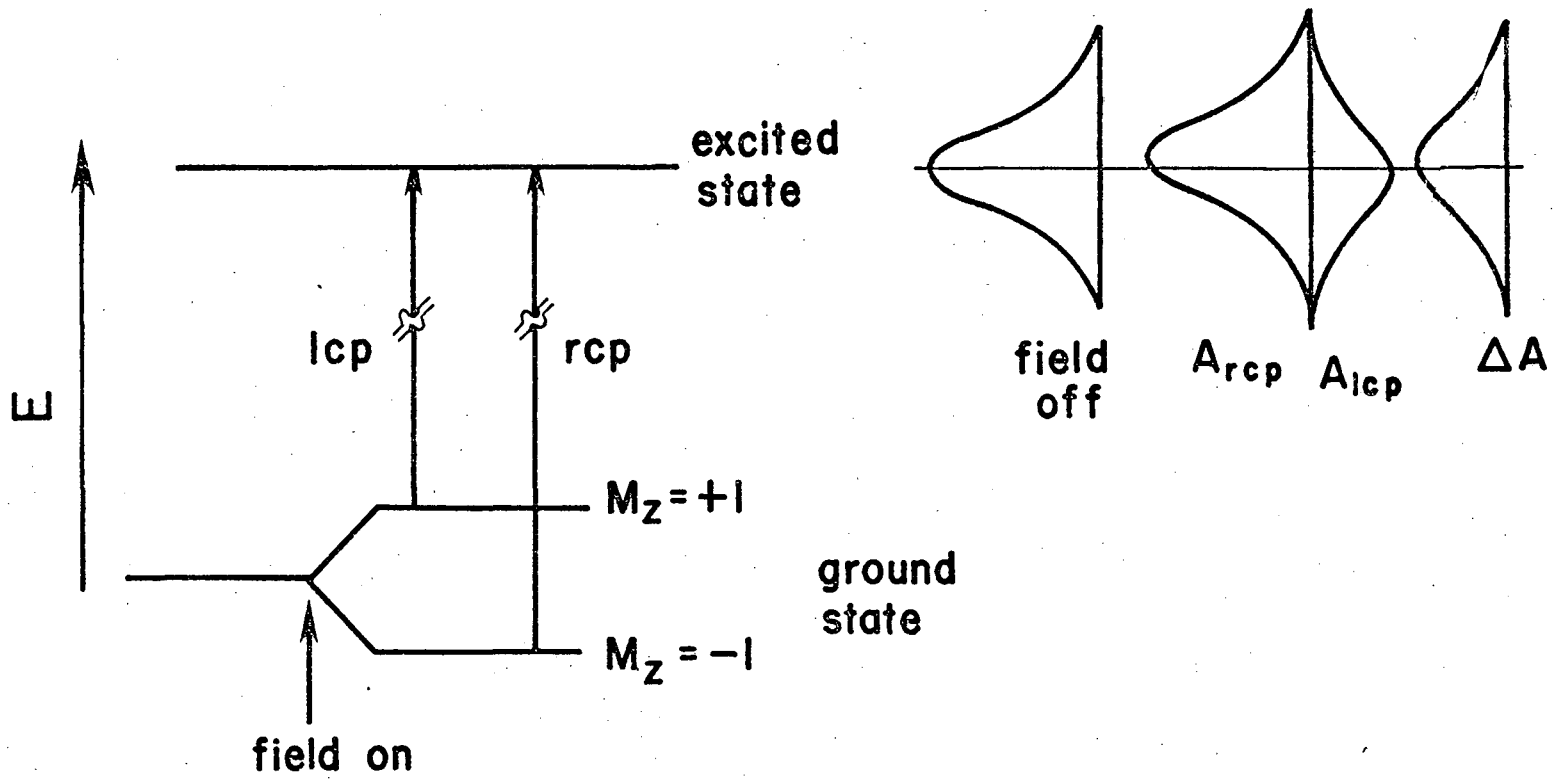

XBL 769-9579

Fig. III-5. a) Effect of a magnetic field on a degenerate ground state and the selection rules for lcp and rcp.
b) Resultant MCD C term.

splitting of the Soret band is not visible in the absorption spectrum and the Soret band has a derivative shape in the MCD spectrum. Upon metallation the porphyrin electronic transitions become degenerate and the α and β bands show intense A terms. Comparison of the MCD and absorption spectra by moment analysis (Schatz and McCaffery, 1969; Stephens, 1970) or curve fitting (Dratz, 1966) yields values of the excited state angular momentum. The value of M_z calculated for the α band of Zn deuteroporphyrin is 6.5, while M_z for the Soret band is 0.82. These values of M_z are close to the values of 9 and 1 predicted by the electron-in-a-ring model. The β band, which has been assigned to the 0-1 vibronic overtone of the α band often shows structure in the MCD spectrum, especially at low temperatures (Sutherland, 1976; Gale, et al., 1972; Linder, et al., 1974) and vibronic components which are not resolved in the absorption spectrum may be resolved in the MCD spectrum.

Hyperporphyrins

A class of metalloporphyrins occur, called "hyperporphyrins" by Gouterman (Gouterman, 1973), show a more complicated absorption spectrum. Two examples of hyperporphyrins are Fe^{3+} porphyrins and Mn^{3+} porphyrins. It appears for Fe^{3+} and much more dramatically for Mn^{3+} that the energies of the d orbitals and the porphyrin π orbitals are sufficiently close for large interactions to occur between the e_g^* (π) orbitals of the porphyrin and the e_g (d_{xz}, d_{yz}) orbitals of the metal, perturbing the classic metalloporphyrin spectrum (Boucher, 1970, 1972).

Manganese (III) porphyrins exhibit a wealth of absorption bands in the near IR, visible and near UV region. The simple 4-orbital model breaks down for Mn (III) porphyrins. Boucher proposed that the additional bands that appear in the absorption spectrum of Mn (III) porphyrins result from charge transfer transitions in which an electron is promoted from a filled porphyrin π orbital to an unfilled orbital of the metal (Boucher, 1970; Zerner and Gouterman, 1966).

The absorption spectra of Fe^{3+} porphyrins seem to lie somewhere intermediate between the spectra of the Mn^{3+} porphyrins and the other metal porphyrins (Boucher, 1972). The ferric porphyrins show absorption bands in the near IR which may be charge transfer bands (Smith and Williams, 1969). In addition, other bands sometimes appear in the visible region. Ferricytochrome c shows an absorption band at 695 nm, for example. It is possible that this band is a charge transfer transition from the porphyrin to the metal (Smith and Williams, 1969). Thus, it appears that there is more interaction between the porphyrin and the metal in Fe^{3+} porphyrins than in the typical metal porphyrin complex.

Absorption and MCD Spectra of Mn (III) Etioporphyrin I

Figure 6 shows the structure of manganese (III) etioporphyrin I (MnETP), indicating that the porphyrin macrocycle is substituted with ethyl and methyl groups about the ring. The metal is coordinately unsaturated and may bind additional ligands. In coordinating solvents such as alcohols the fifth and sixth ligand positions on the manganese are replaced by the solvent (Boucher, 1972). Thus, the absorption

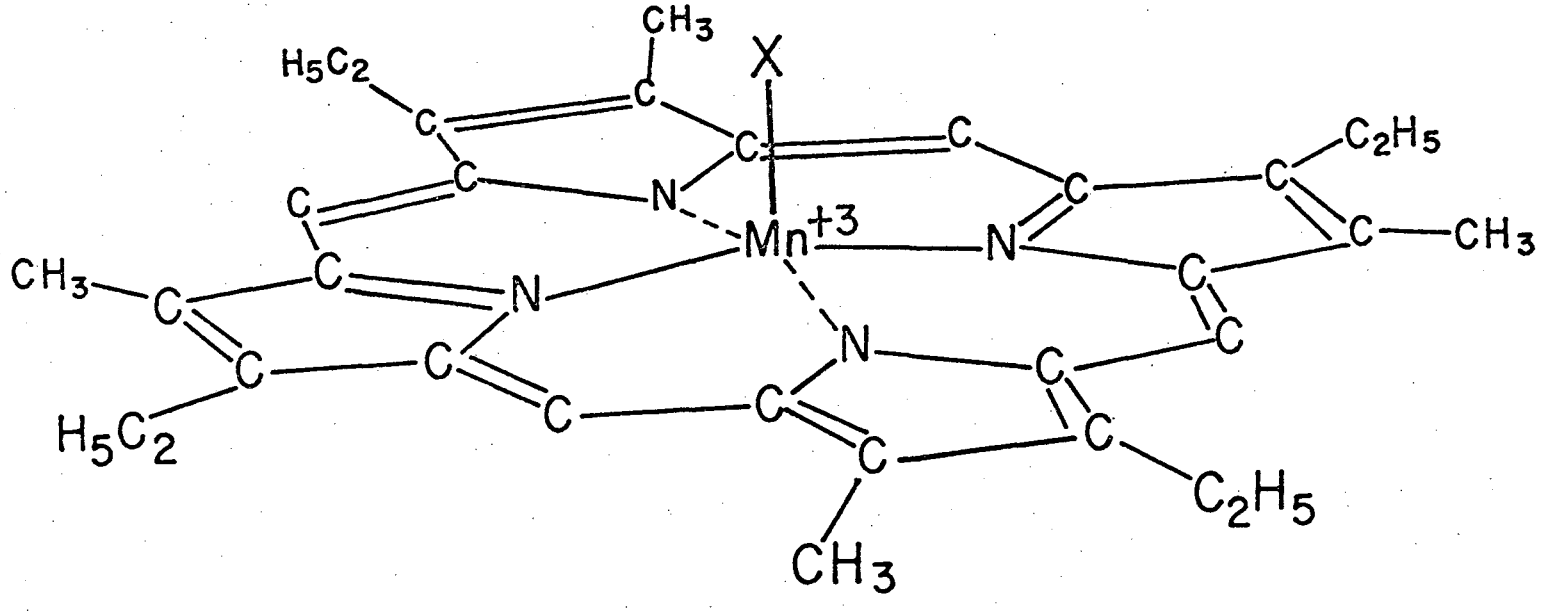

XBL 769 - 9578

Fig. III-6. Structure of Mn (III) Etioporphyrin I.

spectra of different axial complexes of MnETP appear to be identical in coordinating solvents. However, the absorption spectra of different axial complexes of MnETP are well differentiated in poorly coordinating solvents such as benzene, CS_2, $CHCl_3$, etc.

The manganese ion is d^4, high-spin in Mn (III) porphyrins. There are no reports of any low spin complexes of Mn (III) porphyrins (Boucher, 1972). Figure 7 shows a qualitative molecular orbital model for the ground state of Mn (III) porphyrins (Boucher, 1972). The four lowest d orbitals are singly occupied, with the $d_{x^2 - y^2}$ orbital highest in energy and unoccupied.

The UV and visible absorption spectra of the F^-, Cl^-, Br^- and I^- complexes of MnETP are shown in Fig. 8 and are tabulated in Table II. The molar absorptivities of MnETP in n-butanol were determined by dissolving a carefully weighed amount of MnETP in n-butanol, measuring the absorption spectrum and calculating the molar absorptivities using Beers' Law. The other molar absorptivities in Table II were determined with reference to the molar absorptivities of MnETP in n-butanol. The molar absorptivities for MnETP-X (X = F^-, Cl^-, Br^-, I^-) in $CHCl_3$ were determined by preparing concentrated stock solutions of each of the complexes in $CHCl_3$. Ten µl aliquots of the stock solutions were added to a cuvette containing 2.3 ml $CHCl_3$ and to a cuvette containing 2.3 ml of n-butanol. The concentrations of the stock solutions and the molar absorptivities for each of the halide complexes were determined from the previously calculated molar absorptivities of MnETP n-butanol.

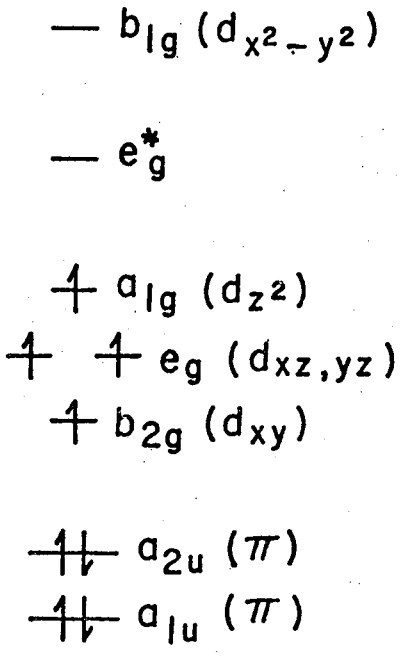

Fig. III-7. Molecular orbital model for the ground state of Mn (III) porphyrins.

Table II. Absorption Spectral Values of MnETP-X (X=F, Cl, Br, I) in $CHCl_3$ (freshly distilled from P_2O_5), n-butanol and in MCP.

Band	III		IV		V				V_a	VI				
Halide or Solvent	λ_{max}	ϵ_{max}	λ_{max}	ϵ_{max}	λ_{max}	ϵ_{max}	$\Delta\nu_{1/2}$	Area	λ_{max}	λ_{max}	ϵ_{max}	$\Delta\nu_{1/2}$	Area	R
F	584	7.53×10^3	551	1.04×10^4	450	7.92×10^4	900	0.71		350	6.08×10^4	3800	2.31	1.30
Cl	592	5.66×10^3	560	1.12×10^4	474	5.25×10^4	760	0.40	428	357	7.32×10^4	3100	2.27	0.72
Br			562		479		790		432	361		2390		0.46
I			570	9.0×10^3	493	2.73×10^4	1070	0.29		369	9.71×10^4	2300	2.23	0.28
n-butanol	576	6.35×10^3	543	9.1×10^3	457	5.75×10^4	780	0.49	413	365	6.80×10^4	3300	2.24	0.85
MCP (RT)	580		550	8.74×10^3	457	4.61×10^4	1050	0.48	415	362	6.4×10^4	3450	2.21	0.72
MCP (122°K)	574	7.62×10^3	542	1.01×10^4	456	9.33×10^4	582	0.54	411	365	8.45×10^4	2820	2.41	1.10

λ_{max} = peak maximum (nm), ϵ_{max} = molar absorptivity $\left(\frac{\text{liter}}{\text{mole-cm.}}\right)$,

$\Delta\nu_{1/2}$ = full width at half height (cm^{-1}), Area = $\frac{\epsilon_{max}\cdot\Delta\nu_{1/2}}{10^8}\left(\frac{\text{liter}}{\text{mole-cm}^2}\right)$

$R = \frac{\epsilon_{max}(\text{band V})}{\epsilon_{max}(\text{bandVI})}$, MCP = solution of 20% n-butanol, 60% methyl cyclohexane, and 20% 2-methylpentane (by volume).

The absorption bands in Fig. 8 are labeled using a numbering scheme introduced by Boucher (Boucher, 1972). Bands I and II appear at about 780 and 680 nm, respectively, with molar absorptivities of about 10^3 (Boucher, 1972). Bands III and IV appear between 550 - 600 nm. Band V appears between 450 - 500 nm while band VI appears between 350 - 370 nm. Boucher proposed that the additional bands that appear in the absorption spectrum of Mn (III) porphyrins, especially band V, result from charge transfer transitions. These occur when an electron is promoted from a filled porphyrin orbital to an unfilled orbital of the metal, or vice versa (Boucher, 1972; Zerner and Gouterman, 1966). Boucher has assigned the near IR absorption bands of Mn (III) porphyrins to d → d and/or charge transfer transitions. The visible bands III and IV were assigned to charge transfer and/or Q transitions. Band V was assigned to a charge transfer transition from an a_{1u}, a_{2u} occupied π orbital to the d_{xz}, d_{yz} orbitals of the metal, and band Va was assigned to a charge transfer transition from an inner occupied porphyrin π orbital to the d_{z^2} orbital of the metal. Band VI was assigned to an admixture of the Soret band and a charge transfer transition from an inner π orbital to the d_{xz}, d_{yz} orbitals of the metal.

The spectra in Fig. 8 display a number of interesting features. As the axial halide varies from F^- through I^- the absorption bands broaden and the molar absorptivities decrease until band III is no longer resolved in the I^- complex. However, the low temperature MCD spectrum (T = 193°) of Mn ETP-I^- in CS_2 resolves band III as an additional component underlying the low energy shoulder of band IV. As Table II indicates, the decrease in the molar absorptivity of band IV is only about 10% through the halide series, while the band maxima shift by 600 cm^{-1} to the red.

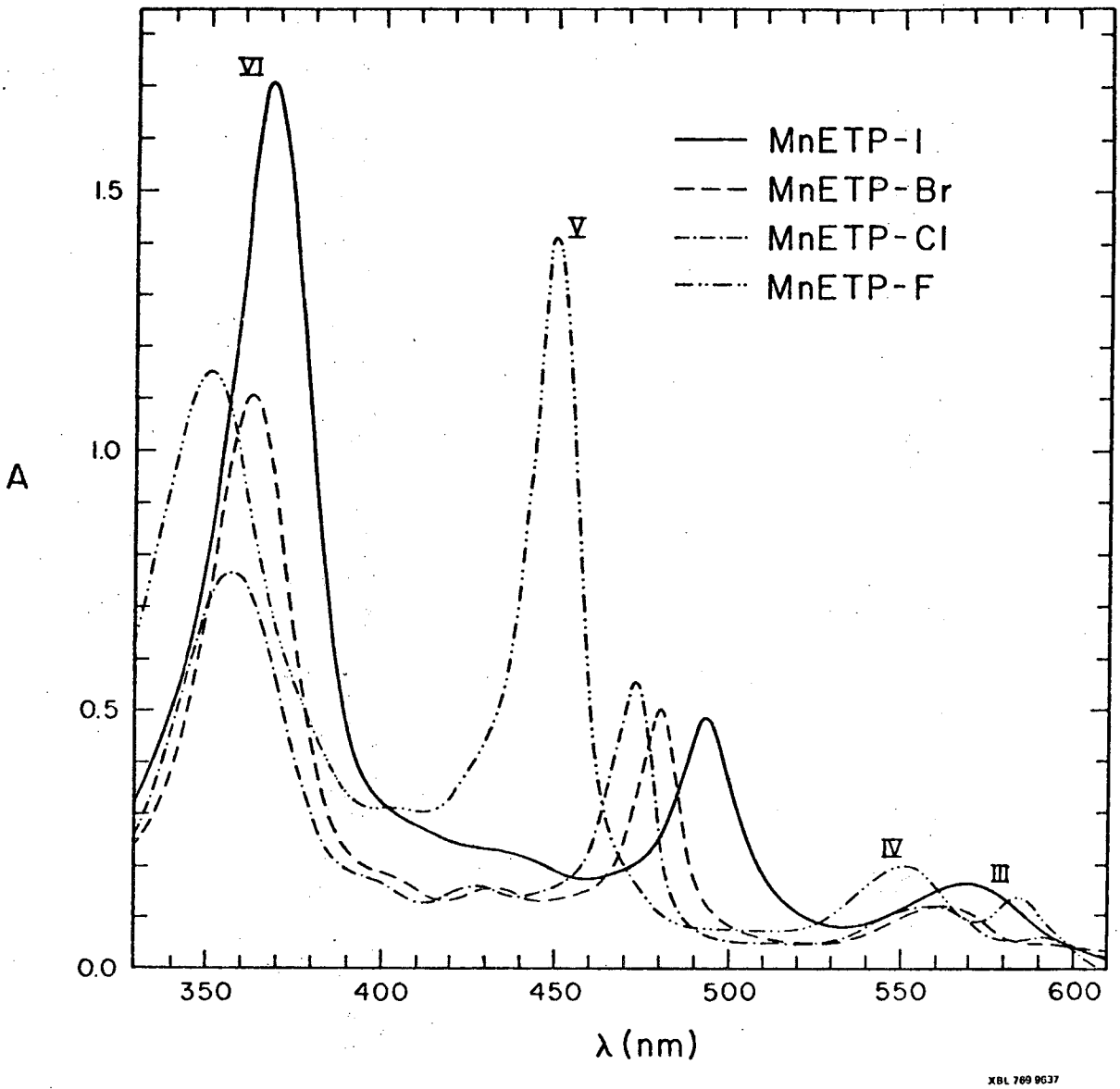

Fig. III-8. Absorption spectra of MnETP-X (X=F^-, Cl^-, Br^- and I^-) in freshly distilled $CHCl_3$. Concentrations: MnETP-F^-=1.86 × 10^{-5}M; MnETP-Cl^-=1.06 × 10^{-5}M; MnETP-Br^-=10^{-5}M; MnETP-I^-=1.75 × 10^{-5}M.

Band VI shows a 60% increase in its molar absorptivity between the F^- and I^-, but the halfwidth decreases proportionately. Thus, the integrated area remains identical to within 1% for each of the halide complexes in $CHCl_3$ and for MnETP-X in n-butanol. The absorption maximum of band VI shifts 1471 cm^{-1} between the I^- and F^- complexes.

Band V shows a much stronger dependence on the axial ligand. The molar absorptivity of band V decreases by 66% in the I^- compared to the F^- complex. The integrated absorption in energy units decreases by 60% in this case. The position of the band maximum shifts to the red by 1940 cm^{-1} in the I^- compared to the F^-.

The energy and the molar absorptivity of band V shows the largest dependence on the axial ligand. This is consistent with the assignment of band V to a charge transfer band, because an axial ligand affects the energies of the d orbitals of the metal more than the porphyrin π orbitals. Thus, the energy of the excited state formed by a charge transfer transition should be more affected by a change in axial ligation than the energy of an excited state formed by a $\pi \rightarrow \pi^*$ transition.

To characterize the electronic transitions of MnETP further, MCD spectra of MnETP were obtained in a solution which forms a clear glass at liquid nitrogen temperatures. The solution (abbreviated MCP) contained 20% n-butanol; 60% methyl cyclohexane and 20% 2-methyl pentane. Figure 9 shows the room and low temperature absorption and MCD spectra of MnETP in MCP. Bands III and IV show A terms in both the room and low temperature MCD spectra, with crossovers at the absorption band maxima. Both the absorption maxima and the crossover points of the A terms shift to higher energy as the temperature is lowered.

The magnitude of the A term for band III doubles at 122°K. However, the increase is somewhat less than the factor of 2.4 expected if the MCD spectrum is purely from C terms. Additionally, both bands III and IV narrow in the absorption spectrum. The narrowing is more obvious in the MCD spectrum where the peak to trough splitting decreases by 46% for band III with a concomitant increase in the magnitude of the A term (Table III). The MCD spectrum of bands III and IV resembles the MCD spectra of the α and β bands of other metalloporphyrins (Sutherland, 1976; Dratz, 1966; Gale, et al., 1972). In addition, the A term of band IV shows structure at 122°K which is consistent with its assignment to the β band of metalloporphyrins (Linder, et al., 1974; Gale, et al., 1972).

Band V shows a much larger temperature dependence in both the MCD and adsorption spectra than do bands III, IV and VI. Band V narrows from a $\Delta\nu_{\frac{1}{2}}$ (full width at half height) of 1050 cm^{-1} at room temperature to $\Delta\nu_{\frac{1}{2}}$ = 582 cm^{-1} at 122°K. Additionally, the peak to trough splitting of the MCD spectrum, measured from the higher intensity positive peak to the trough, decreases from 860 cm^{-1} at room temperature to 180 cm^{-1} at 122°K. The magnitude of an A term is proportional to the reciprocal of the square of the peak to trough separation (Stephens, et al., 1966). Thus the 17 fold increase in magnitude of the MCD spectrum may be accounted for by the greater than four-fold narrowing of the peak to trough separation. There is no evidence for a C term contribution to band V.

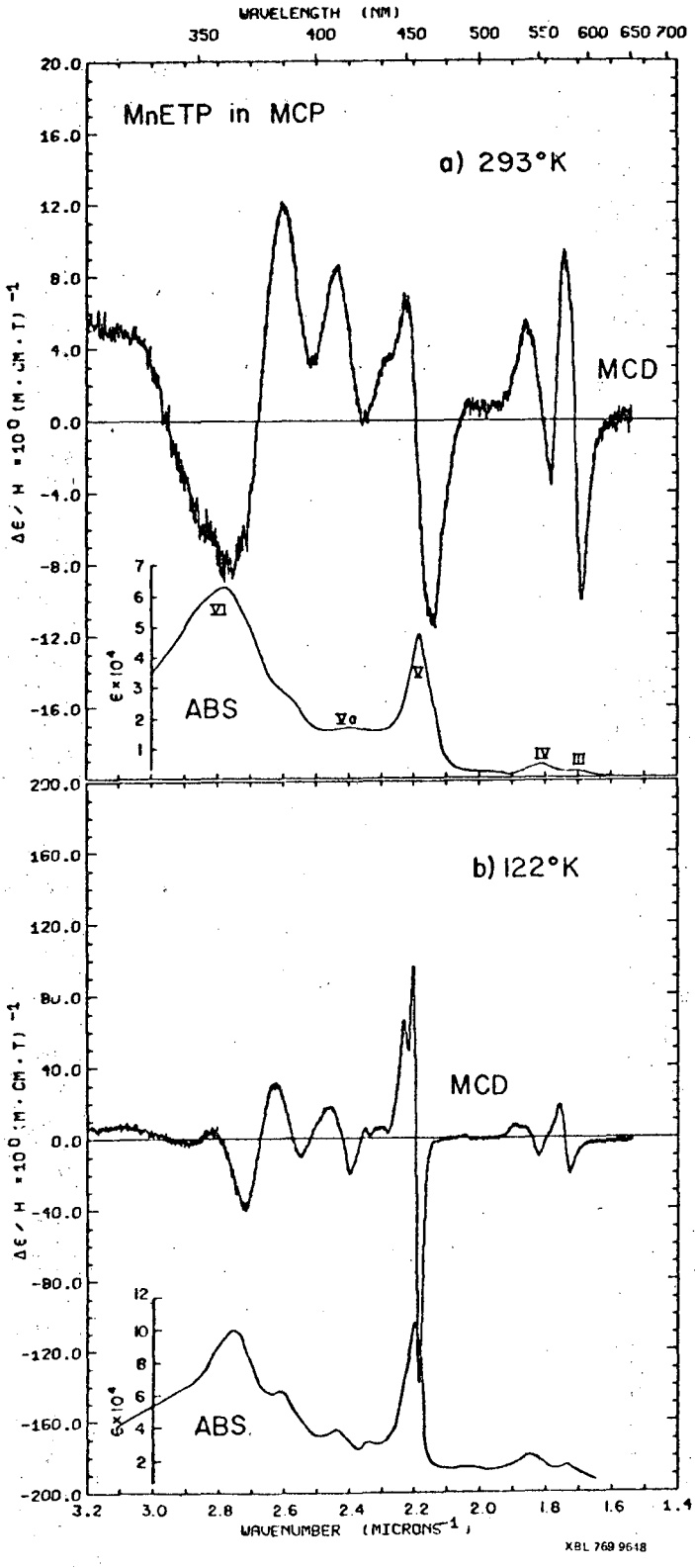

Fig. IV-9 MCD and absorption spectra of MnETP in MCP. Pathlength=0.23 cm. Conc.=8.9 X 10^{-5} M; Slitwidth=0.5 mm. Scan speed=5 nm/min. Magnetic field=0.79 Tesla. a) 293 °K b) 122 °K.

Table III. Energies (cm^{-1}) of the extrema and crossovers in the MCD spectra of MnETP in MCP at room temperature at 122°K (Fig. 9).

		Energies (cm^{-1})	
Band		Room Temperature	122°K
III	MIN	16,890	17,280
	CROSSOVER	17,100	17,460
	MAX	17,450	17,580
	Δ^a	560	300
IV	MIN	17,870	18,220
	CROSSOVER	18,110	18,440
	MAX	18,580	18,780
	Δ^a	710	560
V	MIN	21,410	21,860
	CROSSOVER	21,910	21,960
	MAX	22,270	22,040
	MAX	22,800	22,320
	Δ^a	860	180
Va and VI	MIN		24,000
	CROSSOVER		24,220
	MAX		24,640
	CROSSOVER		25,220
	MIN		25,530
	CROSSOVER		25,760
	MAX	26,000	26,300
	CROSSOVER	26,780	26,730
	MIN	27,700	27,200

Δ is peak to trough separation (cm^{-1})

The MCD spectrum of band V at 122°K shows a splitting which corresponds to an asymmetry present in the absorption spectrum. The crossover of band V in the MCD spectrum occurs within 30 cm^{-1} of the position of the absorption maximum, both at room temperature and at 122°K. As the temperature is lowered the MCD spectrum narrows symmetrically about the crossover point, which shifts ~ 50 cm^{-1} to higher energy paralleling the shift of ~50 cm^{-1} in the absorption spectrum. Although it is possible that the features in the MCD spectrum are due to overlapping B and/or C terms, the lack of three corresponding features in the absorption spectrum and the symmetric narrowing of the MCD spectrum suggests that at least the lower energy peak and the trough have an A term contribution, in agreement with Boucher's assignment (Boucher, 1972). A less likely alternative would invoke overlapping B and C terms resulting from multiple electronic or vibronic transitions which have equal narrowing and energy shifts as the temperature is lowered. The absorption spectrum of band V shows a shoulder at about 22,170 cm^{-1} at 122°K, indicating the presence of another electronic or vibronic transition. No corresponding peak or trough appears at this energy in the MCD spectrum. However, a peak appears in the MCD spectrum at 22,320 cm^{-1}. No corresponding feature is resolved in the absorption spectrum at this energy. The asymmetry of the A term which has a crossover at 21,960 cm^{-1} suggests the existence of an overlapping negative component which decreases the magnitude of the positive lobe. Possibly the peak at 22,320 cm^{-1} is the positive lobe of an overlapping A term. Thus, the MCD spectrum

of band V may result from the overlap of two A terms of different peak to trough widths, which are resolved on the high energy side but which overlap at lower energy to give an asymmetric shape to the A term which has a crossover at the peak of the absorption band. The separation between the A terms would be about 300 cm^{-1}.

The second A term may arise from either another electronic transition or a vibronic overtone of band V. An absorption spectrum of MnETP-I^- in CS_2 at 213°K (Fig. 10) shows an unresolved shoulder at 21,000 cm^{-1} on the high energy side of band V, while the maximum of band V is at 19,800 cm^{-1}. Corresponding features appear in the MCD spectrum with an A term centered at 19,800 and another peak at 21,500 cm^{-1}.

Band V shows no splitting of the A term in CS_2 at 193°K. The feature at 21,500 cm^{-1} may correspond to the peak observed at 22,320 cm^{-1} in the MCD spectrum of MnETP in MCP (Fig. 9). The two peaks in the room temperature MCD spectrum of MnETP in MCP are separated by 530 cm^{-1} while the separation is about 1300 cm^{-1} for MnETP-I^- in CS_2. Resonance Raman spectra obtained by Shelnutt, et al. from MnETP-I^- (Shelnutt, et al., 1976) show an excitation profile maximum both at the absorption maximum of band V and at about 1200 cm^{-1} to higher energy. To explain the two nonequal excitation profile maxima, they invoked a non-adiabatic coupling mechanism. However, the presence of another electronic transition would also explain their results.

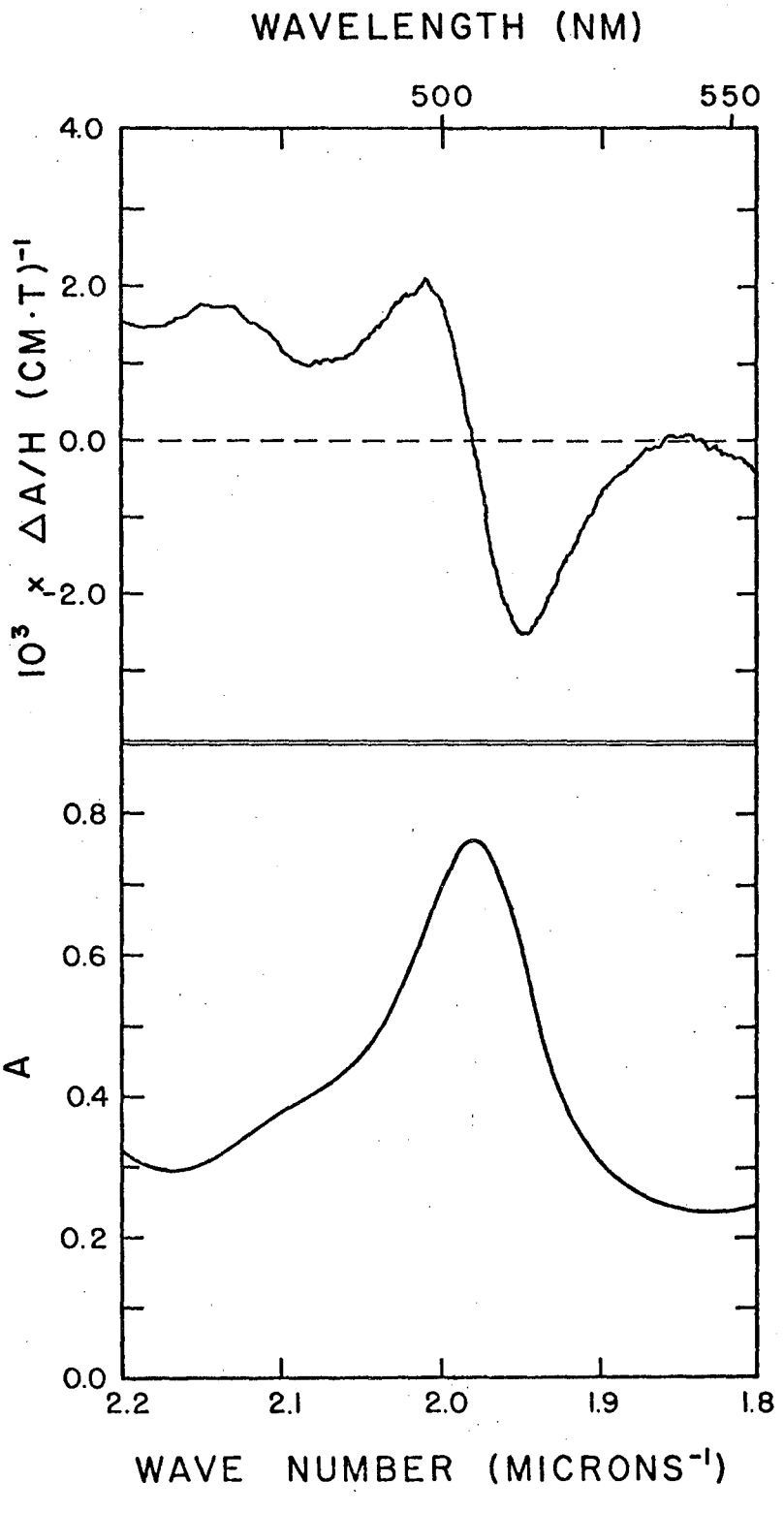

Fig. IV-10 MCD and absorption spectra of MnETP-I$^-$ in CS_2. T=193 °K. Pathlength=0.4 cm. Slitwidth=0.5 mm. Scan speed=5 Å/sec. Magnetic field=0.8 Tesla. Conc. ca. 9 X 10^{-5} M.

The absorption and MCD spectra are much more complex for bands Va and VI. Band VI resolves into 3 components in the low temperature absorption spectrum: a peak at 26,040 cm^{-1}; the main peak at 27,470 cm^{-1} and a high energy shoulder at 28,000 cm^{-1}. The MCD spectrum is very complicated. None of the features in the MCD spectrum clearly coincides with any of the resolved features in the absorption spectrum. The feature (in both the room temperature and 122°K MCD spectrum) that simulates an A term with a crossover at about 26,750 cm^{-1} appears between two resolved components of band VI in the absorption spectrum.

The complexity of the MCD spectrum suggests that band VI contains more electronic transitions than are resolved in the low temperature absorption spectrum and that the complexity of the MCD spectrum results from the overlap of these bands.

Assignments of the Electronic Transitions of Mn ETP

The narrowing of band V at low temperature probably results from the increased ordering of the solvent cage around the MnETP. The major interaction of the solvent with MnETP is through the axial ligation of butanol. An increased ordering of the solvent should effect the d orbitals of the metal more than the π orbitals of the porphyrin. Thus, a charge transfer transition which involves the d orbitals of the metal would be expected to narrow more than a $\pi \rightarrow \pi^*$ transition.

The unique narrowing of band V at low temperature and the dependence of its intensity on the axial ligand implicates band V as a charge transfer band, in agreement with Boucher's conclusions. The MCD spectra of bands III and IV are consistent with the assignment

of these bands to the α and β bands of metalloporphyrins. Band V shows at least one A term, indicating that a degenerate ground or excited state is involved in the electronic transition.

The ground state of MnETP is $^5B_{1g}$ in D_{4h} symmetry. The only allowed charge transfer transitions for MnETP in this point group are from the porphyrin π orbitals to the metal, because the ground state is gerade while the excited state must be ungerade for the transition to be allowed. Transitions of the d electrons of the metal to the e_g^* (π) orbitals are formally forbidden by symmetry since the excited state would be gerade. A charge transfer transition to a doubly degenerate excited state is allowed from any of the 4 highest occupied porphyrin π orbitals, which are of a_{1u}, a_{2u} and b_{2u} symmetry (Gouterman, 1973), to the d_{xz}, d_{yz} orbitals of e_g symmetry. Thus, one possible assignment of band V is a transition from an a_{1u} or a_{2u} orbital to the d_{xz}, d_{yz} orbitals of the metal. The additional feature underlying band V may result from the other transition from either the a_{1u} or a_{2u} porphyrin orbital.

Boucher (Boucher, 1973) has proposed a mechanism to account for the dependence of the oscillator strength of band V on the axial ligand. As the halide anion increases in size, the metal is pulled further out of the plane of the porphyrin due to non-bonded repulsions between the electron cloud of the anion and the porphyrin π orbitals. The overlap of the d orbitals of the metal and the porphyrin π orbitals decreases, resulting in a decrease in the transition moment. That the decrease in oscillator strength is an effect of the out-of-plane distance of the metal and is not an effect of the ligating atom was shown by a comparison

of the absorption spectra of MnETP with imidazole and piperidine as ligands. Non-bonded interaction of the N-H with the porphyrin ring forces the metal further out of the ring in the piperidine complex than in the imidazole complex (Boucher, 1973). Boucher observed that the molar absorptivity of band V in the piperidine complex is only 60% of the value for the imidazole complex and concluded that the further the metal lies out of the plane of the porphyrin the more unfavorable is d and π orbital overlap and the less allowed the transition will be.

Recently Shelnutt, et al., (1976) proposed that band V, Va and VI result from mixing via configuration interaction of the excited states involved in the Soret band with the excited states reached by a charge transfer transition. However, the unique dependence of the oscillator strength of band V on the axial ligand without a concomitant reverse dependence of the oscillator strengths of bands Va and VI suggests that there is no mixing of the excited states involved in band V with the excited states in band VI and that band V may be a pure change transfer transition. If band V results from the mixing of the Soret band and a charge transfer band, reduction of the oscillator strength of band V by increasing the out-of-plane distance of the metal from the ring should change the overlap of the d and π orbitals with a resulting change in the mixing coefficients. Conservation of oscillator strength under the Thomas-Kuhn sum rule predicts that the oscillator strengths of bands Va and/or VI should increase proportionately to the decrease in V (Merzbacher, 1970).

The electronic transitions which give rise to bands Va and VI may arise from configuration interaction between an excited state reached by a charge transfer transition and an excited state involved in the Soret band. The resulting absorption and MCD spectra would be very complex and would be difficult to interpret in the absence of good molecular orbital calculations.

REFERENCES

Boucher, L.J., J. Am. Chem. Soc. 92, 2725 (1970).

Boucher, L.J., Coord. Chem. Rev. 7, 289 (1972).

Boucher, L.J., N.Y. Acad. Sci. 206, 409 (1974).

Caughey, W.S., Deal, R.M., Weiss Jr., C. and Gouterman, M., J. Mol. Spectrosc. 16, 451 (1965).

Dratz, E.A., The Geometry and Electronic Structure of Biologically Significant Molecules as Observed by Natural and Magnetic Optical Activity, Ph.D. Thesis, Univ. of Calif., Berkeley (1966), UCRL 17200.

Falk, J.E., Porphyrins and Metalloporphyrins, Biochim. Biophys. Acta Library Vol. 2, Elsevier Publishing Co., N.Y. (1964).

Gale, R., McCaffery, A.J. and Rowe, M.D., Chem. Soc., Dalton Trans., 596 (1972).

Gouterman, M., J. Chem. Phys. 30, 1139 (1959).

Gouterman, M., J. Mol. Spectrosc. 6, 138 (1961).

Gouterman, M., Excited States of Matter, Vol. 2, C.W. Shoppee, Ed., pgs. 63-103, Grad. Studies, Texas Tech. Univ. (1973).

Gurinovich, G.P., Sevchenko, A.N. and Solovev, K.N., Soviet Physics Uspekhi 6, 67 (1963).

Gurinovich, G.P., Sevchenko, A.N. and Solovev, K.N., in Spectroscopy of Chlorophyll and Related Molecules, AEC-TR-7199, U.S. Atomic Energy Commission, Division of Technical Information (1968).

Linder, R.E., Barth, G., Bunnenberg, E., Djerassi, C., Seamans, L. and Moscowitz, A., J. Chem. Soc. Perkin II, 1712 (1974).

McCaffery, A.J., Nature, Physical Sciences 232, 137 (1971).

Merzbacher, E., Quantum Mechanics, Wiley, N.Y. (1970).

Platt, J.R., Radiation Biology vol. III, McGraw-Hill (1956).

Schatz, P.N. and McCaffery, A.J., Quart. Rev. Chem. Soc. 23, 552 (1969).

Shelnutt, J.A., O'Shea, D.C., Yu, N-T, Cheung, L.D. and Felton, R.H., J. Chem. Phys. 64, 1156 (1976).

Simpson, W.T., J. Chem. Phys., 17, 1218 (1949).

Smith, D.W. and Williams, R.J.P., Structure and Bonding 7, 1 (1970).

Stephens, P.J., Suetaka, W. and Schatz, P.N., J. Chem. Phys. 52, 3489 (1970).

Sutherland, J.C., The Porphyrins, D. Dolphin, ed., Academic Press (in press) (1976).

Zerner, M. and Gouterman, M., Theoret. Chim. Acta. 4, 44 (1966).

CHAPTER IV

RESONANCE RAMAN SPECTROSCOPY OF MANGANESE (III) ETIOPORPHYRIN I AND CHROMIUM (III) TETRAPHENYLPORPHIN

Introduction

Resonance Raman spectroscopy is a technique for the selective observation of the vibrational spectra of dilute molecular species. Other molecules in the medium which are not resonantly enhanced exhibit much weaker Raman scattering on a per molecule basis. Resonance Raman spectroscopy may therefore be used as a selective technique for the study of one molecular species in a medium that contains a myriad of other components, provided that excitation occurs within an absorption band of the molecule of interest which does not overlap with the absorption bands of the other components of the medium. The vibrational structure of a molecule is dependent on the force constants and bond distances which are, in turn, dependent on intermolecular interactions such as hydrogen bonding. Thus, the resonance Raman spectrum of a molecule may contain environmental information. The selectivity of the resonance Raman technique and the environmental information that it may yield makes it a potentially powerful tool for the study of chromophores in biological systems.

Porphyrins, which appear in biologically important molecules such as hemoglobin and the cytochromes, have intense absorption bands which occur at longer wavelengths than the absorption bands of proteins, nucleic acids and most of the

other components of the cell. The enzymatic properties of the heme in the cytochromes and the oxygen binding properties of the heme in hemoglobin appear to be modulated by the surrounding protein matrix (Smith and Williams, 1970). Thus, a study of the resonance Raman spectra of these molecules might yield information on the interactions between the metalloporphyrin and the protein.

The potential utility of resonance Raman spectroscopy as a probe of the interactions between the heme and the protein has led to intensive studies of the resonance Raman spectra of a wide variety of porphyrins, and porphyrin-protein complexes: free-base porphyrins (Verma, et al., (1974); Mendelsohn, et al., 1975a; Berjot, et al., 1975; Plus and Lutz, 1974); metalloporphyrins (Solovyov, et al., 1973; Verma and Bernstein, 1974a, b, c, and d; Mendelsohn, et al., 1975a and b; Felton, et al., (1974); Kitagawa, et al., 1975a and b; Sunder, et al., 1975; Berjot, et al., 1975; Spaulding, et al., 1975; Gaughan, et al., 1975; Asher and Sauer, 1976; Shelnutt, et al., 1976; Kitagawa, et al., 1976, a and b; Spiro 1972a, 1973; Spiro and Strekas, 1972, 1973; Yamamoto, et al., 1973; Brunner and Sussner, 1973; Strekas, et al., 1973; Sussner, et al., 1974; Spiro, 1975, Rimai, et al., 1975; Szabo and Barron, 1975; Kitagawa, et al., 1975c, 1976; Ozaki, et al., 1976); the cytochromes (Strekas and Spiro, 1972b; Spiro and Strekas, 1972, 1973; Brunner, 1973; Salmeen, et al., 1973; Nafie, et al., 1973; Friedman and Hochstrasser, 1973; Collins et al., 1973; Pezolet, et al., 1973; Nestor and Spiro, 1973; Adar and Erecinska, 1974; Adar, 1975; Kitagawa,

et al., 1975d, Ikeda-Saito, et al., 1975; Spiro, 1975; Collins, et al., 1976; Yamamoto, et al., 1976); horseradish peroxidase (Rakshit and Spiro, 1974; Felton, et al., 1976; Rakshit, et al., 1976); and cobalt substituted hemoglobin and myoglobin (Woodruff, et al., 1974, 1975).

From these studies, it appears that excitation within $\pi \rightarrow \pi^*$ electronic transitions involving the macrocyclic ring enhances vibrations within the macrocycle (Spiro and Strekas, 1976; Brunner and Sussner, 1973; Strekas and Spiro, 1973; Mendelsohn, et al., 1975a; Plus and Lutz, 1974; Verma and Bernstein, 1974a).

The vibrations of atoms that are not intimately conjugated to the aromatic structure of the ring make only a small contribution to the resonance Raman spectrum; and,as a result, changes in peripheral substituents about the porphyrin ring produce relatively small differences in the vibrational frequencies observed (Mendelsohn, et al., 1975a and b; Verma and Bernstein 1975a; Sunder, et al., 1975; Adar, 1975; Spiro, 1975). The alterations of the resonance Raman spectra produced by changes in peripheral substituents appear to be induced mainly by changes in the symmetry of the porphyrin macrocycle (Sunder, et al., 1975).

Changes in the central metal also result in differences in the RR spectra. Variations in the spin state, oxidation state (Spiro and Strekas, 1974; Brunner and Sussner, 1973, Strekas, et al., 1973; Brunner, 1973) or in the planarity of the metal with respect to the porphyrin plane shift the

energy and polarization of some of the resonance enhanced vibrations (Woodruff, et al., 1974; Verma and Bernstein, 1974b; Felton, et al., 1974; Spaulding, et al., 1975; Kitagawa, et al., 1975). These shifts in energy and polarization are due to a change in the structure, which may be a doming of the porphyrin when the metal lies farther from the porphyrin ring plane (Spiro and Strekas, 1974; Brunner and Sussner, 1973; Strekas, et al., 1973; Brunner, 1973; Felton, et al 1974; Spiro, 1975) or an expansion of the porphyrin core resulting in a decrease of the metal-to-porphyrin-center distance (Spaulding, et al., 1975).

Another possibility is that the shifts in energy are due to a change in the conjugation between the metal orbitals and the porphyrin π orbitals which affects the stretching force constants of the ring (Kitagawa, et al., 1975b; Spiro and Burke, 1976). The effect of axial ligation on porphyrin macrocycle vibrations depends on the extent that the ligand induces a change in the displacement of the metal from the ring plane (Felton, et al., 1974).

There have been few reports of axial ligand vibrations in heme proteins and metalloporphyrins (Brunner, 1974; Kitagawa, et al., 1976b, Spiro and Burke, 1976), which are of very weak intensity when excitation occurs in a $\pi \rightarrow \pi^*$ transition (Kitagawa, et al., 1976b).

The only feature directly sensitive to the environment of the prophyrin macrocycle is the dispersion with respect

to frequency of the depolarization ratio. Since the depolarization ratio is a function of porphyrin symmetry, it can be influenced by environmental factors such as axial ligation (Verma and Bernstein, 1974; Felton, et al., 1974), and peripheral substitution (Pezolet, et al., 1973; Mendelsohn, et al., 1975b; Felton, et al., 1974; Collins, et al., 1973). However, the dispersion of the depolarization ratio could also be explained by the overlap of two Raman bands of different depolarization ratios which have different excitation profiles (Spaulding, et al., 1975).

The lack of enhancement of axial ligand vibrations in $\pi \rightarrow \pi^*$ transitions is not surprising in view of the fact that there is little mixing between the porphyrin π orbitals and the metal d orbitals in the α,β and Soret bands of metalloporphyrins (Zerner and Gouterman, 1966). Since the axial ligand is bound to the metal, metal-axial ligand vibrations are effectively isolated from the $\pi \rightarrow \pi^*$ transitions of the porphyrin macrocycle. However, axial ligand vibrations might be enhanced by excitation in electronic transitions, such as charge transfer or d→d transitions, which involve the metal orbitals.

MANGANESE (III) ETIOPORPHYRIN

Bands III, IV and V

The visible and near UV absorption spectrum of Mn(III) ETP acetate in n-butanol is shown in Fig. 1. The bands are labeled using the numbering scheme introduced by Boucher (Boucher, 1970, 1972) and the locations are shown for the laser lines used to excite the resonance Raman spectra shown in Fig. 2. The laser line at 568.2 nm lies between bands III and IV, while the line at 530.9 nm lies on the high energy side of band IV. The 457.9 nm line is in resonance with peak V, an electronic transition that has been assigned as a possible charge transfer transition (Chapter III). The solvent contributions to the Raman spectra are noted in the figures. Table I contains the energies and relative intensities for each of the Raman peaks shown in Fig. 2.

Apart from the rising baseline, the spectra shown in Figs. 2a and b are qualitatively similar. It is unclear whether the rising baseline in Fig. 2a which peaks at 15,900 cm^{-1} (630 nm) represents emission from MnETP or an impurity, but there are no obvious features in the absorption spectrum that would give rise to fluorescence at this wavelength.

The Raman spectra shown in Figs. 2a and b show strong correlations in frequency and intensity. However, differences appear for peaks at 757, 988 and 1313 cm^{-1}. The intensities of these three peaks show greater enhancement

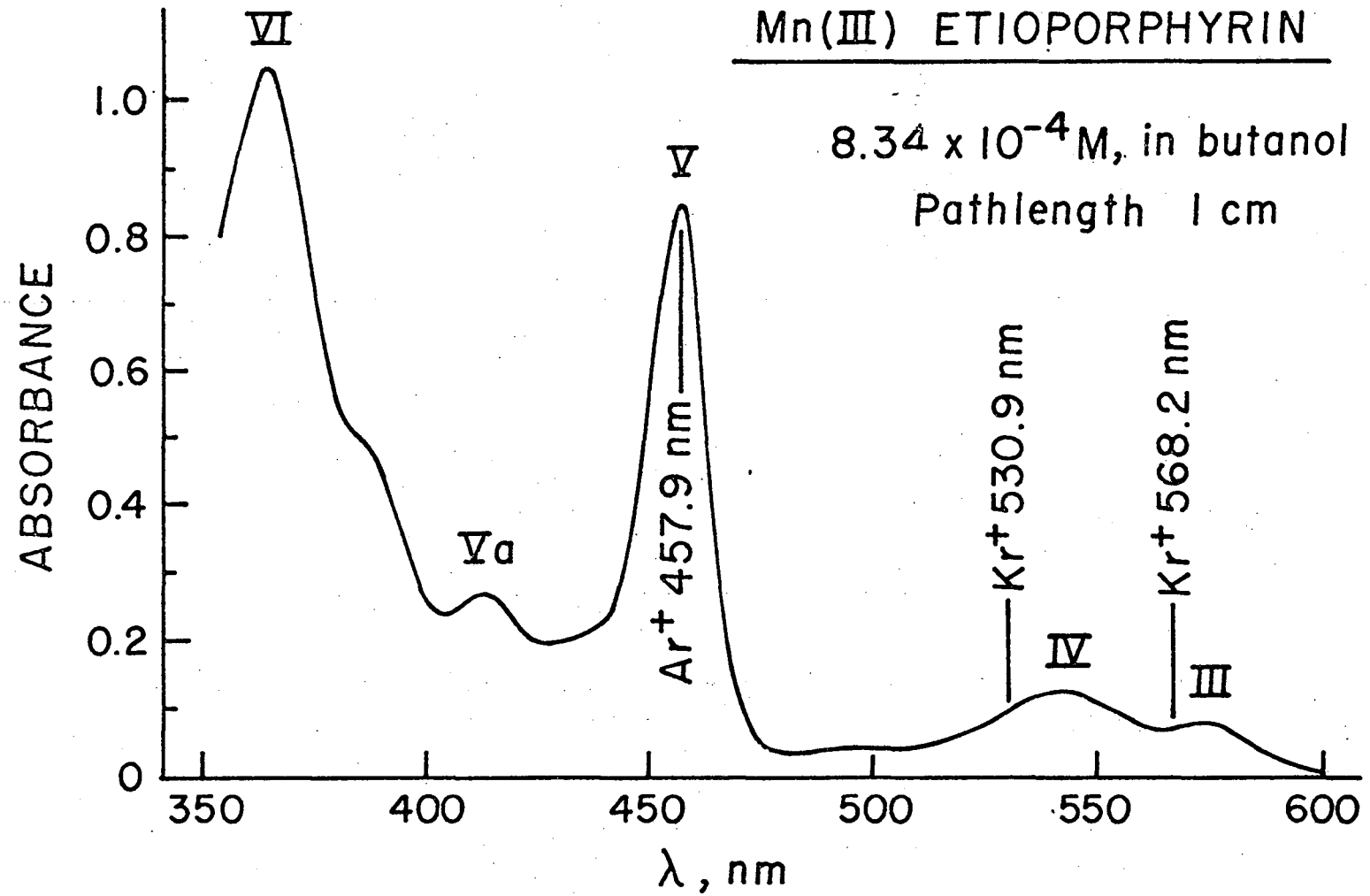

XBL753-5119

Fig. IV-1. Absorption spectrum of Mn(III) etioporphyrin I in butanol. Path length = 1 cm, conc. = 8.34×10^{-4}M. The bands are labeled in Boucher's nomenclature (Boucher, 1970,1972). The position and source of the laser lines used in the Raman spectra are indicated.

Fig. IV-2. a) Resonance Raman spectrum of Mn(III)ETP in butanol. λ_{ex} = 568.2 nm, power = 160 mw. Slit width = 5 cm^{-1}, scan speed = 50 cm^{-1}/min. Conc. ca 10^{-3}M. Because of an increasing background the offset was changed in mid scan. The wavenumber shifts in the figures and tables for all of the Raman spectra in this figure were obtained by averaging over several spectra.

b) Resonance Raman spectrum of Mn(III)ETP in butanol. λ_{ex} = 530.9 nm, power = 50 mw. Slit width = 6.4 cm^{-1}, scan speed = 25 cm^{-1}/min. Conc. ca 10^{-3}M.

c) Resonance Raman spectrum of Mn(III)ETP in butanol. λ_{ex} = 457.9 nm, power = 250 mw. Slit width = 6.4 cm^{-1}, scan speed = 50 cm^{-1}/min. Conc. ca 10^{-3}.

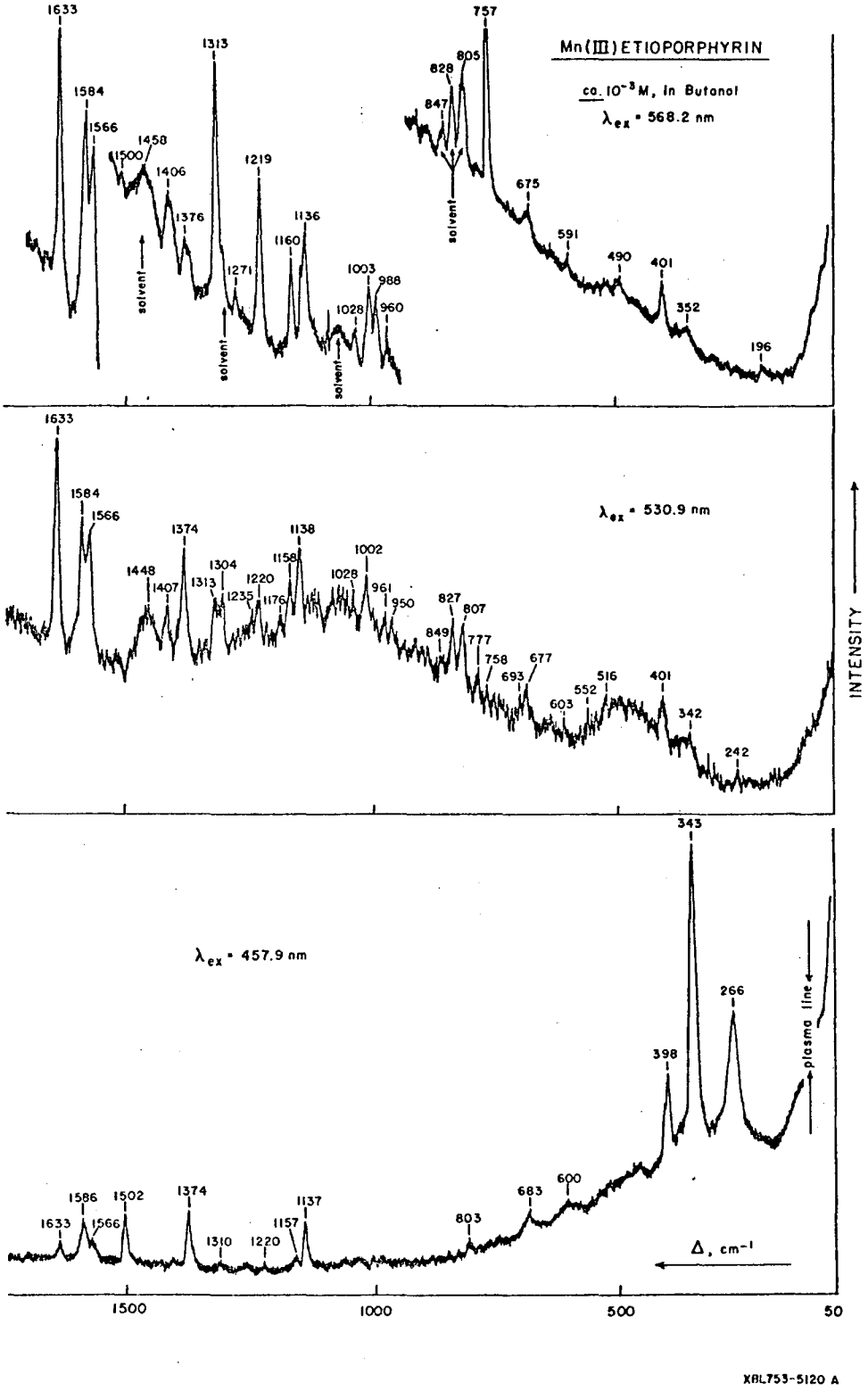
Mn(III) ETIOPORPHYRIN
ca. 10⁻³ M, In Butanol
λex = 568.2 nm
λex = 530.9 nm
λex = 457.9 nm
solvent
plasma line
INTENSITY
Δ, cm⁻¹
1500
1000
500
50
XBL753-5120 A

Fig. IV-2.

TABLE I

Observed vibrational frequencies and relative intensities of the Raman bands of MnETP in BuOH excited by laser lines at 457.9, 530.9 and 568.2 nm. Relative intensities: vs - very strong; s - strong; m - medium; w - weak; vw - very weak; sh - shoulder.

Exciting line:	457.9	530.9		568.2	
$\Delta\nu$ cm^{-1}	I	$\Delta\nu$ cm^{-1}	I	$\Delta\nu$ cm^{-1}	I
				196	vw
		242	w		
266	s	265	vw		
343	vs	342	w	352	w
398	s	401	w	401	w
				490	vw
600	vw	603	vw	591	vw
683	w	677	w	675	w
		693	w		
		758	w	757	s
803	(solvent)	807	(solvent)	805	(solvent)
		827	(solvent)	828	(solvent)
		849	(solvent)	847	(solvent)
		950	w		
		961	w	960	m
				988	m
		1002	m	1003	m
		1028	w	1028	w

TABLE I (cont.)

exciting line: 457.9		530.9		568.2	
$\Delta\nu$ cm^{-1}	I	$\Delta\nu$ cm^{-1}	I	$\Delta\nu$ cm^{-1}	I
1137	m	1138	m	1136	s
1157	vw	1158	m	1160	s
1220	vw	1220	m	1219	vs
				1271	w
1310	vw	1304	(solvent)	1313	vs
1374	m	1374	s	1376	m
		1407	m	1406	m
		1448	(solvent)	1458	(solvent)
1502	m			1500	w
1566	sh	1566	s	1566	vs
1586	m	1584	vs	1584	vs
1633	w	1633	vs	1633	vs

with excitation in band III than with excitation in band IV. Conversely, the peak at 1374 cm^{-1} is more intense with excitation in band IV rather than in band III. The most intense features of both spectra appear between 1550 and 1650 cm^{-1}. There are few well resolved features below 500 cm^{-1}.

Comparison of the spectra obtained with excitation in bands III and IV with the spectrum obtained with excitation in band V showsmore dramatic differences. The most intense features in Fig. 2c are vibrations at frequencies less than 500 cm^{-1}. This is the region in which manganese pyrrole nitrogen vibrations are expected to occur (Burger, et al., 1971; Ogashi, et al., 1971; 1972, 1973; Boucher and Katz, 1967; Warshel, 1976). Higher frequency vibrations are still visible, but their relative intensities are small. A number of peaks are conspicuous by their absence. The bands at 757 and 1002 cm^{-1} seen in Figs. 2a and 2b do not appear with excitation in absorption band V; instead a new peak appears at 1502 cm^{-1}.

In order to determine whether the low frequency vibrations (less than 500 cm^{-1}) in the Raman spectrum of MnETP are metal related, the Raman spectra of the F^-, Cl^-, Br^-, and I^- salts were measured. These Raman spectra are shown in Fig. 3. Table II lists the frequencies and relative intensities of the Raman bands of MnETP-X between 100 and 500 cm^{-1}. All of the Raman bands in Fig. 3 are polarized. Carbon disulfide was used as the solvent

Fig. IV-3. Raman spectra of Mn(III)ETP-X (X-F^-, Cl^-, Br^-, and I^-). CS_2 is the solvent for the F^-, Cl^-, and Br^- complexes. $CHCl_3$ is used for I^- complex. λ_{ex} = 457.9 nm for F^-, 476.5 nm for the Cl^- and 488.0 nm for the Br^- and I^- complexes. Power = 10 mw. Slit width = 5 cm^{-1}, scan speed = 12 cm^{-1}/min. Conc. ca 10^{-3}M. The gaps in the spectrum of MnETP-I indicate solvent interference. The 260 cm^{-1} shoulder in the spectrum of the bromide complex is more pronounced in other recorded spectra.

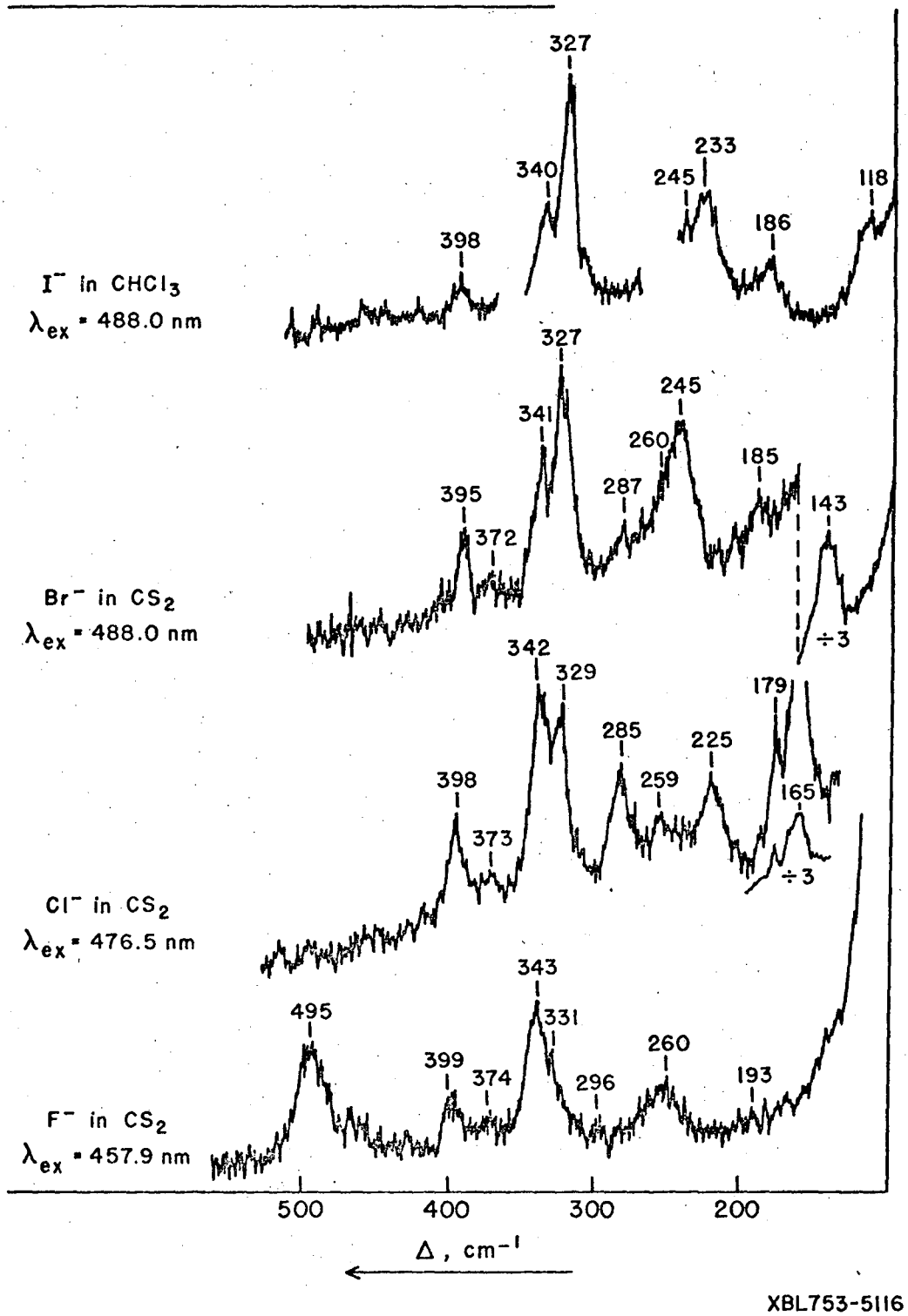

Fig. IV-3.

TABLE II

Observed Raman bands of the halide salts of MnETP. Intensities are labeled as in Table I. ρ is depolarization ratio: p, polarized; dp, depolarized; ap, anomalously polarized.

F^-			Cl^-			Br^-			I^-		
$\Delta\nu, cm^{-1}$	I	ρ	$\Delta\nu, cm^{-1}$	I	ρ	$\Delta\nu, cm^{-1}$	I	ρ	$\Delta\nu, cm^{-1}$	I	ρ
									118	s	p
						143	s	p			
			165	s	p						
193			179	s	p	185	vw		186	w	
			225	m	p				233	s	p
						245	s	p	245	w	p
260	s	p	259	m	p	260	sh	p	$CHCl_3$	interference	
			285	s	p						
296	w	p				287	vw				
331	sh	p	329	s	p	327	vs	p	327	vs	p
343	s	p	342	s	p	341	s	p	340	m	p
374	vw		373	w		372	w		$CHCl_3$	interference	
399	m	p	398	m	p	395	m	p	398	m	p
495	s	p									
			754	m	ap						
									805	w	p
									923	w	ap
1002	w	p	1002	w	p	1002	m	p	1003	w	p

TABLE II (cont.)

F^-			Cl^-			Br^-			I^-		
$\Delta\nu, cm^{-1}$	I	ρ	$\Delta\nu, cm^{-1}$	I	ρ	$\Delta\nu, cm^{-1}$	I	ρ	$\Delta\nu, cm^{-1}$	I	ρ
						1057	w				
1138	s	p	1136	s	p	1136	s	p	1138	s	p
1256	w		1254	w	p	1256	w	p	1256	w	p
						1308	m	ap	1309	w	ap
1376	s	p	1374	s	p	1375	s	p	1376	s	p
1505	m		1502	m	p	1502	w	p	1506	w	p
1568	sh		1564	w	ap	1569	sh				
1585	w		1583	m	ap	1585	s	dp	1586	w	dp
1637	w										

for the F^-, Cl^-, and Br^- salts. Because of insufficient solubility in CS_2, chloroform was used for the I^- salt: The exciting laser light was changed in order to stay in maximum resonance with peak V.

The Raman spectra of the halide salts are clearly a function of the axial ligand. Unique peaks appear for each of the halide salts. A number of important differences and similarities appear among these spectra. The similarities will be discussed first. In the Raman spectra of all of these complexes peaks appear at about 398, 374, 342, 327 and 260 cm^{-1}, and these frequencies are virtually independent of the mass of the axial ligand. The 260 cm^{-1} peak decreases by 1 cm^{-1} from the F^- to the Cl^- complex and appears as a shoulder near 260 cm^{-1} for the Br^- complex. The Raman spectrum of the solvent, $CHCl_3$ masks this region in the I^- complex. The spectrum of MnETP in butanol (Fig. 2c) shows a peak appearing at 266 cm^{-1}.

The relative intensity of the 329 cm^{-1} peak is found to be sensitive to the axial ligand. A distinct increase in intensity occurs as the axial ligand is changed from F^- through I^-. The 329 cm^{-1} peak is not evident for MnETP in butanol. Because the peaks at 329 and 342 cm^{-1} both show a small frequency dependence on the ligand, there must be some metal contribution to these vibrational modes. The change in axial ligand has a small effect through the metal but, because the effects are small, these modes must also have a large porphyrin contribution. The peak at

about 400 cm^{-1} appears in all of the spectra. The exact position is difficult to obtain since a very weak Raman line of CS_2 also appears in this region. The position of this peak does not appear to shift appreciably with a change in the ligand, since this peak appears at 398 cm^{-1} for MnETP in butanol and at 398 cm^{-1} for the I^- complex in $CHCl_3$.

A number of peaks do not correlate between spectra. The peak at 495 cm^{-1} in the F^- complex does not have any counterpart in the other spectra. The 285 cm^{-1}, 225 cm^{-1} and 165 cm^{-1} peaks in the Cl^- complex also show no counterparts in the other spectra. This is also true of the 245 and 143 cm^{-1} peaks of the Br^- and the 186 and 118 cm^{-1} peaks of the I^- complex. The peaks at 495 in the F^-, 285 in the Cl^-, 245 in the Br^- and 233 in the I^- appear to correspond with Mn-X vibrations observed in the far IR spectra of Mn(III) protoporphyrin IX dimethyl ester halides (Boucher, 1968). All of these peaks are shifted between 43 and 23 cm^{-1} to higher frequency from the Mn-halide stretches in Mn(III) protoporphyrin IX dimethyl ester which appear at 462, 262, 211 and 190 cm^{-1} for F^-, Cl^-, and I^- respectively, presumably because the spectra shown in Fig. 3 are for the molecules in solution rather than in the solid state mulls that were used for the far IR spectral measurements.

Another indication that these peaks represent the Mn-halide stretches is shown by isotopic substitution of ^{35}Cl and ^{37}Cl in the MnETP-Cl complex (Fig. 4 and Table III).

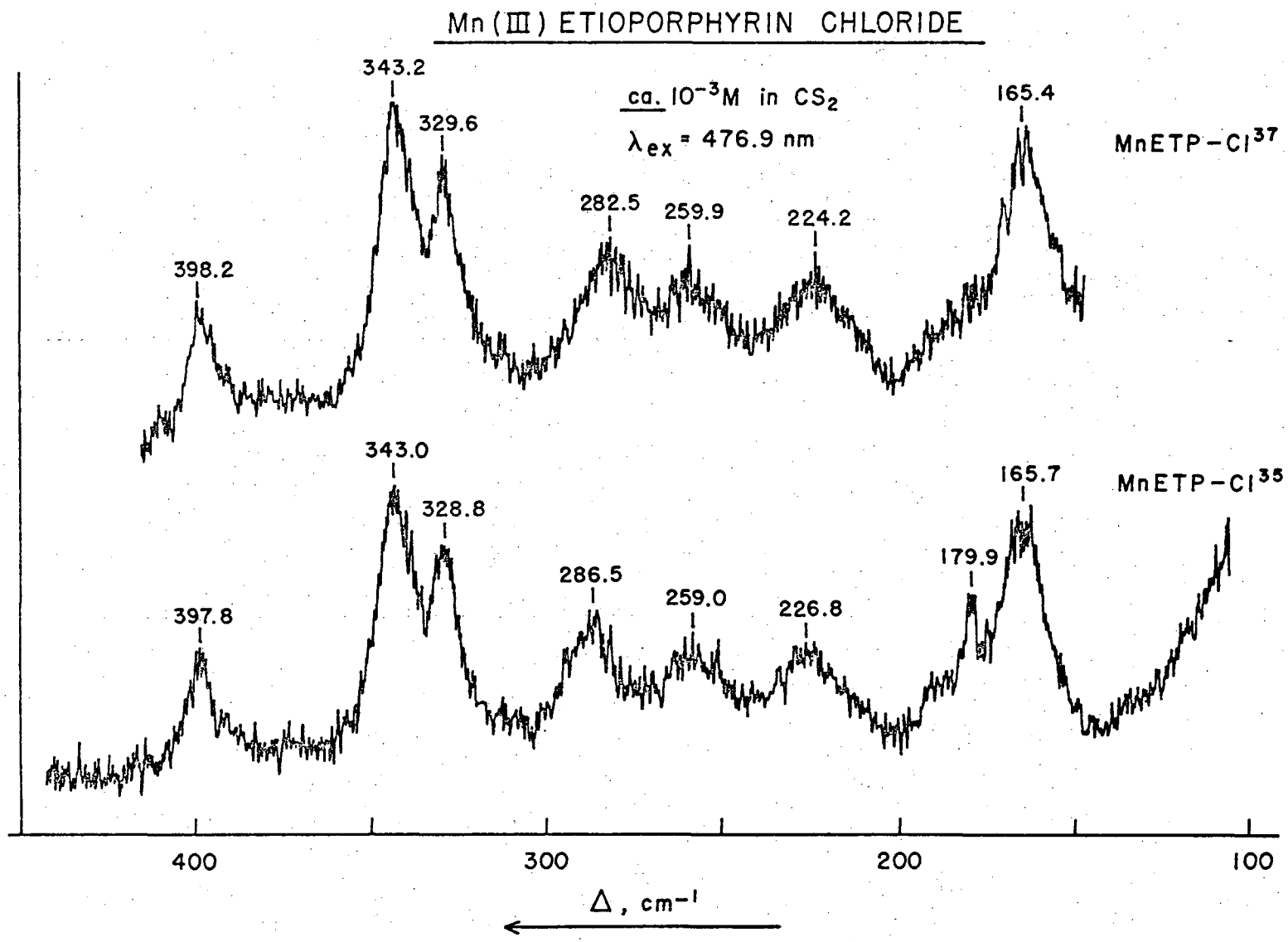

Fig. IV-4. Raman spectra of MnETP-^{35}Cl and ^{37}Cl in CS_2. λ_{ex} = 476.9 nm, power = 10 mw. Slit width = 2 cm^{-1}, scan speed = 1.2 cm^{-1}/min, time constant = 10 sec. Conc. ca 10^{-3}M.

XBL753-5115

TABLE III

Observed vibrational frequencies (cm^{-1}) and shifts of the Raman bands of MnETP ^{35}Cl and ^{37}Cl in CS_2. λ_{ex} = 476.5 nm; $\Delta(\Delta\nu) = \Delta\nu_{^{35}Cl} - \Delta\nu_{^{37}Cl}$

MnETP-^{35}Cl	MnETP-^{37}Cl	$\Delta(\Delta\nu)$
165.7	165.4	
179.9		
226.8	224.2	+2.6
259.0	259.9	
286.5	282.5	+4.0
328.8	329.6	
343.0	343.2	
397.8	398.2	

All of the low energy peaks are constant in frequency, within experimental precision ± 1 cm^{-1}, except for the peaks at 285 and 225 cm^{-1} (Table III). The peaks at 285 and 225 cm^{-1} show a shift of 4 and 2.6 cm^{-1}, respectively, to lower frequency when the axial ligand is changed from ^{35}Cl to ^{37}Cl. Using a harmonic oscillator model, the energy shift for the 285 cm^{-1} peak is 0.8 cm^{-1} less than the shift of 4.8 cm^{-1} expected if this were a pure Mn-Cl vibration. The peak at 225 cm^{-1} shows a smaller shift, and the vibrational mode responsible for it must also involve motion of the metal against the porphyrin macrocycle.

The peaks at 165 and 143 cm^{-1} in the Cl^- and Br^- complexes and the two peaks at 186 and 118 cm^{-1} in the I^- complex appear also to be axial-ligand dependent. The 165 cm^{-1} peak, the dominant feature in the Raman spectrum of the Cl^- complex shows no frequency change with isotopic substitution. A correlation of the 225 cm^{-1} peak in Cl^- with the 143 cm^{-1} peak in Br^- and the 118 cm^{-1} peak in I^- seems reasonable. The peaks exhibit a decrease in frequency with mass, and may reflect a vibration of the metal and halide against the porphyrin. Although the corresponding peak is not apparent in the F^- complex, it may lie within the broad feature at 260 cm^{-1}. This is supported by a polarization study in which the RR peaks recorded with the analyzer oriented either parallel or perpendicular to the electric vector of the incident radiation showed different maxima separated by about 3 cm^{-1}.

Table IV summarizes the assignments for the low frequency region of the Raman spectra of the halide complexes of MnETP.

The higher frequency region 500-1700 cm^{-1} of these metal complexes shows no pronounced changes with substitution of the axial ligand, in agreement with the observations made by Kitagawa, et al., for the F^-, Cl^-, Br^- and I^- complexes of Fe(III) octaethylporphyrin (Kitagawa, et al., 1975b) and by Spirc and Burke for the F^-, Cl^- and μ-oxo complexes of Fe(III) mesoporphyrin IX (Spiro and Burke, 1976). Table V lists a compilation of low frequency vibrations observed in the far IR spectra of metalloporphyrins.

There appears to be a correspondence between some of the far IR spectral peaks observed for other metalloporphyrins with the 260, 330, 340 and 400 cm^{-1} Raman peaks measured for MnETP-X. The symmetry of the axial halide complexes of MnETP-X is C_{4v}. Thus A_1 vibrations are allowed in both the IR and Raman spectra. Since all of the low frequency Raman peaks are polarized, they correspond to A_1 vibrations. The far IR spectra listed in Table V indicate that vibrational modes which are metal-dependent occur between 203-275 cm^{-1}, 337-351 cm^{-1} and 385-420 cm^{-1}. Additionally, these modes show isotope shifts when Zn^{64} is substituted for Zn^{68}; Ni^{58} is substituted for Ni^{64}; and Fe^{54} is substituted for Fe^{56}. These vibrations must, therefore, have a significant metal contribution to the vibrational mode. The IR bands that are observed for Fe(III)octaethylporphyrin-X^-($X=F^-$, Cl^-,Br^-,I^-,NCS^-

TABLE IV

Assignment of the low energy Raman bands of the MnETP halides

F^-	Cl^-	Br^-	I^-	Assignments
495				
	285			
		245		manganese halide stretch
			233	
374	373	372		porphyrin + manganese
343	342	341	340	porphyrin + manganese
331	329	327	327	out of plane porphyrin + manganese vibration
260	259	260 sh		porphyrin + manganese
	225			porphyrin + Mn + Cl^-
260	162	143	118	porphyrin + Mn + Halide

TABLE V

Far infrared absorption bands of various metalloporphyrins

Fe	Co	Ni	CU	Zn	Pd	Ag	Cd	Mg	porphyrin moiety	isotope exchange	Δν	assignment	reference
	267		235	202					OEP	$Zn^{64\to68}$	1.8		Bürger et al (1972)
270									OEP	$Fe^{54\to56}$	4		Ogashi et al (1973)
	264	287	234	203	275			214	OEP			M-N	Ogashi et al (1971)
		290	246	202					porphyrin	$Zn^{64\to68}$	3.7	ν(M-N)+δ(CCN)	Ogashi et al (1972)
	349	353	348	349	352	350	352	342	protoporphyrin dimethylester			porphyrin deformation	Boucher & Katz (1967)
	348	352	346	346	346	348	346	337	hematoporphyrin			porphyrin deformation	Boucher & Katz (1967)
	366	346	348						porphin			δ(CCN)+ν(C-C, CN) + ν(M-N)	Ogashi et al (1972)
	356												
	351	356	338	337					OEP	$Ni^{58\to64}$, $Zn^{64\to68}$	2.3,-0.2		Bürger et al (1972)
	351	355	336	334	348			336	OEP			ν(M-N)+Ligand	Ogashi et al (1971)
355				381					OEP	$Fe^{54\to56}$	4		Ogashi et al (1973)
		420	392	385					porphin	$Zn^{64\to68}$	0.3	δ(CCN)	Ogashi et al (1972)

OEP - octaethylporphyrin

Δν - isotope shift (cm^{-1})

ν - stretching

δ - in plane bending

XBL 769-9649

and N_3^-) at ca 350, 340, 260, and 220 cm^{-1} show a small energy dependence on the axial halide (Ogashi, et al., 1973) similar to the small energy dependence on the axial ligand observed for MnETP-X^- in Fig. 3.

However, care is warranted in comparing vibrational peaks observed in IR and Raman Spectroscopy. Recently Kitagawa, et al., measured both the IR and Raman spectra of a variety of metal porphyrins (Kitagawa, et al., 1976b). The IR spectrum of Ni octaethylporphyrin shows a strong band at 355 cm^{-1}. On deuteration of the methine carbons this peak appears to shift to 334 cm^{-1}, implying a large contribution of methine bridge stretching to the vibrational mode. In contrast, the resonance Raman spectrum of Ni octaethylporphyrin shows a weak doublet appearing at 364 and 344 cm^{-1} which shifts only a few wavenumbers on deuteration, implying that the bands observed in the IR and Raman spectra are fortuitously close in energy but result from different vibrational modes.

Warshel, in a recent normal mode calculation on metalloporphyrins, found a large contribution of metal-pyrrole nitrogen stretching for an A_{1g} mode at 360 cm^{-1} (Warshel, 1976). It is interesting that the doublet observed by Kitagawa at 364 and 344 cm^{-1} in Ni octaethyl porphyrin shifts on substitution of Cu, Co and Pd. In addition, a weak Raman peak at 263 cm^{-1} for Cu octaethylporphyrin appears to shift to 254 cm^{-1} in the Co complex and shifts to 275 cm^{-1} in Pd. It thus appears,

that on exciting into band V of MnETP, a specific enhancement occurs for vibrational modes about the metal, such as modes involving Mn-pyrrole nitrogen stretches and axial ligand stretches.

The lack of enhancement of these vibrations in $\pi\rightarrow\pi^*$ transitions and their selective enhancement in charge transfer transitions can be accounted for by an examination of the Raman tensor. In Chapter II the Raman tensor for the vibrational transition i→j for the normal mode a was detailed as (eq. 20):

$$(\alpha_{\rho\sigma})_{gi,gj} = A'' + B'''$$

$$A'' = \sum_{v} \frac{(g^o|R_\rho|e^o)(e^o|R_\sigma|g^o)}{E_e^o - E_g^o - E_o^o + i\Gamma_e} \langle i|v\rangle\langle v|j\rangle$$

$$B''' = -\sum_{s}\sum_{a} [(g^o|R_\rho|e^o)(e^o|h_a|s^o)(s^o|R_\sigma|g^o) \qquad (1)$$

$$+ (g^o|R_\sigma|e^o)(e^o|h_a|s^o)(s^o|R_\rho|g^o)]$$

$$\chi \frac{(E_e^o - E_g^o)(E_s^o - E_g^o) + E_o^2}{[(E_e^o - E_g^o)^2 - E_o^2 + i\Gamma_e][(E_s^o - E_g^o)^2 - E_o^2]} \langle i|Q_a|j\rangle$$

where $\alpha_{\rho\sigma}$ is the $\rho\sigma$th component of the polarizability tensor and ρ and σ are coordinates within the molecule-fixed coordinate system. $|g^o\rangle$ represents the ground electronic state. $|e^o\rangle$ represents the excited electronic state in resonance. $|s^o\rangle$ is a different excited electronic state. $|i\rangle$ and $|j\rangle$ are vibrational states of the ground electronic state. $|v\rangle$ is a vibrational state of the excited electronic state $|e\rangle$. R_ρ and R_σ are the dipole moment operators. h_a is the change in the electronic Hamiltonian with the vibration of the ground state normal mode a. Q_a is the displacement of the ath normal mode. E_e and E_s are the energies of the excited states $|e\rangle$ and $|s\rangle$ and E_o is the energy of the incident laser light. Γ_e is a damping factor.

The B term contributes to Raman intensity through the vibrationally induced mixing of different electronic states produced by perturbation by the vibrational mode, a. The vibrational mode that is most active in mixing the states will show the greatest Raman intensity. This accounts for the lack of resonance enhancement of vibrations of peripheral substituents in the Raman spectrum of porphyrins. Thus, vibrations at the periphery of the ring which do not perturb the electronic states of the porphyrin sufficiently for mixing to occur between different electronic states show little resonance enhancement.

What this argument intends to show is that the enhanced vibrations of a metalloporphyrin with excitation in a charge transfer band are different from the enhanced vibrations with excitation in a $\pi \rightarrow \pi^*$ transition. It is necessary to resolve the spatial properties of $\langle e| \partial H / \partial Q_a |s\rangle$.

The only part of the electronic Hamiltonian that depends on nuclear position is the coulomb potential between electrons and nuclei (Albrecht, 1961)

i.e. $$(\partial H/\partial Q_a) = -e \sum_j \sum_n \partial(z_n/r_{jn})/\partial Q_a \qquad (2)$$

where the summation is over all of the electrons j and nuclei n, e is the electronic charge, z_n is the charge on nucleus n and r_{jn} is the distance between electron j and nucleus n. $\partial H/\partial Q_a$ is, thus, a one electron operator. For any one-electron operator, G (Albrecht, 1961; Tang and Albrecht, 1964, 1972)

$$G = -e \sum_j G(r_j) = \int G(r)\, dr \qquad (3)$$

where $G = \partial H/\partial Q_a$

and $$\langle e|G|s\rangle = \langle e|\int G(r)\rho(r)dr|s\rangle = \int \langle e|\rho(r)|s\rangle G(r)dr \qquad (4)$$

where $\langle e|\rho(r)|s\rangle$, the transition density, (Murrell and Pople, 1956; Longuet-Higgins, 1956), represents the spatial overlap of $|e\rangle$ and $|s\rangle$. As Albrecht has pointed out, for mixing by a vibrational perturbation to occur, the mixed electronic states must lie within the same region of the molecule.

We will consider excitation within three types of possible porphyrin transitions $\pi\rightarrow\pi^*$, d→d and $\pi\rightarrow$d, a charge transfer transition. The results for a $d\rightarrow\pi^*$ charge transfer transition would be the same, but these transitions would not be allowed for Mn porphyrins under D_{4h} symmetry. The ground state for Mn(III) porphyrins is illustrated in Fig. 7 of Chapter III.

$$|g\rangle = \psi_{por}\,\psi_{metal} = NA\prod_{i}^{m}\phi^2_{por_i}\,\phi^{*o}_{por}d^1_{xy}d^1_{xz}d^1_{yz}d^1_{z^2}d^o_{x^2-y^2} \quad (5)$$

The lowest energy $\pi\rightarrow\pi^*$ excited states may be written:

$$\left.\begin{aligned}|e\rangle &= N_eA\prod_{i}^{m-1}\phi^2_{por_i}\,\phi^1_{por_m}\phi^{*1}_{por}d^1_{xy}d^1_{xz}d^1_{yz}d^1_{z^2}\,d^o_{x^2-y^2}\\ |s\rangle &= N_sA\prod_{i}^{m-2}\phi^2_{por_i}\phi^1_{por_{m-1}}\phi^2_{por_m}\phi^{*1}_{por}d^1_{xy}d^1_{xz}d^1_{yz}d^1_{z^2}\,d^o_{x^2-y^2}\end{aligned}\right\} \quad (6)$$

An excited state reached by a d→d transition may be written:

$$|d\rangle = N_dA\prod_{i}^{m}\phi^2_{por_i}\,\phi^{*o}_{por}d^1_{xy}d^o_{xz}d^1_{yz}d^1_{z^2}\,d^1_{x^2-y^2} \quad (7)$$

The electron is promoted from one of the degenerate d orbitals to the $d_{x^2-y^2}$ orbital. Although there are no d→d transitions allowed under D_{4h} symmetry, a d→d transition from one of the degenerate d orbitals to the $d_{x^2-y^2}$ orbital is allowed under C_{4v} symmetry. The change from D_{4h} to C_{4v} symmetry in a metalloporphyrin can occur by axial ligation. An excited state reached by an allowed charge transfer excitation of an electron from the porphyrin to the metal may be written

$$|c\rangle = N_cA\prod_{i}^{m-1}\phi^2_{por_i}\,\phi^1_{por_m}\phi^{*o}_{por}d^1_{xy}d^1_{xz}d^2_{yz}d^1_{z^2}\,d^o_{x^2-y^2} \quad (8)$$

Ψ_{por} and Ψ_{metal} represent the wavefunction of the porphyrin and metal, respectively, $|e\rangle$ is the excited state in resonance. N is the normalization factor. A is the anti-symmetrizer. ϕ_{por_i} are the occupied molecular orbitals in the ground state configuration of the porphyrin. ϕ^*_{por} is the lowest unoccupied porphyrin molecular orbital. The product of orbitals is in order of increasing energy (Boucher, 1972). $d_{xy}, d_{xz}, d_{yz}, d_{z^2}, d_{x^2-y^2}$ represent the atomic orbitals of the manganese. The superscripts indicate the electron occupancy of the orbitals.

An examination of the transition density matrix element indicates which vibrational modes are enhanced by excitation within a particular type of electronic transition. The types of transition density matrix elements that must be examined are between states reached by $\pi \rightarrow \pi^*$ transitions, charge transfer transitions and $d \rightarrow d$ transitions.

If the two states $|e\rangle$ and $|s\rangle$ that couple are both reached by a $\pi \rightarrow \pi^*$ transition:

$$\langle e|\rho(r)|s\rangle = -e\int \phi^1_{por_{m-1}}\, \delta(r-r_j)\, \phi^1_{por_m}\, dr_j \qquad (9)$$

since the integral equals unity for electrons not involved in the transition. This is a spatial integral over the two highest energy occupied molecular orbitals of the ground state. Spatially, these orbitals occur within the porphyrin macrocycle and occupy similar regions; as a result, the vibrational modes, a, that are picked out by the electron density matrix element $\langle e|\partial\mu/\partial Q_a|s\rangle$ are those within the

macrocycle.

For coupling of a charge transfer band in which an electron goes to a d_{yz} or d_{xz} orbital, for example, with an excited state reached by a $\pi \rightarrow \pi^*$ transition from the same occupied molecular orbital, the required vibrational perturbation matrix element is $\langle c|\partial H/\partial Q_a|e\rangle$ and the transition density is:

$$\langle c|\rho(r)|e\rangle = -e\int d^1_{yz}\delta(r-r_j)\phi^{*1}_{por}dr_j \qquad (10)$$

This integral represents the spatial overlap of a d orbital of the metal and a π orbital of the porphyrin. The region of maximum overlap will occur around the metal and pyrrole nitrogens. The vibrational modes picked out by the transition density operator in this case will be those around the central metal, such as vibrations involving the manganese-pyrrole nitrogen bonds. Vibrations involving the axial ligand on the manganese may also be picked out, because the metal-ligand vibration should perturb the d orbitals, affecting the excited state reached by the charge transfer transition.

For coupling of two different excited states formed by charge transfer transitions in which the excitation is from the same porphyrin ground state occupied molecular orbital, then

$$\langle c_1|\rho(r)|c_2\rangle = -e\int d^1_1\delta(r-r_j)d^1_2dr_j \qquad (11)$$

where $|c_1\rangle$ and $|c_2\rangle$ represent two different charge transfer states and d_1 and d_2 are the two different d orbitals that

are occupied by the promoted electron. This term will be small since the two different d orbitals occupy different regions of space, unless axial ligand vibrations and the constraints imposed by the pyrrole nitrogens mix the d orbitals. This may be the term that allows the vibrations of axial ligands to be enhanced. For coupling between two charge transfer states $|c_1\rangle$ and $|c_3\rangle$ that terminate in the same d orbital but are initiated from different porphyrin π orbitals

$$\langle c_1|\rho(r)|c_3\rangle = -e\int \phi^1_{por_m}\,\delta(r-r_j)\,\phi^1_{por_{m-1}}\,dr_j \qquad (12)$$

and vibrations active in the macrocycle will show intensity. States differing by the occupancy of more than one electron cannot couple under the vibrational perturbation so that charge transfer transitions differing in occupancy of both porphyrin and d orbitals cannot couple.

Coupling may not occur between a state $|d\rangle$, reached by a d→d transition and a state $|e\rangle$, reached by a $\pi\rightarrow\pi^*$ transition because a difference in occupancy of two electrons exists between the two states. State $|d\rangle$ may couple with a charge transfer state $|c\rangle$ if the electron is promoted to the same d orbital in both transitions. The vibrations picked out by this transition density matrix element involve the central metal.

Looking at the form of the polarizability tensor for excitation within (1) a charge transfer band and (2) a $\pi \rightarrow \pi^*$ transition we find:

1. There are terms in the polarizability tensor containing $\langle c|\rho(r)|d\rangle$, $\langle c|\rho(r)|s\rangle$ and $\langle c_1|\rho(r)|c_2\rangle$. The $\langle c|\rho(r)|s\rangle$ and $\langle c|\rho(r)|d\rangle$ terms enhance vibrations active about the metal while the $\langle c_1|\rho(r)|c_2\rangle$ terms enhance vibrations both within the macrocycle and around the metal, including vibrations involving the axial ligand.

2. There are terms containing both $\langle e|\rho(r)|s\rangle$ and $\langle e|\rho(r)|c\rangle$. $\langle e|\rho(r)|s\rangle$ enhances vibrations active in the macrocycle, while $\langle e|\rho(r)|c\rangle$ enhances vibrations about the metal.

In this argument we have neglected configuration interaction of the Q and B states but, as Gouterman (Gouterman, 1959, 1961, 1973) has pointed out, this is a major phenomenon in porphyrins; as a result the B and Q states are mixed and the excited states should be written more precisely:

$$|Q\rangle = M|Q^o\rangle + N|B^o\rangle \quad \text{and} \quad |B\rangle = P|B^o\rangle + T|Q^o\rangle$$

where M,N,P and T are the coupling coefficients and $|Q^o\rangle$ and $|B^o\rangle$ and the zero order $|Q\rangle$ and $|B\rangle$ states. The transition density matrix elements are then:

$$\langle Q|\rho(r)|B\rangle = MT\langle Q^o|\rho(r)|Q^o\rangle + NP\langle B^o|\rho(r)|B^o\rangle + (MP+NT)\langle B^o|\rho(r)|Q^o\rangle \qquad (13)$$

The overlap of the $|Q\rangle$ and $|B\rangle$ states with themselves would

equal unity. As a result the terms in the polarizability tensor containing $\langle Q|\rho(r)|B\rangle$ would dominate and, for excitation in a Q band, we would expect to see vibrations in the porphyrin macrocycle as the major enhanced vibrations.

Differentiation of metal and porphyrin vibrational modes can also occur via the diagonal part of the polarizability tensor, Albrecht's A term (Albrecht and Hutley, 1971). The A term enhances those vibrational modes which have large Franck-Condon overlap factors within the resonant electronic transition. Excitation within a $\pi\rightarrow\pi^*$ transition will enhance vibrations which are associated with the porphyrin macrocycle, while excitation in a charge transfer transition will enhance both vibrations in the macrocycle and vibrations about the metal. This results from an examination of the A term.

$$A = \sum_{v}\left[\frac{\langle g|R_o|e\rangle\langle e|R_\rho|g\rangle}{E_e^o - E_g^o - E_o^o + i\Gamma}\right]\langle i|v\rangle\langle v|j\rangle \qquad (14)$$

Using the Born-Oppenheimer approximation, the wavefunction for a molecule in a state $|e\rangle$ may be separated into an electronic and vibrational wavefunction

$$\psi_e = \Phi(q,Q)\chi(Q) \qquad (15)$$

where Φ is the electronic wavefunction which is dependent on the electronic coordinates q, and the nuclear coordinates Q; χ represents the vibrational wavefunction and is a function of only the nuclear coordinates. $\chi(Q)$ may be expanded

as the product of orthonormal modes, a

$$\chi(Q) = \prod_a \Lambda_a^v \tag{16}$$

where the superscript labels the quantum level of the vibrational mode a. It is convenient to separate $\chi(Q)$ into 2 parts, $\chi(Q) = \chi_p(Q)\ \chi_m(Q)$. $\chi_p(Q)$ represents modes which are mainly associated with the porphyrin macrocycle and $\chi_m(Q)$ represents modes associated with the metal. These two sets may be differentiated experimentally by their energy dependence with metal or axial ligand substitution, or theoretically by a correlation of the atoms which contribute to each of the normal modes.

We may then rewrite equations (5)-(7) as:

$$\begin{aligned} |gi\rangle &= \Phi_{por}\ \Phi_{met}\ \chi_p^i\ \chi_m^i \\ |gj\rangle &= \Phi_{por}\ \Phi_{met}\ \chi_p^j\ \chi_m^j \\ |ev\rangle &= \Phi_{por}^e\ \Phi_{met}\ \chi_p^{ev}\chi_m^v \\ |cu\rangle &= \Phi_{por}^{*+}\ \Phi_{met}^{*-}\ \chi_p^{u^{*+}}\ \chi_m^{u^{*-}} \end{aligned} \tag{17}$$

For resonance with state $|e\rangle$, a state reached by $\pi\rightarrow\pi^*$ transition, the Franck-Condon factors have the form:

$$\sum_v \langle\chi_p^j\ \chi_m^j|\chi_p^{ev}\chi_m^v\rangle\langle\chi_p^{ev}\chi_m^v|\chi_p^i\ \chi_m^i\rangle = \tag{18}$$

$$\sum_v \left|\langle\chi_p^j|\chi_p^{ev}\rangle\langle\chi_p^{ev}|\chi_p^i\rangle\right|\ \left|\langle\chi_m^j|\chi_m^v\rangle\langle\chi_m^v|\chi_m^i\rangle\right|$$

Since the $\pi \rightarrow \pi^*$ transition occurs mainly in the porphyrin macrocycle, the maximum change in the electronic configuration of the excited state vs. the ground state occurs within the macrocycle as opposed to about the metal. Concomitantly, the equilibrium nuclear configuration shows its maximum change within the macrocycle. This results in different potentials within the Hamiltonian for the excited state compared to the ground state. This means that

$$\langle \chi_p^j | \chi_p^{ev} \rangle \langle \chi_p^{ev} | \chi_p^i \rangle \neq \delta_{ij} \qquad (19)$$

and Raman intensity may derive from the A term with $j = i+1$.

However, the change in potential about the metal is small, and

$$\langle \chi_m^j | \chi_m^v \rangle \langle \chi_m^v | \chi_m^i \rangle \cong \delta_{ij} \qquad (20)$$

We would not expect to see metal modes so enhanced as porphyrin modes by the A term.

Following a similar argument, it can be shown that both porphyrin and metal modes will be enhanced by the A term if excitation occurs in a charge transfer transition, since a large change in potential occurs in the macrocycle and about the metal.

The above arguments provide a means of distinguishing a charge transfer band from a $\pi \rightarrow \pi^*$ transition. The vibrations most enhanced by excitation in band V are vibrations involving the central metal, while the vibrations most enhanced by excitation in bands III and IV are porphyrin

macrocycle vibrations. Thus, band V is assigned to a charge transfer transition, and bands III and IV are identified as the α and β bands of metalloporphyrins, respectively.

A comparison of the resonance Raman spectra of MnETP in bands III and IV with the resonance Raman spectra of CuETP(I) also favors these assignments (Mendelsohn, et al., 1975b). The resonance Raman spectra of CuETP(I) excited in the α and β bands show many similarities to the Raman spectra of MnETP excited in bands III and IV. In all of these spectra the enhanced vibrations are those of the porphyrin macrocycle. The vibrations at 757, 988 and 1313 cm^{-1} in MnETP are maximally enhanced with excitation in band III. Analogously, vibrations at 754, 984 and 1314 cm^{-1} in the spectra of CuETP(I) are maximally enhanced with excitation in the α band. The vibration at 1374 cm^{-1} in MnETP shows maximum enhancement with excitation in band IV. The corresponding vibration in CuETP(I) at 1380 cm^{-1} shows maximum enhancement with excitation in the β band.

Many of the low frequency vibrations enhanced by excitation in the charge transfer band are metal and axial ligand dependent. Some of these vibrations may be assigned to manganese-halide stretches. The intensity but not the frequency of the vibration at 329 cm^{-1} is strongly dependent on the axial ligand (Fig. 3). Therefore, it may be assumed that this band is only indirectly influenced by the axial ligand. One possible way to account for this intensity

dependence is to assume that the 329 cm^{-1} peak is an out-of-plane vibrational mode of the manganese porphyrin. As the ligand increases in size the metal is pulled out of the plane of the porphyrin (Felton, et al., 1974; Boucher, 1973). When the metal lies farther out of the plane, an out-of-plane vibration which puts the metal back into the ring will show increasing enhancement. This could be due to increased coupling between the excited charge transfer state and the π^* state.

The out-of-plane distance of the metal with respect to the porphyrin also has an effect on the molar absorptivity (Boucher 1970, 1972, 1973). For the fluoride complex the ratio of band V to band VI is high. It decreases as the size of the anion increases. That this must be an effect of the out-of-plane distance of the metal and is not an effect of the ligating atom can be shown by a comparison of the absorption spectra of MnETP with imidazole and piperidine as ligands. Nonbonded interaction of the N-H with the porphyrin ring forces the metal further out of the ring in the piperidine complex than in the imidazole complex (Boucher, 1973). The molar absorptivity of band V in the piperidine complex is only 60% of the value for the imidazole complex. The further the metal lies out of the plane of the porphyrin the more unfavorable is d and π orbital overlap and the less allowed the transition will be.

After completion of this work two studies on the

resonance Raman spectra of manganese (III) porphyrins were reported (Gaughan, et al., 1975; Shelnutt, et al., 1976). The first report by Gaughan, et al., also noted selective enhancement of low frequency Raman modes upon excitation in band V of Mn(III) tetraphenylporphyrin. However, the intensity pattern of these low frequency peaks were radically different. The most prominent feature that they observed was a band at 400 cm^{-1}. Both their study and ours show little dependence of the intensity or frequency of this band on the axial ligand.

In contrast to our study, Gaughan, et al., did not observe enhancement of axial ligand vibrations. Yet, the chloride and bromide complexes of both Mn(III) etioporphyrin I and Mn(III) hematoporphyrin IX show enhancement of the Mn halide vibrations when excitation is in band V. The lack of axial ligand vibrations in the Raman spectra of Mn(III) tetraphenylporphyrin may reflect a difference in the structure of Mn(III) tetraphenylporphyrin compared to Mn(III) etioporphyrin, or it may indicate that a reevaluation of the resonance Raman spectra of Mn(III) tetraphenylporphyrin is in order.

The second study, by Shelnutt, et al., (Shelnutt et al., 1976) also investigated Mn(III) etioporphyrin. They observed enhancement of low frequency modes upon excitation in band V. However, Shelnutt, et al., in their report emphasized the enhancement profiles observed in band V. To account for the nonsymmetric doubly peaked excitation profiles, they

invoked a non-adiabatic coupling mechanism. We believe that the excitation profiles reported may alternatively be accounted for by the presence of a second electronic transition underlying band V. A study of the absorption spectrum of band V of MnETP-I^- in CS_2 (Chapter III) clearly shows a high energy shoulder evident at 480 nm, while the main peak occurs at 505 nm. The MCD spectrum shows the presence of an electronic transition at about 480 nm. The intensity and the frequency separation of this electronic transition from the main peak is a function of the axial ligand and the solvent system. Thus, the excitation profiles that Shelnutt, et al., report may be a consequence of the presence of two transitions underlying band V. In this event, non-adiabatic coupling need not be invoked to account for the Raman excitation profiles. Furthermore, the fixed laser frequencies used and the uncertainties in intensity determinations indicated by the error bars in Shelnutt, et al., make a precise determination of the excitation profile maxima difficult.

Band VI

As Chapter III indicated, band VI shows a very complex absorption and MCD spectrum, indicating that numerous electronic transitions underlie band VI. A resonance Raman spectrum of MnETP in n-butanol excited at 3577.1Å is shown in Figure 5. The broad background in Fig. 5 between 200-500 cm^{-1} results from the Raman spectrum of the quartz

Fig. IV-5. Resonance Raman spectrum of MnETP in n-butanol. λ_{ex} = 3577.1 Å, energy = 10^{-4} joule/pulse. Pulse repetition rate 10 Hz, scan speed = 4.5 Å/min. Slitwidth = 1.0 Å. Monochromator was used in second order. Conc ~ 10^{-3}M.

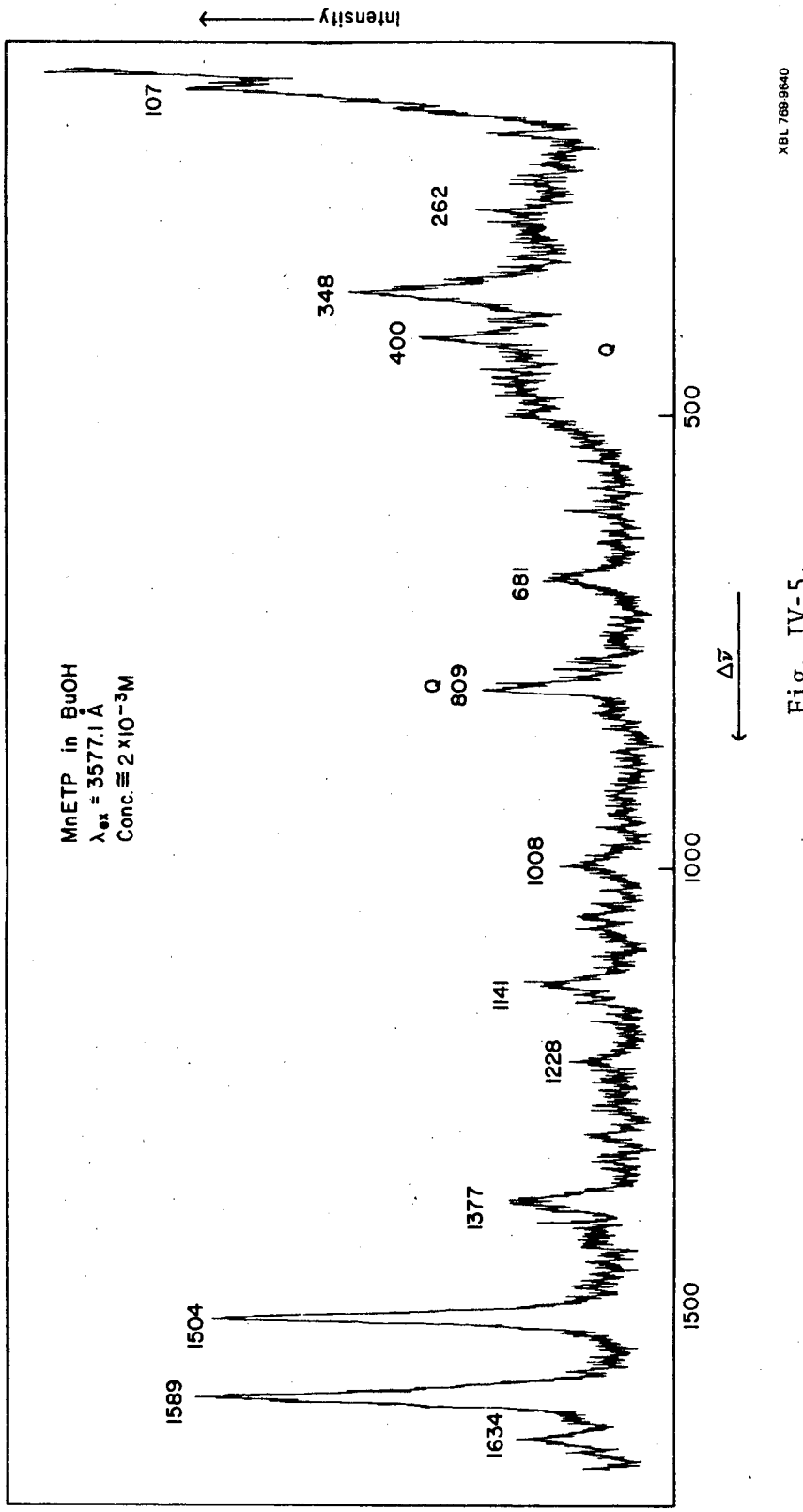

Fig. IV-5.

cuvette that contains the MnETP solution.

The Raman peaks of the solvent, n-butanol, are not visible over the background. All of the features in Fig. 5 except for the broad background below 500 cm^{-1} and the 809 cm^{-1} peaks are due to MnETP. The 809 cm^{-1} peak is a composite band resulting from the overlap of the Raman spectrum of quartz and the resonance Raman spectrum of MnETP. Each of the Raman peaks in Fig. 5 has a close correspondence to the resonance Raman spectra obtained by excitation in Bands III, IV and V (Fig. 2). The major difference is the increase in enhancement of the 1504 cm^{-1} peak and the disappearance of the 1566 cm^{-1} peak. In contrast to depolarization measurements with excitation in bands III, IV and V, which indicated that the peak at 1586 cm^{-1} was anomalously polarized, depolarization measurements in band VI show that the band is polarized. Excitation profiles for the Raman peaks observed in band VI are shown in Fig. 6. Since the Raman peaks for the solvent, n-butanol were not visible over the background, the broad Raman spectrum of quartz between 200-500 cm^{-1} was used as an internal standard. The intensities of the Raman peaks in each of the Raman spectra used in the excitation profiles were normalized to the quartz band. The sampling occurred by 75°scattering from a quartz curvette and the geometry was held fixed between spectra. With excitation below 330 nm the Raman peaks of the solvent are observed over the background. The ratios of the intensities of the solvent peaks to the quartz background remains constant to within 15% for the spectra excited at wavelengths below 330 nm.

A number of features are evident in Fig. 6. The 1504, 1589 and 1377 cm^{-1} Raman bands show their maximum intensity

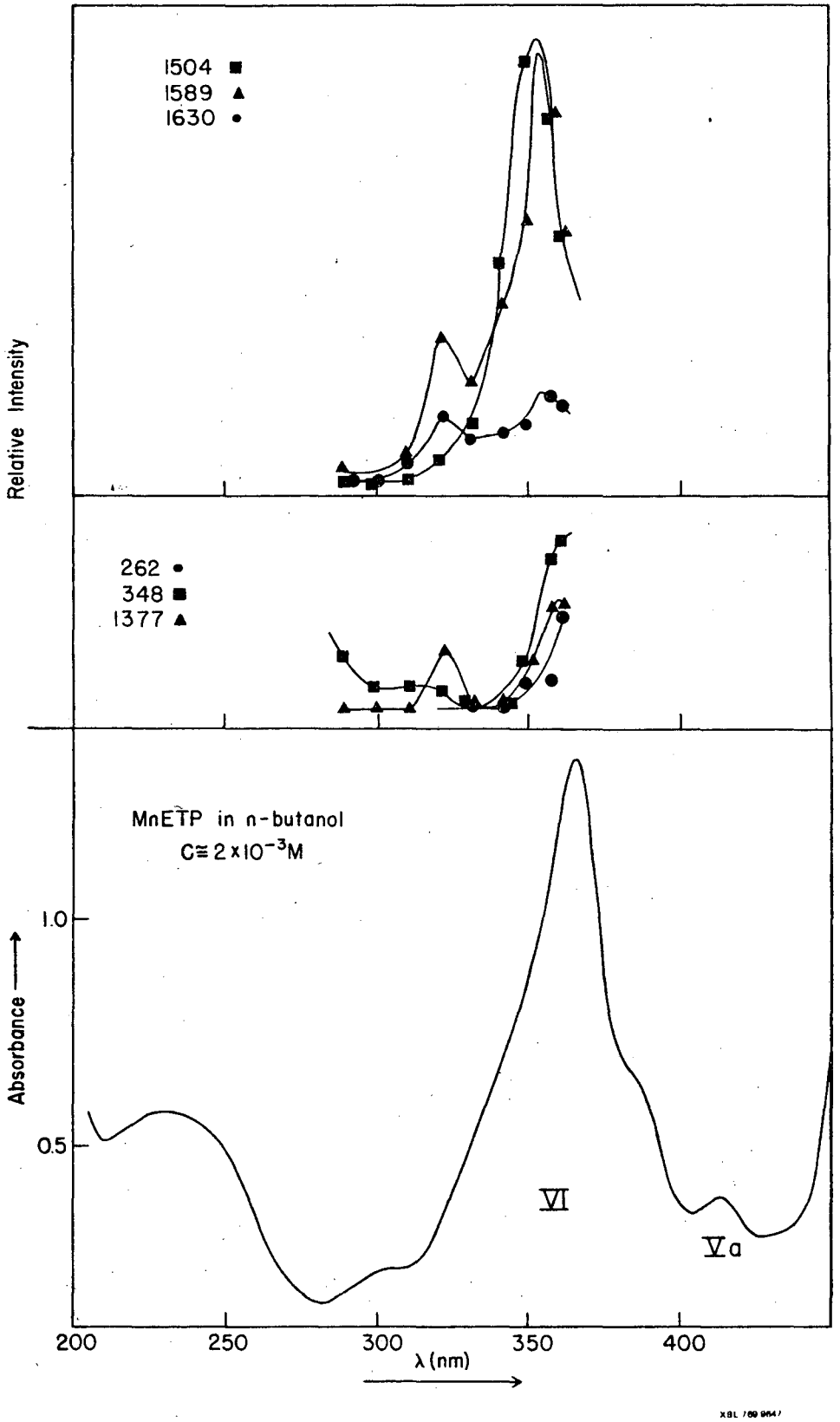

Fig. IV-6. Absorption spectrum and excitation profiles in band VI for some vibrations of MnETP-acetate in n-butanol.

and 1633 cm^{-1} peaks at about 320 nm. The 262 and 348 cm^{-1} peaks appear to be in resonance with an electronic transition which lies above 362 nm. Unfortunately, due to the lack of laser intensity above 362 nm, the remainder of band VI lying to longer wavelength could not be probed.

The peak in the excitation at ca 320 nm has no corresponding feature in the room temperature absorption spectrum, or in either the room or low temperature MCD spectrum. However, a faint shoulder occurs in the low temperature (77°K) absorption spectrum of MnETP in MCP. The excitation profile indicates that an electronic transition which is not resolvable in the MCD and is poorly resolved in absorption lies at about 320 nm. In addition, the selective enhancement of higher energy Raman bands (>1000 cm^{-1}) suggests that the electronic transition at 320 nm results from a $\pi \rightarrow \pi^*$ transition. An interesting point is the lack of enhancement of the 1504 cm^{-1} peak at 320 cm^{-1}. Another, larger maximum occurs for the 1634, 1589 and 1504 cm^{-1} vibrations at ca 354 nm, 3000 cm^{-1} to lower energy than the ca 320 nm maximum. The 1377 cm^{-1} vibration shows its maximum intensity a few hundred wavenumbers to lower energy (ca 359 nm) from the excitation profile maxima of the 1634, 1589 and 1504 cm^{-1} bands. The intensity of the 348 and 262 cm^{-1} bands continues to rise at 362 nm.

There is no absorption or MCD feature which suggests the presence of an electronic transition at 355 nm to account for the excitation profile maxima. The progression of excitation profile maxima exhibited by the set of peaks at 1634, 1589 and 1504 cm^{-1}, the peak at 1377 cm^{-1} and the two peaks at 348 and 262 cm^{-1} suggests that the resonance Raman bands are in resonance with a 0-1 vibronic overtone of a 0-0 electronic transition lying to lower energy. An examination of the denominator of the resonance Raman tensor expression (eq. 1) indicates that an intensity maximum will occur for Raman scattering at the 0-0 vibronic level of an electronic transition. The energy denominator, $E_e^o - E_g^o - E_o + i\Gamma$ vanishes, except for the damping factor. At the 0-1 vibronic overtone, $E_e^o(0\text{-}1) = E_e^o + h\Omega$, where Ω is the vibrational frequency. When $E_o = E_e^o + h\Omega$, the denominator again vanishes except for the damping factor, predicting a progression of excitation profile maxima which occur at an energy equal to the sum of the energy of the (0-0) electronic transition and the energy of the vibrational mode. Spiro (Spiro, 1975) experimentally observed the excitation profile progressions in his studies of ferrocytochrome c excited in the β band. As the theory predicts, the excitation profile maximum for a vibration of energy $h\Omega$ in ferrocytochrome c occurs at an energy, $h\Omega$, greater than the energy of the absorption maximum of the α band.

The 1634, 1589 and 1504 cm^{-1} bands show excitation profile maxima at about 354 nm (28,250 cm^{-1}).

If the excitation profile maxima are a result of enhancement in a 0-1 vibronic transition, subtraction of 1550 cm^{-1} from the excitation profile maximum predicts the 0-0 transition to be at ca 26,700 cm^{-1}. Both the room and low temperature MCD spectra show a derivative shaped feature with a cross-over at 26,700. On decreasing the temperature, the MCD feature narrows but the cross-over does not shift. Thus, the feature which has the shape of an A term and has a cross-over at ~26,700 cm^{-1} may result from the (0-0) component of an electronic transition.

Verma and Bernstein noted in an excitation profile study of protohemin (Verma and Bernstein, 1974b) that a spin-state sensitive, polarized vibration at ~1500 cm^{-1} appeared to be selectively enhanced by the Soret band. By analogy, the selective enhancement of the 1500 cm^{-1}, polarized vibration in band VI suggests a Soret band contribution. However, the enhancement of the low frequency 262,348 and 399 cm^{-1}, vibrations which appear to have significant contribution from metal - pyrrole nitrogen stretching vibrations and which may be diagnostic of charge transfer character, suggests a change transfer contribution to band VI. Unfortunately, there have been few reports of the resonance Raman spectra of porphyrins excitated in the Soret band; this is due to the unavailability of laser lines in the region between 360 - 440 nm. Lutz (Lutz, 1974) reported Raman spectra excited at the maximum of the absorption band of chlorophyll b. The dominant features in the Raman

spectrum occurred at energies above 1000 cm^{-1}. Nafie, et al., (Nafie, et al., 1973) excited on the high energy side of the Soret band of ferrocytochrome c. They observed only very weak features below 600 cm^{-1}. On the other hand, excitation at 4416 Å, close to the Soret band of cytochrome c oxidase (Salmeen, et al., 1973) or of hemoglobin and myoglobin (Rimai, et al., 1975) resulted in enhancement of low frequency modes. For example, vibrations at 215 and 340 cm^{-1} in cytochrome c oxidase, were enhanced to the extent that they were comparable in intensity to the higher frequency modes.

The limited data available suggests that band VI contains both a charge transfer and Soret transition. The derivative shaped feature at ca 26,700 cm^{-1} may result from a A term occuring at a 0-0 electronic transition and the high energy shoulder in the absorption spectrum of band VI may result from the contribution of a 0-1 vibronic overtone.

CHROMIUM (III) TETRAPHENYLPORPHIN

The absorption spectrum of chromium (III) tetraphenylporphin (CrTPP) in the visible and near UV spectral regions qualitatively appears similar to the absorption spectra of other "normal" metalloporphyrins (Fig. 7). Two absorption bands, III and IV, which have been assigned to the α and β bands, are observed between 500-610 nm (Gouterman, et al., 1975). The very intense absorption band at 447 nm for CrTPP-Cl^- in $CHCl_3$ (band V) has been assigned to the Soret band (Gouterman, et al., 1975). However, additional bands occur in both the near IR and UV spectral regions.

The UV absorption spectrum of CrTPP-Cl^- shows a complex series of moderately strong ($\varepsilon \cong 2 \times 10^4$) bands (labeled VI) between 280-400 nm, while several weak bands (I and II) ($\varepsilon \cong 10^3$) are found in the near IR between 650-800 nm (Gouterman, et al., 1975). Additionally, a shoulder appears on the short wavelength side of band IV. Gouterman has proposed that the extra bands in the UV may result from charge transfer transitions. He suggests, that the energies of charge transfer transitions from the a_{1u}, a_{2u} porphyrin π orbitals to the d_{xz}, d_{yz} metal orbitals for the series of metalloporphyrins containing Cr(III), Mn(III) and Fe(III), occur in the order Cr(III)> Mn(III)> Fe(III). Thus, charge transfer bands would occur in the visible spectral region for Fe(III) porphyrins, in the blue for Mn(III) porphyrins and in the UV for Cr(III) porphyrins

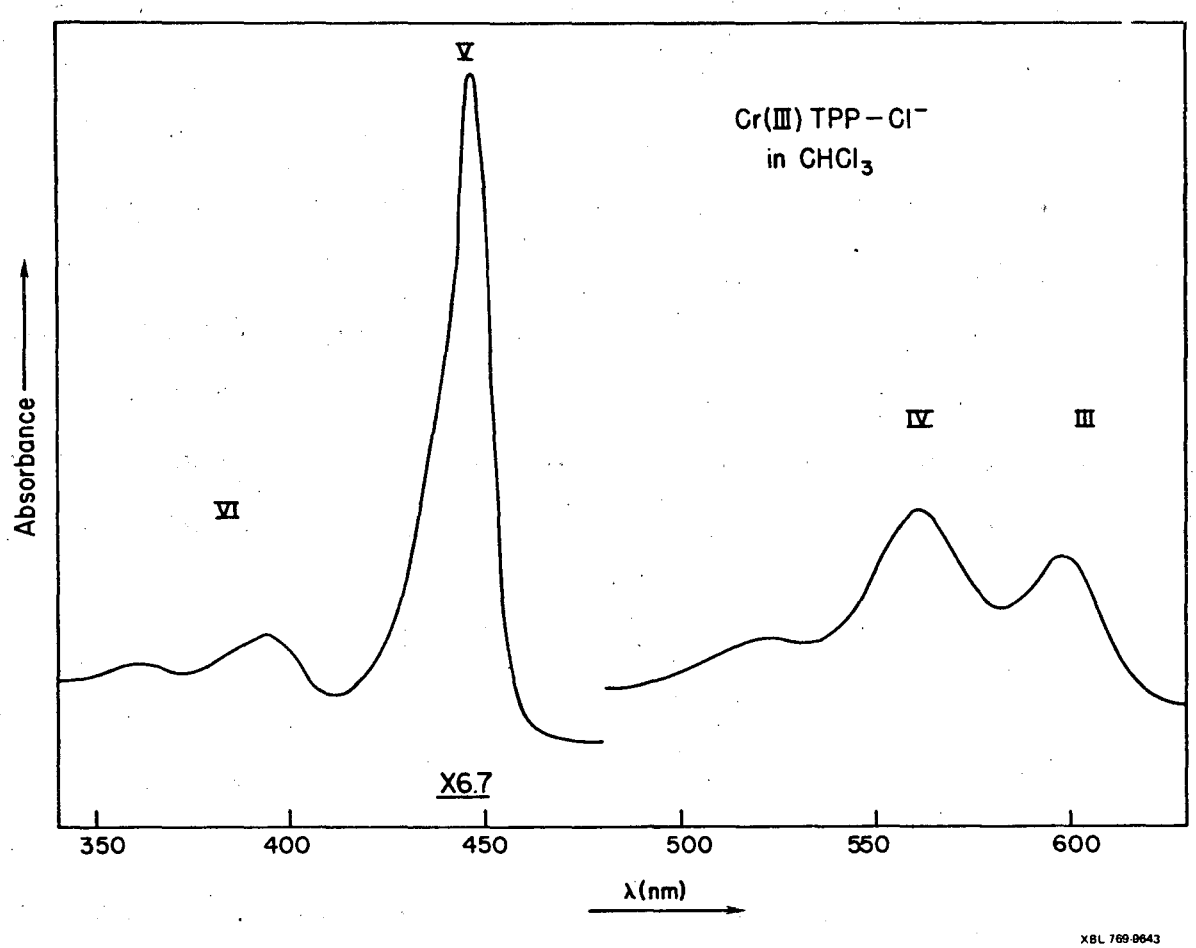

Fig. IV-7. Absorption spectrum of Cr(III)tetraphenylporphin-Cl^- in $CHCl_3$. The bands are labeled after Gouterman et al., (Gouterman, et al., 1975).

(Gouterman, et al., 1975).

To test the assignments of bands III, IV and V, resonance Raman spectra were measured on a solution of Cr(III) TPP-Cl^- in CS_2. Fig. 8 shows the absorption spectrum of Cr(III) TPP-Cl^- in CS_2 and indicates the positions of the excitation wavelengths used in the resonance Raman spectra shown in Figs. 9, 10 and 11.

The resonance Raman spectrum of Cr(III)TPP-Cl^- obtained by excitation at 4581.0Å in band V (Fig. 9) shows as its most prominent feature a peak at 400 cm^{-1}. Other features appear at higher frequencies (>800 cm^{-1}). However, except for the very weak peak at 336 cm^{-1} the region below 400 cm^{-1} is blank. The very strong peak at 656 cm^{-1} and the moderately intense peak at ca 800 cm^{-1} are due to CS_2. Spectra obtained with excitation at 4518.2Å, 4552.9Å and 4619Å show spectra similar to Fig. 9. The major difference lies in the variation of enhancement of the Cr(III)TPP peaks over the 656 and 800 cm^{-1} peaks of the solvent, CS_2.

Table VI lists the Raman peaks observed for CrTPP-Cl in CS_2. The resonance Raman peaks observed by excitation in band V of CrTPP correlate well with Raman spectra reported for free base tetraphenylporphin (Mendelsohn, et al., 1975a) and for various metal complexes (Mendelsohn, et al., 1975a; Solovyov, et al., 1973; Gaughan, et al., 1975; Shelnutt, et al., 1976). For example, Raman peaks are observed at 1005, 1232, 1372, 1495, 1548 and 1593 cm^{-1} for the free-base form of tetraphenylporphin (Mendelsohn, et al., 1975a). For

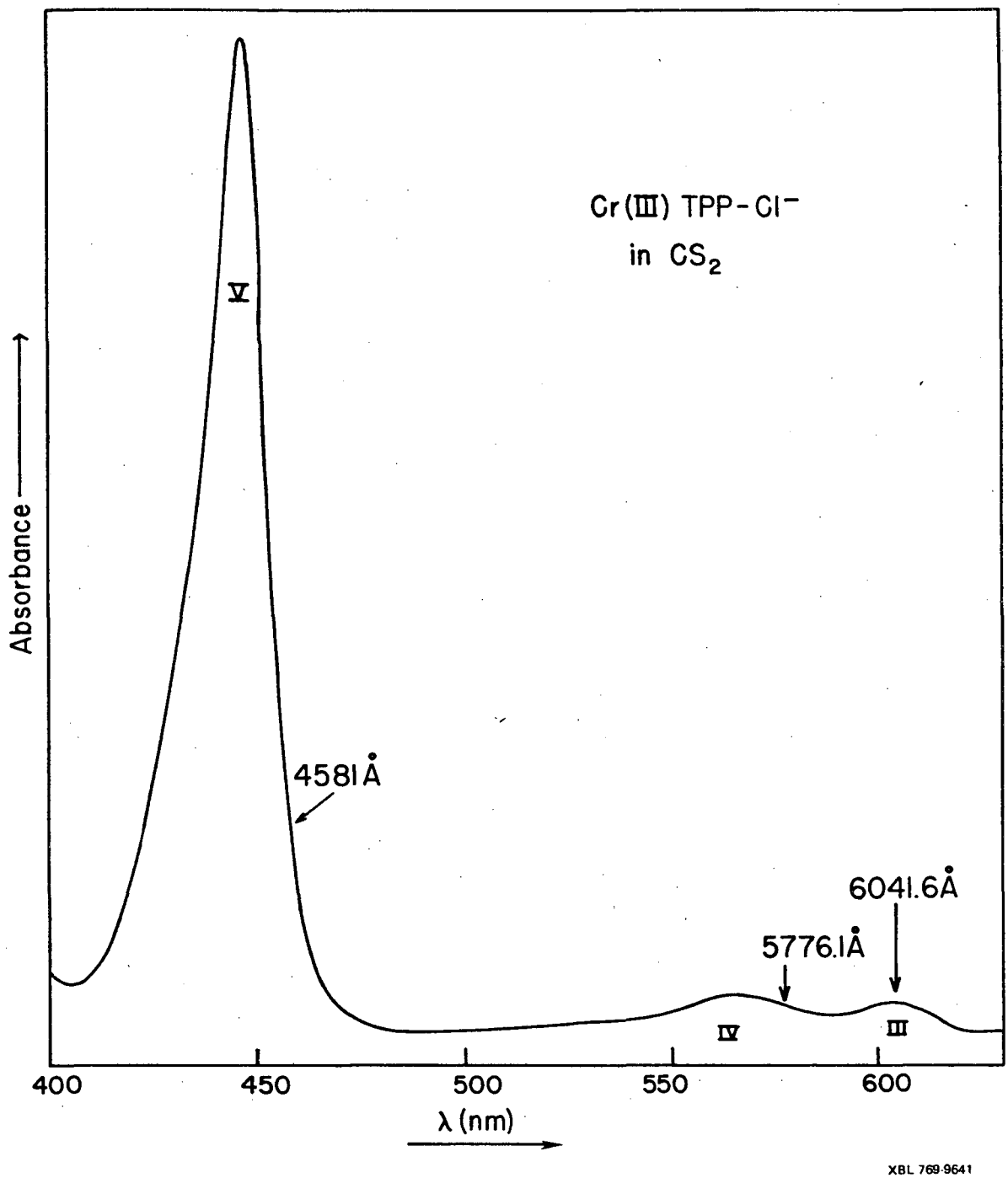

Fig. IV-8. Absorption spectrum of Cr(III) tetraphenylporphin in CS_2. Pathlength = 1 cm. The bands are labeled after Gouterman (Gouterman, et al., 1975). The position of the laser lines used in the Raman spectra are indicated.

Fig. IV-9. Resonance Raman spectrum of Cr(III)tetraphenylporphin in CS_2. λ_{ex} = 4581.0. Energy = 7×10^{-4} joule/pulse. Pulse repetition rate = 10 Hz. Scan speed = 9 Å/min, Slitwidth = 0.85 Å, conc ~ 10^{-3}M. Position of solvent bands is indicated in the figure.

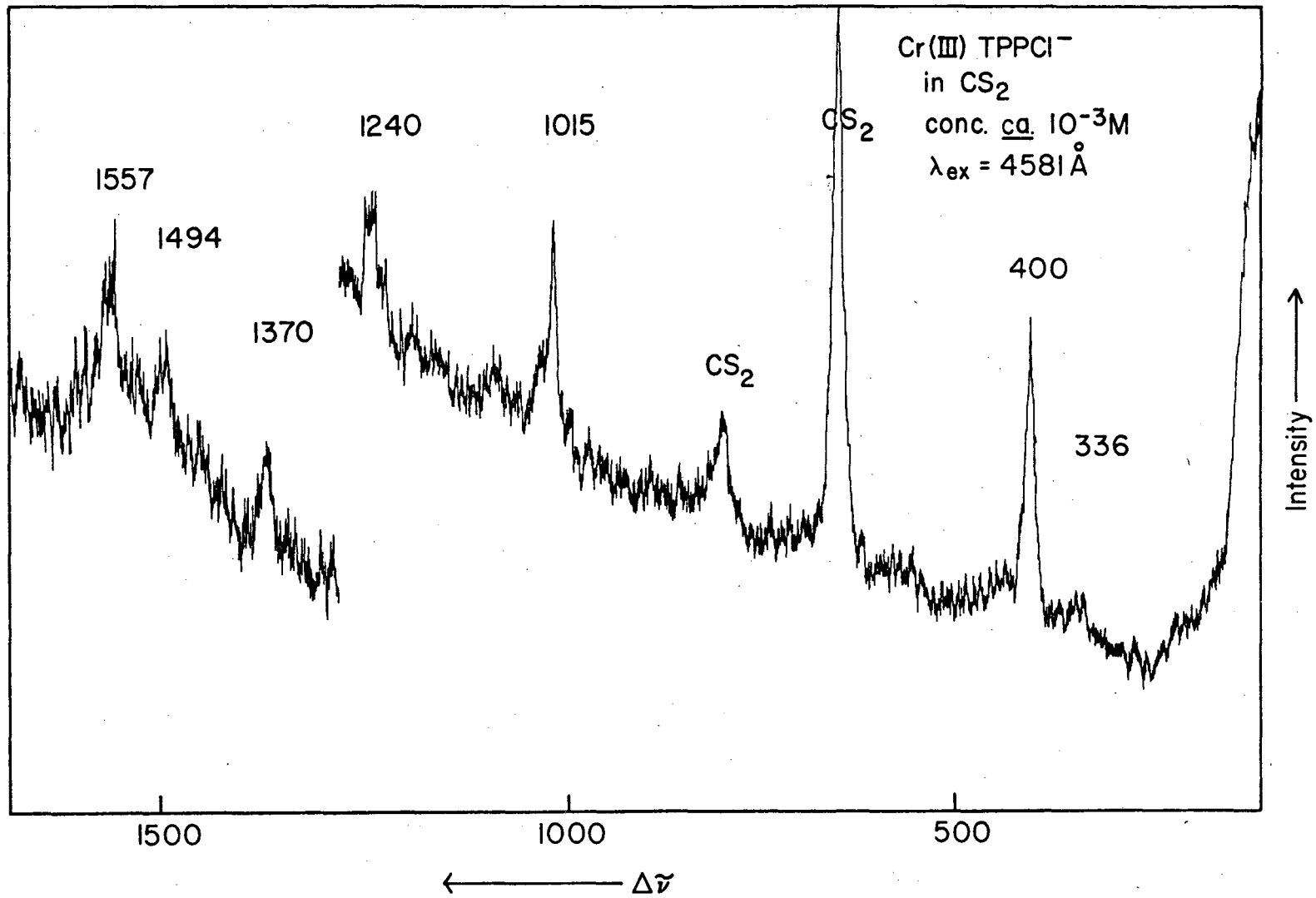

Fig. IV-9.

XBL 769-9644

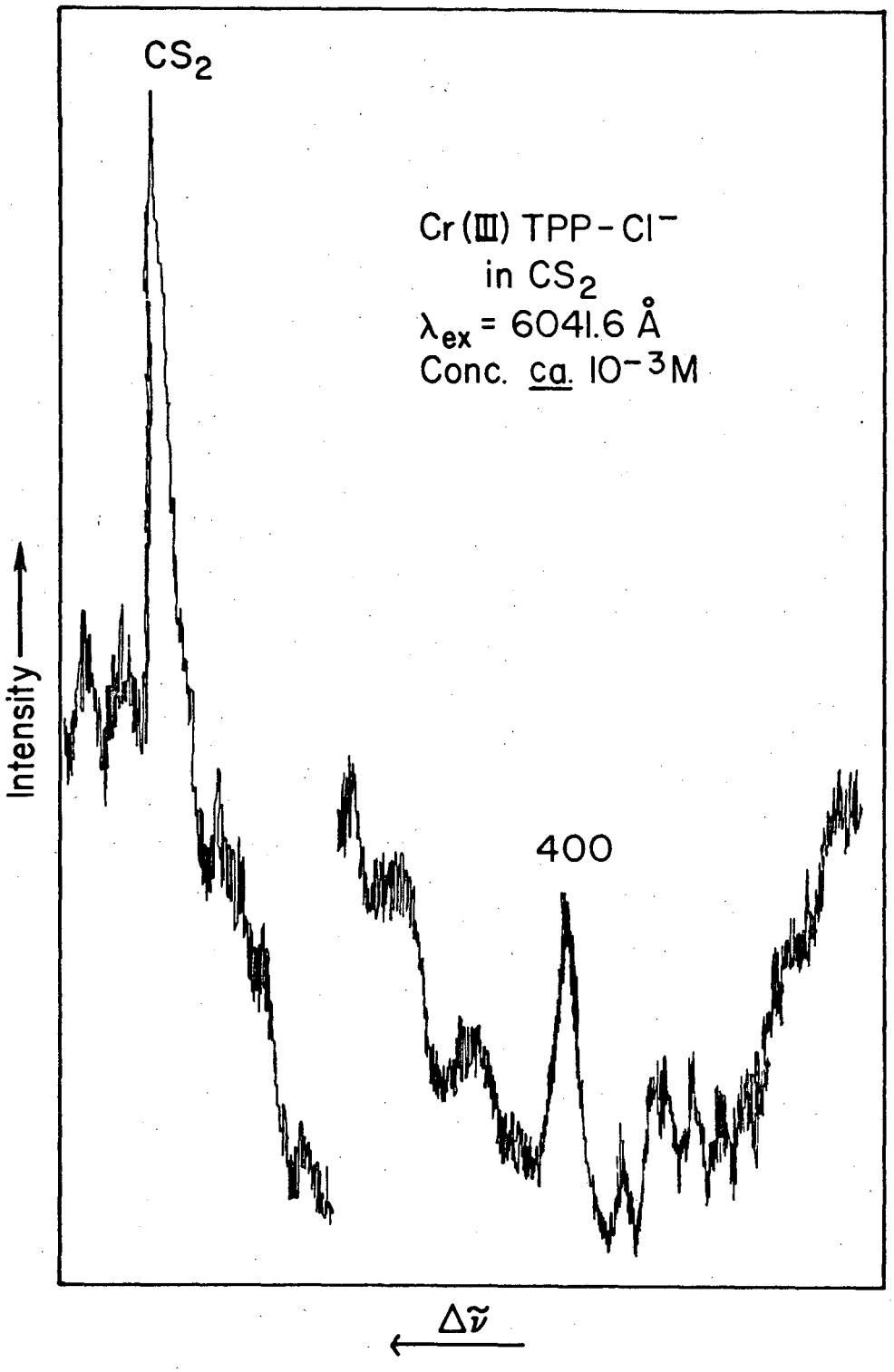

Fig. IV-10. Resonance Raman spectrum of Cr(III)tetraphenylporphin in CS_2. λ_{ex} = 6041.6 Å. Energy = 3×10^{-3} joule/pulse. Pulse repetition rate = 30 Hz. Scan speed = 14 Å/min. Slitwidth = 1.5 Å. Conc ~ 10^{-3}M. Position of solvent band is indicated in figure.

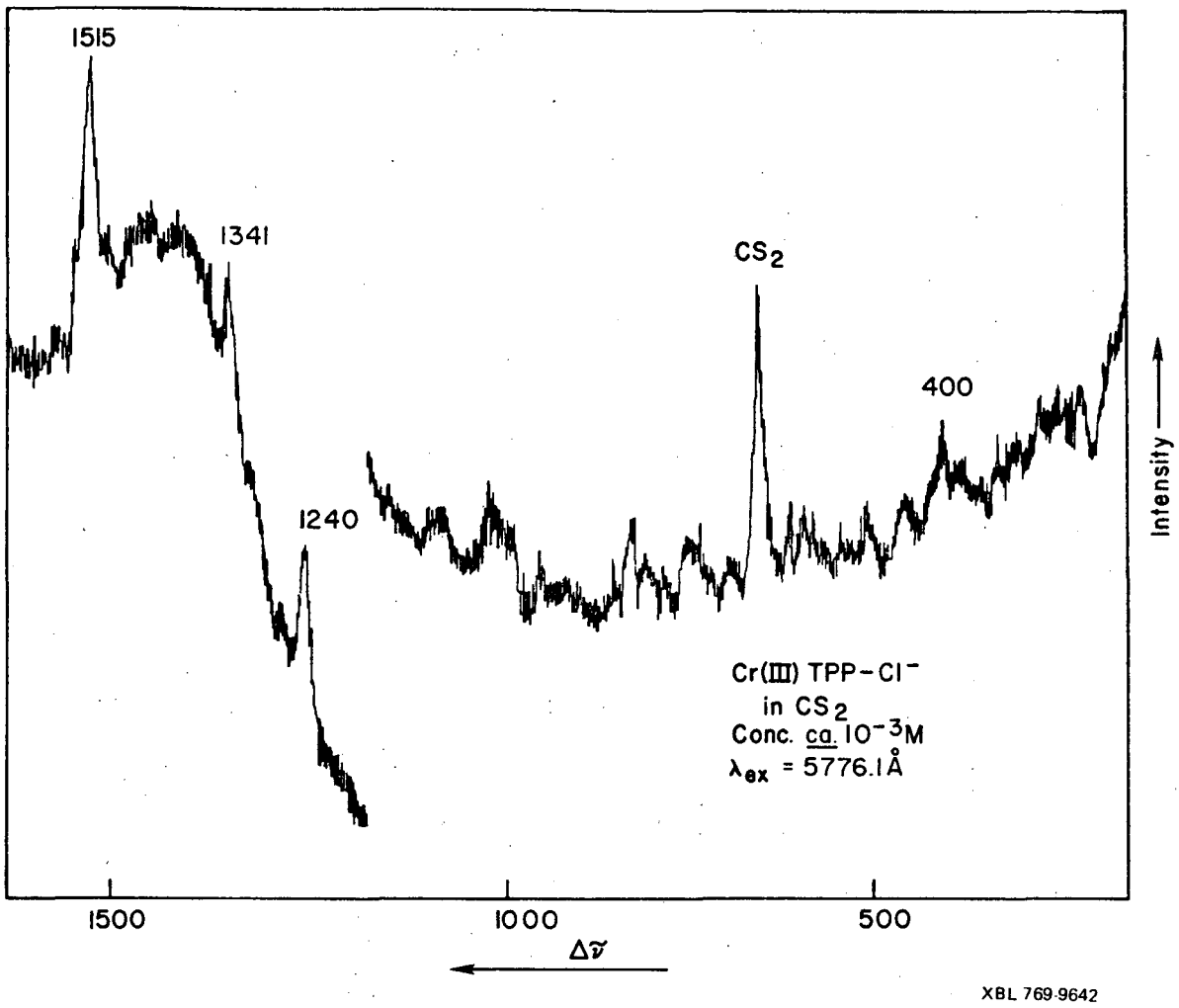

Fig. IV-11. Resonance Raman spectrum of Cr(III)tetraphenylporphin in CS_2. λ_{ex} = 5776.1 Å, Energy = 10^{-3} joule/pulse. Pulse repetition rate = 30 Hz. Scan speed = 14 Å/min. Slitwidth = 1.5 Å. Conc ~ 10^{-3}M. Position of solvent band is indicated.

TABLE VI

Observed vibrational frequencies and relative intensities of the Raman Bands of Cr(III)TPP-Cl$^-$ in CS_2. Relative intensities are normalized with respect to the 656 cm^{-1} line of CS_2 and are corrected for spectrometer efficiency. ρ, the depolarization ratio is labeled; p, polarized; dp, depolarized; ap, anomalously polarized.

Exciting line:	4581.0Å			5776.1Å		6041.6Å	
	$\Delta\nu, cm^{-1}$	I	ρ[b]	$\Delta\nu, cm^{-1}$	ρ	$\Delta\nu, cm^{-1}$	I
	336	0.04					
	400	0.61	p	400		400	0.35
	1015	0.33	p				
	1240	0.13	p	1240	ap		
				1341			
	1370	0.10	p				
	1494	0.08	ap	1515	ap		
	1557	0.14	p				
	1583[a]						

[a] only observed with excitation at 4475.6Å

[b] from Shelnutt, et al., 1976

CuTPP and NiTPP, Raman spectra excited at 6328Å show peaks appearing at 1236, 1365 and 1582 for CuTPP, while peaks appear at 1246, 1370 and 1592 for NiTPP (Solovyov, et al., 1973). For Mn(III)TPP Raman peaks are observed at 1497, 1564 and 1583 cm^{-1}. Because of the small dependence on metal substitution of the energies of the Raman peaks which occur above 1000 cm^{-1}, these vibrations are assigned to porphyrin macrocycle modes. The Raman spectrum in Fig. 9 above 400 cm^{-1} agrees qualitatively with the Raman spectrum of CrTPP-Cl^- in CH_2Cl_2, excited at 4579.0Å measured by Shelnutt, et al (Shelnutt, et al., 1976). The major difference is in the lack of clearly resolved, medium intensity peaks below 400 cm^{-1}. Resonance Raman spectra were measured with excitation at 4619, 4581, 4552.9, 4518.0 and 4475.6Å for CrTPP-Cl^- in CS_2 and at 4619Å for CrTPP-Cl^- in CH_2Cl_2. None of these spectra showed any medium intensity features below 400 cm^{-1}. Excitation at the maximum of absorption band V, which occurs at 4530Å, produced two weak, ill resolved peaks at ca 307 and 340 cm^{-1}.

A comparison of the resonance Raman spectrum of MnTPP-Br^- (Gaughan, et al, 1975) and MnETP-Br^-, excited in band V shows low frequency peaks occuring at 395, 327, 245 cm^{-1} for MnETP-Br^- and at 392, 330 and 240 cm^{-1} for MnTPP-Br^-. The major difference between the resonance Raman spectra of MnTPP and MnETP is the large enhancement observed for the 392 cm^{-1} peak in MnTPP. Although all of the low frequency (<500 cm^{-1}) modes of MnTPP are more intense than the high

frequency modes (>500 cm^{-1}), the 392 cm^{-1} peak of MnTPP is almost an order of magnitude more intense than any other peak in the spectrum. The remarkable enhancement of the ca 400 cm^{-1} modes in both CrTPP and MnTPP, in contrast to the lack of enhancement of a corresponding mode in MnETP, suggests that the origin of the enhancement of this mode is peculiar to metallotetraphenylporphins.

Enhancement of the 400 cm^{-1} peak also occurs upon excitation in band III at 6041.6Å (Fig. 10). An intense background occurs in the Raman spectrum of CrTPP measured in bands III and IV, presumably from an impurity which was not removed by chromatography with alumina; as a result, only the low frequency region of the Raman spectrum excited in band III could be measured. The 400 cm^{-1} feature that appeared with excitation in band V appears again with excitation in band III. The Raman peak due to CS_2 at 656 cm^{-1} is shown for comparison.

Excitation at 5776.1Å in band IV results in a somewhat different spectrum. (Fig. 11) The 400 cm^{-1} peak does not appear with much intensity, while peaks at 1240, 1341 and 1515 dominate the spectrum. Both the 1515 and the 1240 cm^{-1} peaks are anomalously polarized with excitation at 5776.1Å. Thus, it appears that the 400 cm^{-1} peak is in resonance with both band III and band V, but not with band IV.

Mendelsohn et al., (Mendelsohn, et al., 1975b) in their study of the resonance Raman spectra of CuETP noted that a 342 cm^{-1} polarized Raman band appeared to be enhanced both

in the α and by the Soret band. Verma and Bernstein (Verma and Bernstein, 1974c) noted that the 342 cm^{-1} polarized peak was the dominant feature in the resonance Raman spectrum of CuETP excited in the α band. If the 400 cm^{-1} peak of CrTPP represents the same vibrational mode as the 342 cm^{-1} peak in CuETP, then the resonance enhancement of the 400 cm^{-1} mode in both bands III and V support the assignments of bands III and V to the α and Soret bands. The enhancement of high frequency, porphyrin macrocycle modes by excitation in band IV is consistant with the assignment of band IV to the β band.

The lack of enhancement of low frequency modes other than the 400 cm^{-1} peak, the lack of a Raman peak assignable to a Cr - Cl^- stretch and the enhancement of porphyrin macrocycle modes indicate that bands III, IV and V result from $\pi \rightarrow \pi^*$ transitions; this supports Gouterman's assignments of bands III, IV and V to the α, β and Soret Bands (Gouterman, et al., 1975).

REFERENCES

Adar, F., Arch. Biochem. and Biophys., 170, 644(1975).

Adar, F. and Erecinska, M., Arch. Biochem. and Biophys., 165, 644(1974)

Albrecht, A. C., J. Chem. Phys., 34, 1476(1961)

Albrecht, A. C., and Hutley, M. C., J. Chem. Phys., 55, 4438 (1971),

Asher, S., and Sauer, K.,.J. Chem. Phys., 64, 4115(1976)

Berjot, M., Bernard, L., Macquet, J. P. and Theophanides, T. J. Raman Spectrosc., 4, 3(1975)

Boucher, L. J., and Katz, J. J., J. Amer. Chem. Soc., 89, 1340(1975)

Boucher, L. J., Coord. Chem. Rev., 7, 289(1972)

Boucher, L. J., J. Amer. Chem. Soc., 92, 2725(1970)

Boucher, L. J., Ann. N.Y. Acad. Sci., 206, 409(1973)

Brunner, H., Biochem. Biophys. Res. Commun., 51, 888(1973)

Brunner, H., Naturwis., 61, 129(1974)

Brunner, H., Mayer, A. and Sussner, H., J. Mol. Biol., 70, 153(1972)

Brunner, H., and Sussner, H., Biochem. Biophys. Acta 310, 20(1973)

Burger, H., Burczyk, K and Fuhrhop, J. H., Tetrahedron 27, 3257(1971)

Collins, D. W., Fitchen, D. B. and Lewis, A., J. Chem. Phys. 59, 5714(1973)

Collins, D. W., Champion, P. N., and Fitchen, D. B., Chem. Phys. Lett., 40, 416(1976)

Felton, R. H., Yu, N-T., O'Shea, D. C. and Shelnutt, J. A., J. Amer. Chem. Soc., 96, 3675(1974)

Felton, R. H., Romans, A. Y., Yu, N-T., and Schonbaum, G. R, Biochem. Biophys. Acta, 434, 82(1976)

Freedman, J. M. and Hochstrasser, R. M., Chem. Phys., 1, 457 (1973)

Gaughan, R. R., Shriver, D. F. and Boucher, L. J., Proc. Natl. Acad. Sci. USA 72, 433(1975)

Gouterman, M., J. Chem. Phys., 30, 1139(1959), J. Mol. Spectros., 6, 138(1961)

Gouterman, M., Excited States of Matter, edited by Shoppee, C. W., (Texas Tech. Univ, Lubbock, TX, 1973), Vol. 2 pp. 63-103.

Ikeda-Saito, M., Kitagawa, T., Iizuka, T., and Kyogoku, Y., FEBS Lett., 50, 233(1975)

Kitagawa, T., Ogashi, H., Watanabe, E. and Yoshida, Z., Chem. Phys. Lett., 30, 451(1975a), J. Phys. Chem. 79, 2629 (1975b)

Kitagawa, T., Iizuka, T., Saito, M., and Kyogoku, Y., Chem. Lett., 849(1975c)

Kitagawa, T., Kyogoku, Y., Iizuka, T., Ikeda-Saito, M. and Yamanaka, T., J. Biochem., 78, 719(1975d)

Kitagawa, T., Kyogoku, Y., Iizuka, T., and Saito, M. I., J. Amer. Chem. Soc., 98, 5169(1976a)

Kitagawa, T., Abe, M., Kyogoku, Y., Ogashi, H., Watanabe, E., and Yoshida, Z., J. Phys. Chem. (in press) (1976b)

Longuet-Higgins, H. C., Proc. R. Soc. London A235, 537(1956)

Lutz, M., J. Raman Spectrosc., 2, 497(1974)

Mendelsohn, R., Sunder, S. and Bernstein, H. J., J. Raman Spectrosc., 3, 303(1975a)

Mendelsohn, R., Sunder, S., Verma, A. L., and Bernstein, H. J. J. Chem. Phys., 62, 37(1975b)

Murrell, J. N., and Pople, J. A., Proc. Phys. Soc. London Sect. A, 69,245(1956)

Nafie, L. A., Pezolet, M., and Peticolas, W. L., Chem. Phys. Lett., 20, 563(1973)

Nestor, J. and Spiro, T. G., J. Raman Spectrosc., 1, 539(1973)

Pezolet, M., Nafie, L. A. and Peticolas, W. L., J. Raman Spectrosc., 1, 455(1973)

Plus, R., and Lutz, M., Spectrosc. Lett., 7, 73 and 133(1974)

Ogashi, H., Masai, N., Yoshida, Z. I., Takemoto, J., and Nakamoto, K., Bull Chem. Soc., Japan 44, 49(1971)

Ogashi, H., Saito, Y., and Nakamoto, K., J. Chem. Phys., 57, 4194(1972)

Ogashi, H., Watanabe, E., Yoshida, Z., Kincaid, J., and Nakamoto, K., J. Amer. Chem. Soc., 95, 2845(1973)

Ozaki, Y., Kitagawa, T., and Kyogoku, Y., FEBS Lett., 62, 369(1976)

Rakshit, G., and Spiro, T. G., Biochem., 13, 5317(1974)

Rakshit, G., Spiro, T. G., and Uyeda, M., Biochem. Biophys. Res. Comm., 71, 803(1976)

Rimai, L., Salmeen, I., and Petering, D. H., Biochem., 44, 378(1975)

Salmeen, I., Rimai, L., Gill, D., Yamamoto, T., Palmer, G., Hartzell, C. R., and Beinert,H., Biochem. Biophys. Res. Comm., 52, 1100(1973)

Shelnutt, J. A., O'Shea, D. C., Yu, N-T., Cheung, L. D. Felton, R. H., J. Chem. Phys., 64, 1156(1976)

Smith, D. W., and Williams, R. J. P., Structure and Bonding 7, 1(1970)

Solovyov, K. N., Ksenofontova, N. M., Shkirman, S. F., and Kachura, T. F., Spectrosc. Lett 6, 455(1973)

Spaulding, L. D., Chang, C. C. Yu, N-T., and Felton, R. H., J. Amer. Chem. Soc., 97, 2517(1975)

Spiro, T. G., and Strekas, T. C., Proc. Natl. Acad. Sci., USA, 69, 2622(1972)

Spiro, T. G. and Strekas, T. C., J. Amer. Chem. Soc., 96, 338(1974)

Spiro, T. G., Biochem. Biophys. Acta., 416,169(1975)

Spiro, T. G. and Burke, J. M., J. Amer. Chem. Soc., 98, 5482(1976)

Strekas, T. C. and Spiro, T. G., Biochem. Biophys. Acta., 263, 830(1972a), 278,188(1972b)

Strekas, T. C. and Spiro, T. G., J. Raman Spectrosc., 1 387(1973)

Strekas, T. C., Packer, A. J., and Spiro, T. G., J. Raman Spectrosc., 1, 197(1973).

Sunder, S., Mendelsohn, R. and Bernstein, H. J., Biochem. Biophys. Res. Comm., 62, 12(1975)

Sussner, H., Mayer, A., Brunner, H. and Fasold, H. Eur. J. Biochem., 41, 465(1974)

Szabo, A., and Barron, L. D., J. Amer. Chem. Soc., 97, 660(1975)

Tang, J., and Albrecht, A. C., J. Chem. Phys., 49, 1144(1964)

Tang, J. and Albrecht, A. C., Raman Spectroscopy edited by Szymanski, H. A., (Plenum, NY (1971)), Vol II.

Verma, A. L., and Bernstein, H. J., Biochem. Biophys. Res. Comm., 57, 255(1974a), J. Raman, Spectrosc., 2, 163(1974b) J. Chem. Phys., 61, 2560(1974c)

Verma, A. L., Mendelsohn, R., and Bernstein, H. J., J. Chem. Phys., 61, 383(1974d)

Warshel, A., Annual Review of Biophysics and Bioengineering Vol. 6 (in press) (1976)

Woodruff, W. H., Spiro, T. G. and Yonetani, T., Proc. Natl. Acad. Sci., USA 71, 1065(1974)

Woodruff, W. H., Adams, D. H., Spiro, T. G. and Yonetani, T., J. Amer. Chem. Soc., 97, 1695(1975)

Yamamoto, T., Palmer, G., Gill, D., Salmeen, I. T., and Rimai, L., J. Biol. Chem., 248, 5211(1973)

Yamamoto, T., Palmer, G., and Crespi, H., Biochem. Biophys. Acta., 439, 232(1976)

Zerner, M., and Gouterman, M., Theoret. Chem. Acta., 4, 44 (1966)

Chapter V

RESONANCE RAMAN SPECTROSCOPY OF HEMOGLOBIN

Introduction

Hemoglobin (Hb), a metalloporphyrin-protein complex, reversibly binds and transports molecular oxygen from the alveoli of the lungs through the circulatory system to the cells where respiration occurs. Vertebrate Hb consists of 4 non-covalently linked subunits, each of which contains one molecule of iron protoporphyrin IX (heme) (Antonini and Brunori, 1971). The subunits can be differentiated into 2 types called the α and β subunits. The tetrameric hemoglobin molecule consists of 2 α and 2 β subunits. Although the α and β chains are somewhat different in their amino acid sequences, they have similar tertiary structures (Perutz, et al., 1968). Both the α and β chains bind heme in a hydrophobic cavity of the protein by the axial linkage of the imidazole group of the "proximal histidine" to the iron atom of the heme. Further interactions between the protein and the heme occur through Van der Waals interactions with side chains of the protein protruding into the heme cavity (Perutz, 1970).

Reversible binding of 0_2 can occur only when the heme iron is in the ferrous (+2) oxidation state (Smith and Williams, 1970). However, ferrous porphyrins are readily oxidized to the ferric (+3) state in the presence of oxygen. One of the roles of the protein is to stabilize the ferrous oxidation state of the heme and prevent oxidation to the ferric state (Stryer, 1975; Antonini and Brunori, 1971).

The subunits of Hb do not bind 0_2 independently; the oxygen binding occurs by a cooperative mechanism in which binding of oxygen by one

subunit facilitates oxygen binding in the unoxygenated subunits (Perutz, 1970). For example, the probability of binding a molecule of oxygen for the two hemoglobins, A and B, where A contains three bound 0_2 and B contains none, is 70 times higher for A than for B (Perutz, 1970). The cooperativity phenomenon serves an important physiological role in oxygen transport by decreasing the oxygen affinity of saturated Hb as oxygen begins to dissociate. As Perutz pointed out (Perutz, 1970), the partial pressure of 0_2 in the tissues is not much lower than in the alveoli. The decrease in oxygen affinity that results from the first dissociation of oxygen triggers further dissociation of oxygen. This leads to a very efficient transport of oxygen from the alveoli to the cells.

A detailed and experimentally testable model for the molecular mechanism of cooperativity has been proposed by Perutz (Perutz, 1970, 1972; Perutz, et al., 1974 a,b,c, 1976) using the allosteric theory of Monod, et al. (Monod, et al., 1965). The model proposes that the increase in oxygen affinity for Hb as it becomes oxygenated results from a transition between 2 quarternary forms. In the relaxed (R) quarternary form, the oxygen affinity of each heme is relatively high, similar to that of the isolated α or β subunits. The tense (T) form of Hb shows a decreased oxygen affinity. Deoxyhemoglobin is in the T form; the iron is high-spin and lies 0.60 Å out of the heme plane (Fermi, 1975). Upon oxygenation, the Fe^{2+} atom becomes low-spin. The ionic radius decreases and the Fe^{2+} atom moves into the heme plane (Perutz and Teneyck, 1971). The distance between the "proximal histidine" and the heme plane should decrease in response to the movement of the Fe^{2+} atom into the heme plane. The pulling of the histidine towards the porphyrin plane would result in changes in the tertiary and quarternary structure of the protein.

Perutz proposed that the change in the distance between the histidine and the porphyrin plane is the trigger mechanism responsible for the tertiary and quarternary structural changes occurring in the transition from the T (low oxygen affinity) to the R (high oxygen affinity) form of Hb.

The R and T forms of Hb can be differentiated by the distance between the iron atoms of the different hemes and by a change in the binding between the α and β subunits (Perutz, et al., 1974a). Inositol hexaphosphate (IHP) stabilizes the T form of Hb (Perutz, et al., 1974b). Along with the characteristic absorption, CD and sulfhydryl reactivity changes observed in the R → T transition, a rise in the paramagnetic susceptibility of the iron occurs, indicating a small shift of the spin-state equilibrium of the iron to the high-spin form. Perutz (Perutz, et al., 1974c) interprets these data as indicating that the protein exerts a tension in the T form, pulling the "proximal histidine" and the iron away from the heme plane. This tension stabilizes the high-spin form of Fe^{2+} and opposes the transition to the low-spin form necessary for combination with oxygen. Perutz (Perutz, 1972; Perutz, et al., 1976) proposes that the interaction between the heme and the globin is a reciprocal one: that oxygenation of one subunit, resulting in an in-plane, low-spin heme, changes the tertiary structure of that subunit. This change induces an alteration in the tertiary and quarternary structures of the other subunits to a form more characteristic of the R conformation. The result is an increase in the oxygen affinities of the unoxygenated subunits.

The absorption spectra of iron porphyrins are more complex than the absorption spectra of "normal" metalloporphyrins. Oxyhemoglobin shows the characteristic α, β, and Soret bands in the visible and near

UV spectral regions, but an additional weak absorption band occurs at ca 900 nm (Antonini and Brunori, 1971). Ferric hemoglobin, which is often called methemoglobin (MetHb), shows a more complicated spectrum. MetHb F^- shows a very diffuse visible and near IR absorption spectrum with peaks or shoulders appearing at 486, 543, 579, 603, 738, 840 and 1110 nm (Perutz, et al., 1974c). MetHb N_3^- shows peaks at 500, 540, 580, 630 and 1000 nm, while MetHb OH^- complex shows peaks at 486, 540, 576, 600, 816, and 980 nm. The additional peaks in the absorption spectra of iron porphyrins compared to "normal" porphyrins appear to be due to charge transfer and/or d → d transitions (Smith and Williams, 1970). The absorption spectrum of MetHb is very sensitive to axial ligation, to pH and to protein conformational changes (Smith and Williams, 1970; Perutz, et al., 1974c). Although most of the visible absorption bands result from electronic transitions polarized in the x,y plane of the porphyrin, the azide complex shows a z-polarized transition at about 640 nm (Eaton and Hochstrasser, 1968). Smith and Williams suggested that charge transfer transitions contribute to the absorption bands of MetHb derivatives between 470-640 nm via configuration interaction with the α and β bands (Smith and Williams, 1970). None of the absorption bands that result can be considered to come from pure $\pi \rightarrow \pi^*$ or charge transfer transitions. The resulting complex absorption spectrum is sensitive to substitution of the axial ligand, which affects the energies of the d orbitals and the amount of configuration interaction occurring between the charge transfer bands and the α and β bands.

In view of the results outlined in Chapter IV, which indicate that excitation in the charge transfer band of MnETP enhances vibrational

Fig. V-1. Resonance Raman spectrum of MetHb N_3^- (0.76 mM heme) containing 0.25 M Na_2SO_4 as an internal standard. λ_{ex}= 5590.8 Å. Energy=10^{-3} joule/pulse. Pulse repetition rate= 30 Hz. Scan speed= 23 Å/min. Slitwidth= 3 Å. Position of Raman lines due to $SO_4^=$ and uncomplexed azide are shown in the figure.

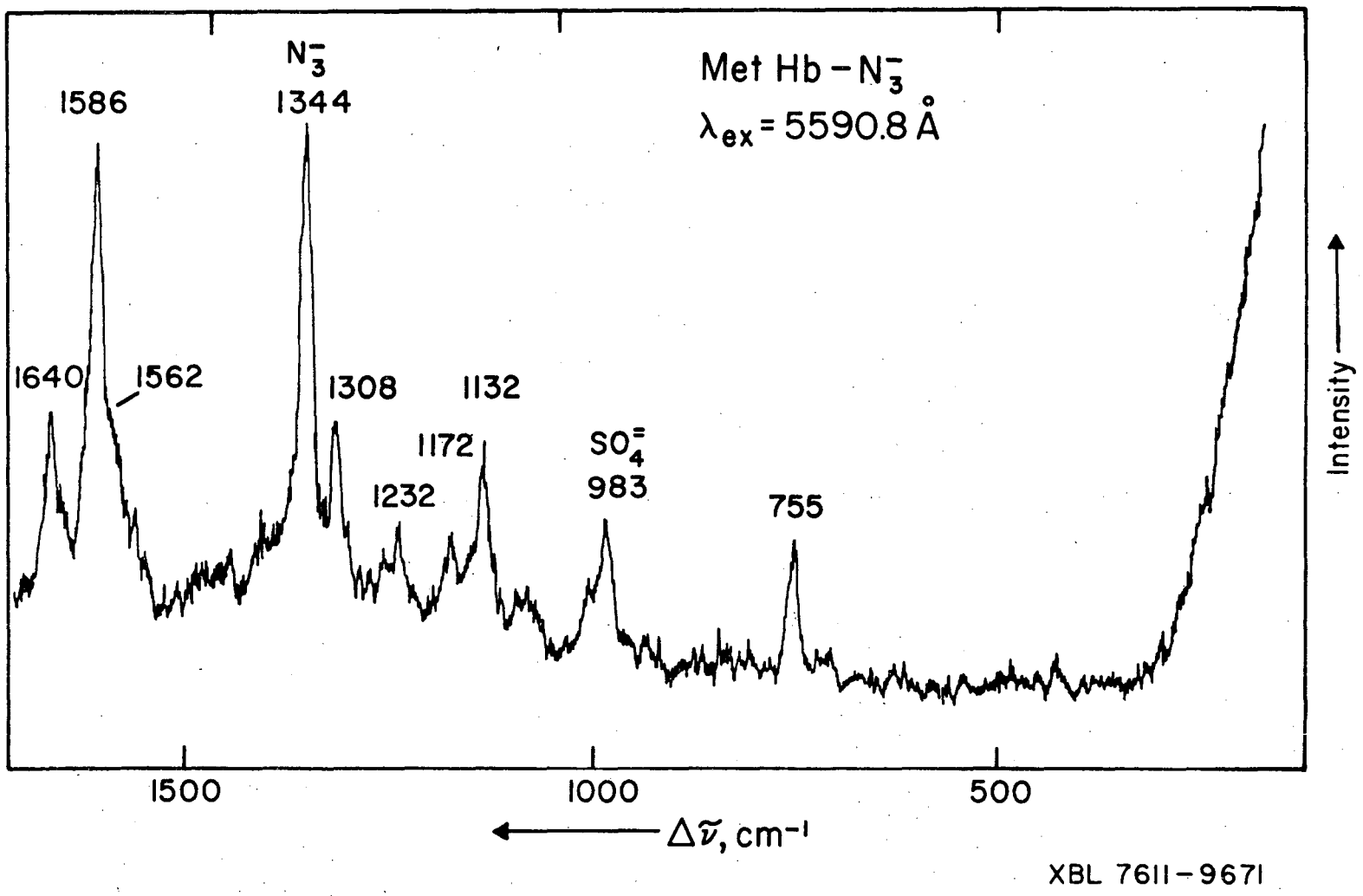
Met Hb – N_3^-
λ_{ex} = 5590.8 Å
N_3^-
1344
1586
1640
1562
1308
1132
1172
1232
$SO_4^=$
983
755
Intensity
1500
1000
500
$\Delta\tilde{\nu}$, cm^{-1}
XBL 7611-9671

Fig. V-1.

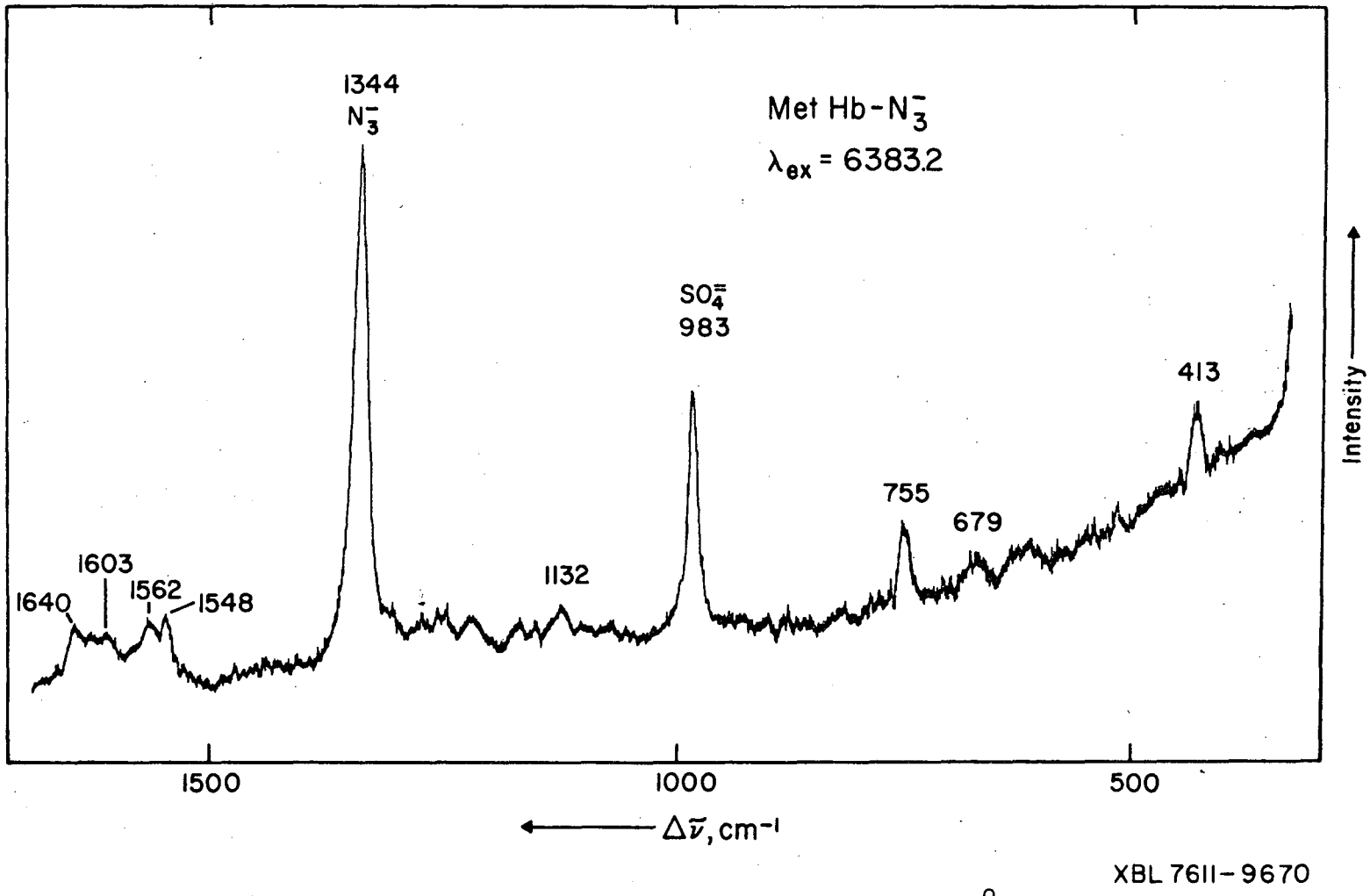

Fig. V-2. Resonance Raman Spectrum of MetHb N_3^-. λ_{ex}=6383.2 Å, conditions as in Fig. V-1.

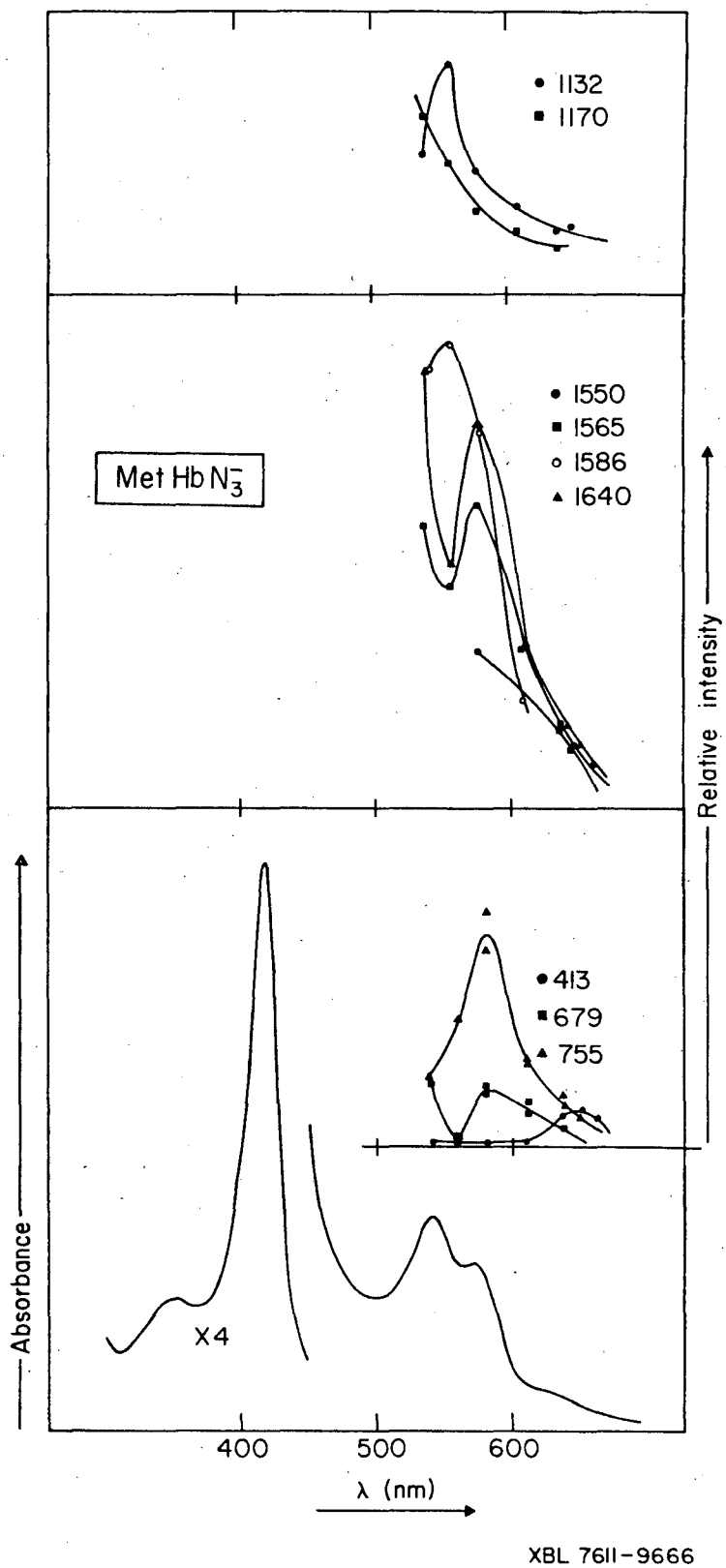

Fig. V-3. Absorption spectrum and excitation profiles of MetHb N_3^-. The intensities of the Raman lines were corrected for the spectrometer response and then normalized against the $SO_4^=$ line at 983 cm^{-1}.

modes about the metal, excitation in the charge transfer bands of hemoglobin might be expected to enhance vibrational modes about the iron atom. These modes should be sensitive to the out-of-plane distance of the iron from the heme plane and may monitor the geometric changes occurring at the heme due to a transition of the protein between the R and T conformations. The OH^-, N_3^- and F^- derivatives of MetHb were studied because each exhibits distinct absorption bands which have been assigned to charge transfer transitions (Smith and Williams, 1970). In addition, the OH^- and N_3^- derivatives are known to undergo changes in both their absorption spectra and spin state equilibria upon addition of IHP. Addition of IHP to MetHb F^- induces changes in the sulfhydryl reactivities and the UV absorption and CD spectra; these changes are similar to those observed in the R to T transition in deoxyHb (Perutz, et al., 1974b). Perutz concluded that IHP addition results in the conversion of the R quarternary form of MetHb F^- to the T form.

Resonance Raman Spectra of Hemoglobin

These studies were carried out in collaboration with Dr. Larry Vickery (Department of Chemistry, University of California, Berkeley), who prepared most of the Hb and myoglobin derivatives and who measured the absorption spectra contained in Figs. 3, 6 and 9.

MetHb N_3^-

Figures 1 and 2 show the resonance Raman spectra of the azide complex of MetHb excited at 5590.8 and 6383.2 Å, respectively. As the absorption spectrum of MetHb N_3^- in Fig. 3 shows, excitation at

5590.8 Å occurs between two absorption bands which have been assigned to the α and β bands of metalloporphyrins (Eaton and Hochstrasser, 1968). Excitation at 6383.2 Å occurs within a weak absorption band at ca 6400 Å, which has been assigned to a charge transfer transition (Eaton and Hochstrasser, 1968). A comparison of Figs. 1 and 2 with the Raman spectrum of an aqueous solution of Na_2SO_4 indicates that the feature in the Raman spectra at 983 cm^{-1} is due to $SO_4^=$, which was added to the Hb solution as an internal standard for the excitation profile measurements shown in Fig. 3. A comparison between the Raman spectrum of an aqueous solution of NaN_3, and a solution of MetHb N_3^- with lower concentrations of N_3^- indicates that the feature at 1344 cm^{-1} is due to uncomplexed azide. The 1344 cm^{-1} peak does not appear with lower concentrations of NaN_3^- (0.04 M). Yet the absorption spectrum of the MetHb solution is still characteristic of the MetHb N_3^- complex.

The dominant features in the resonance Raman spectrum excited between the α and β bands (Fig. 1) appear at energies greater than 600 cm^{-1}, occurring at 1640, 1586, 1308, 1132, and 755 cm^{-1}. From a comparison between the resonance Raman spectra of high and low-spin forms of the ferric and ferrous derivatives of a variety of heme-proteins and iron porphyrin complexes, Spiro and coworkers noted a correlation between the energies of some of the Raman bands and the oxidation and spin-state of the iron (Spiro and Strekas, 1974; Spiro, 1975; Spiro and Burke, 1976). For example, peaks which appear at ∿ 1640 and ∿ 1590 cm^{-1} in the low-spin form of heme-proteins and Fe^{3+} mesoporphyrin IX dimethyl ester shift to ∿ 1633 and 1575 cm^{-1} in the high-spin form (Spiro and Burke, 1976). However, exceptions to these correlations occur for some heme proteins. For example, for

MetHb F^- and Met myoglobin fluoride (MetMb F^-) which are in the high-spin state, peaks appear at 1608 and 1555 cm^{-1}. In contrast, peaks appear at 1632 and 1572 for Fe^{+3} mesoporphyrin IX dimethyl ester-F^-. The increased shift of the Raman peaks in MetHb F^- and MetMb F^- over the values expected for other high-spin heme-proteins and Fe^{+3} porphyrins appears to be due to an interaction with the protein, which may result in an increased out-of-plane distance of the Fe^{+3} from the porphyrin plane (Spiro and Burke, 1976). Peaks appear in the Raman spectrum of MetHb N_3^- at 1640 and 1586 cm^{-1}, indicating that MetHb N_3^- is predominantly low-spin, in agreement with paramagnetic susceptibility measurements (Antonini and Brunori, 1971). An oxidation-state dependent vibration occurs at $\sim$ 1374 cm^{-1} for ferric hemes and at $\sim$ 1360 cm^{-1} for ferrous hemes (Spiro, 1975). Due to the interference of the Raman spectrum of the azide ion, the oxidation dependent vibration is not visible in Figs. 1 and 2. However, Raman spectra of MetHb N_3^- obtained with lower concentrations of N_3^- (0.04 M) clearly show a peak at 1375 cm^{-1}, indicating that the iron is in the +3 oxidation state.

The Raman spectrum shown in Fig. 1 is similar to previously reported spectra of the azide complexes of MetHb (Strekas and Spiro, 1972) and Met myoglobin (Mb) (Kitagawa, et al., 1976). All of the features in the Raman spectrum of MetHb N_3^- excited at 5590.8 Å are due to porphyrin macrocyclic vibrational modes (Spiro, 1975).

The resonance Raman spectrum of MetHb N_3^- excited at 6383.2 Å in the charge transfer band (Fig. 2) shows a new Raman peak appearing at 413 cm^{-1}. A depolarization ratio measurement of the 413 cm^{-1} peak indicates that the peak is polarized, while an examination of the excitation profiles in Fig. 3 shows that the 413 cm^{-1} peak is the only peak in resonance with the

charge transfer band at 6400 Å. All of the other Raman peaks which appear with 6383.2 Å excitation are more intense upon excitation at shorter wavelength and appear to be in resonance with the α and β bands.

The 413 cm^{-1} peak enhanced by excitation in the charge transfer band of MetHb N_3^- is close in energy to a vibration observed in the IR spectrum of Fe^{3+} octaethylporphin-N_3^- at 421 cm^{-1}, which was assigned to the Fe-azide stretching vibration (Ogashi, et al., 1973). The unique enhancement of the 413 cm^{-1} peak by the charge transfer band of MetHb N_3^-, the close correspondence between the energies of the 413 cm^{-1} peak and the Fe-N_3^- stretch observed in Fe(III) octaethylporphin-N_3^-, the fact that the peak is polarized, and the selective appearance of the 413 cm^{-1} peak in the resonance Raman spectrum of MetHb N_3^- in contrast to its absence in MetHb OH^- and MetHb F^- (vide infra) all suggest that the 413 cm^{-1} peak results from a vibration of the azide nitrogen against the heme iron.

MetHb N_3^- was prepared with the Na ^{14}N ^{14}N ^{15}N (97% enriched from Koch Isotopes, Inc., Cambridge, Massachusetts). A comparison between the resonance Raman spectra of MetHb-(^{14}N ^{14}N ^{14}N) and MetHb-(^{15}N ^{14}N ^{14}N) was not conclusive for an isotope shift. Binding of the singly, terminally labeled azide results in a 50-50 mixture of the azide complex of MetHb (i.e., Fe - ^{15}N = ^{14}N = ^{14}N and Fe - ^{14}N = ^{14}N = ^{15}N). Using a harmonic oscillator model and assuming that the 413 cm^{-1} peak is due to a pure Fe-N_3^- stretch which is not mixed with any other vibrational modes, substitution of ^{15}N for ^{14}N at the iron is expected to decrease the energy of the 413cm^{-1} peak to 402 cm^{-1}. However, only 50% of the

MetHb N_3^- has the ^{15}N label bound to the iron. Thus, the Raman spectrum of the singly terminally labeled azide complex of MetHb results from the overlap of two Raman peaks, one shifted to lower energy and one remaining at 413 cm^{-1}. Assuming equal amounts of MetHb - $^{15}N = ^{14}N = ^{14}N$ and MetHb - $^{14}N = ^{14}N = ^{15}N$, and that the bands are Gaussian, a shift of 5.5 cm^{-1} is expected for the resultant Raman peak. The intensity of the peak would decrease by 9%, and the full width at half height would increase by 9%. A shift of 5.5 cm^{-1} in a broad Raman peak is not detectable with the present Raman spectrometer, due to the spectral signal-to-noise ratio and the 3 cm^{-1} laser line width. To demonstrate an isotope shift for the Fe-N_3^- vibration it is necessary to use an azide with both termini labeled.

In contrast to the Raman spectra obtained from MnETP excited in the charge transfer band (Chapter IV), no porphyrin vibrational modes are enhanced by excitation in the charge transfer band of MetHb N_3^-. The porphyrin macrocyclic modes appear to derive their intensity from the α and β bands. Even the pyrrole-nitrogen-Fe vibrations are not visibly enhanced. The lack of enhancement of pyrrole-nitrogen-Fe^{3+} vibrations suggests that the electronic transition which is responsible for the absorption band at 6400 Å in MetHb N_3^- is different from the electronic transition which is responsible for band V in MnETP. This conclusion is supported by a polarization study of the absorption spectra of single crystals of MetHb N_3^- (Kabat, 1967) and ferrimyoglobin-N_3^- (MetMb N_3^-) (Eaton and Hochstrasser, 1968), which indicates that a z-polarized electronic transition is responsible for the absorption band at 6400 Å. MCD spectra of MetHb N_3^- show a negative extremum due to the 6400 Å absorption band (Vickery, et al., 1976). In contrast, the

MCD spectra of band V of MnETP show an A term (Chapter III). Since the ground state of MnETP is non-degenerate, the MCD results indicate that the excited state of MnETP is degenerate and therefore x,y polarized, while the electronic transition of MetMb N_3^- is non-degenerate.

MetMb N_3^- shows an absorption spectrum almost identical to that of MetHb N_3^-. The major difference is a shift of all of the absorption bands about 40 Å to longer wavelength (Antonini and Brunori, 1971). The similarity between the absorption spectra of MetHb N_3^- and MetMb N_3^- is due to the similar environments of the heme in MetHb and MetMb. Mb is an oxygen storage and transport heme-protein found in muscle. In contrast to Hb, which is a tetramer, Mb is monomeric. The molecular weight and amino acid sequence is similar to that of the individual α and β subunits of Hb. The heme in Mb is bound in a hydrophobic cavity of the protein by a "proximal histidine". Eaton and Hochstrasser assigned the $\sim$ 6400 Å absorption band of MetMb N_3^- to either an $a_{2u}(\pi) \rightarrow d_{z^2}$ or an azide $\rightarrow$ iron (d) charge transfer band. It is less likely that the band results from a d $\rightarrow$ d transition, because its molar absorptivity ($\varepsilon \sim 10^3$) is an order of magnitude higher than the molar absorptivity expected for a d $\rightarrow$ d transition (Smith and Williams, 1970).

The Raman data do not distinguish the $a_{2u}(\pi) \rightarrow d_{z^2}$ from the azide $\rightarrow$ iron (d) charge transfer transitions. Enhancement of in-plane porphyrin and pyrrole-nitrogen - Fe^{3+} vibrations would not necessarily be expected for a z-polarized electronic transition. However, enhancement of out-of-plane vibrations involving the Fe^{3+}-pyrrole linkages would be expected. Unfortunately, the magnitude of this enhancement is difficult to predict. No new features which might be due to out-of-plane vibrations of the

heme are observed in the Raman spectrum of MetHb N_3^-. The vibration of the Fe-N_3^- linkage is expected to be the major vibration enhanced in an a_{1u} or $a_{2u} \rightarrow d_{z^2}$ transition since the azide is bound by the d_{z^2} orbital of the iron.

A charge transfer transition from the azide to the d orbitals of the iron would be expected to enhance the Raman peak due to the vibration of the Fe-N_3^- linkage. However, internal vibrations of the N_3^- might also be expected to be resonance-enhanced, since an analogous enhancement of pyridine vibrations occurs upon excitation into a $Fe^{2+} \rightarrow$ pyridine charge transfer band at 4765 Å in pyridine complexes of Fe^{2+} mesoporphyrin IX (Spiro and Burke, 1976). Raman spectra of MetHb N_3^- with lower concentrations of N_3^- (0.04 M) show spectra similar to Fig. 2. The only difference is the disappearance of the 1344 cm^{-1} peak, due to free N_3^- present. There is no obvious enhancement of internal azide vibrations upon excitation in the charge transfer band at 6400 Å.

However, from X-ray crystallographic studies of MetMb N_3^-, azide is known to bind at a 111° angle to the normal of the heme plane (Fig. 4a) (Stryer, et al., 1964). Both the symmetric and anti-symmetric vibrations of the N_3^- are at a 111° angle to the z-polarized electronic transition. Thus, these azide vibrations may not couple well with the z-polarized charge transfer transition. It is difficult to predict the enhancement expected for the doubly degenerate azide deformation mode (Fig. 4b). Another possibility is that the charge transfer transition occurs from a nonbonding orbital of the azide to a d_{z^2} orbital of the iron. The transition, which is z-polarized would enhance the vibration between the Fe and azide nitrogen. However, neither the

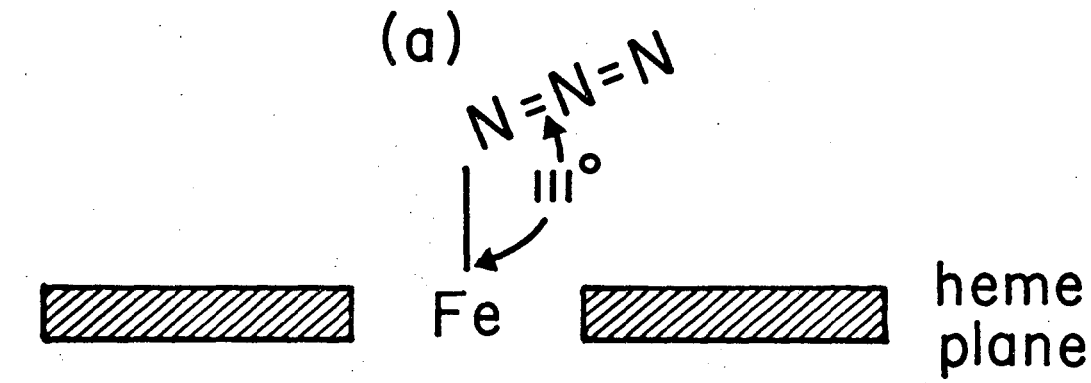

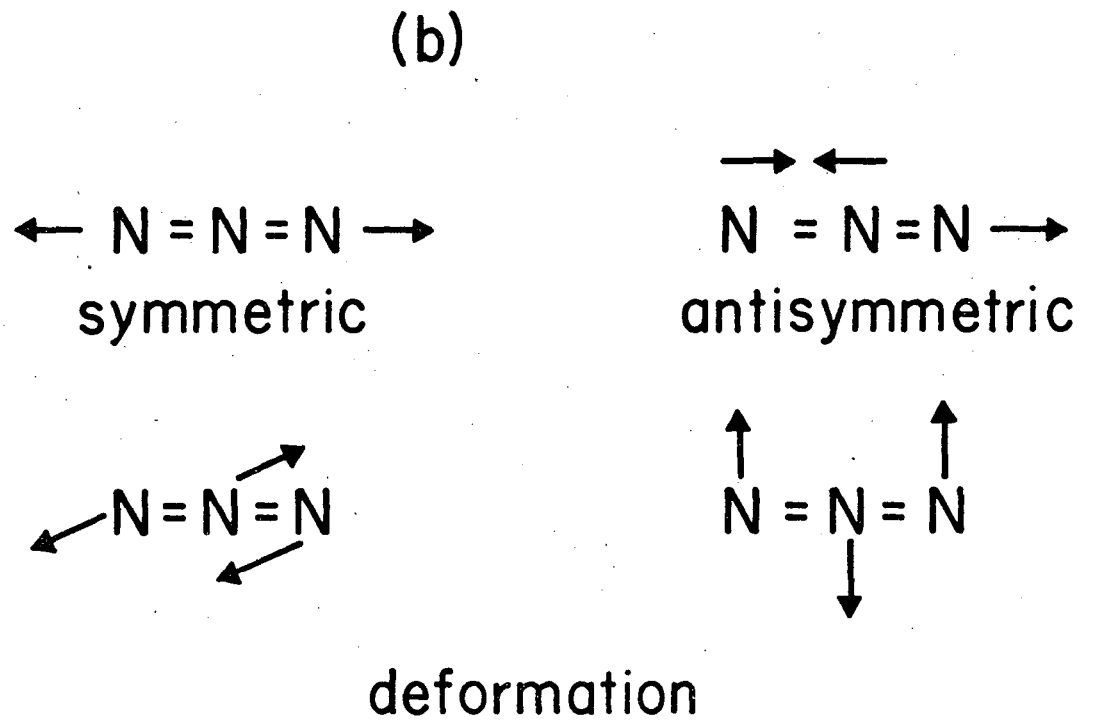

XBL 7611-9672

Fig. V-4. (a) Geometry of the heme-azide complex of MetHb N_3^-.
(b) Vibrational modes of N_3^-.

pyrrole-nitrogen-Fe nor internal azide vibrations would be appreciably enhanced.

MetHb OH^-

In acidic or neutral solutions and in the absence of exogenous coordinating ligands, the sixth axial position of MetHb is occupied by a water molecule. However, in basic solutions the sixth ligand is hydroxide. For human MetHb the pK for the displacement of the axial coordinated water by OH^- is 8.05 (Antonini and Brunori, 1971). Thus, at a pH greater than 10.0 essentially all of the MetHb is complexed to OH^-. In contrast to MetHb N_3 which is predominantly low-spin, MetHb OH^- exists in a spin-state equilibrium with comparable concentrations of the high and low-spin forms (Antonini and Brunori, 1971).

Fig. 5 shows the resonance Raman spectrum of MetHb OH^- at pH = 11.06. The dominant features in the spectrum occur at 497, 755, 1555, 1587 and 1634 cm^{-1}. A number of differences appear between the resonance Raman spectrum of MetHb OH^- and MetHb N_3^-. The 413 cm^{-1} peak is absent in the latter, but there is a new peak at 497 cm^{-1}. An examination of the absorption spectrum and the excitation profiles in Fig. 6 indicates that the 497 cm^{-1} peak is in resonance with the shoulder at 6000 Å in the absorption spectrum. The other Raman bands at 353, 755, 1555, 1587 and 1634 cm^{-1} increase in intensity as the excitation wavelength decreases, indicating that they are resonantly enhanced by the 5700 and/or 5400 Å absorption bands.

The unique enhancement of the 497 cm^{-1} band by the shoulder at 6000 Å is similar to the selective enhancement shown by the 413 cm^{-1} Raman peak in the charge transfer band of MetHb N_3^- at 6400 Å. To determine whether

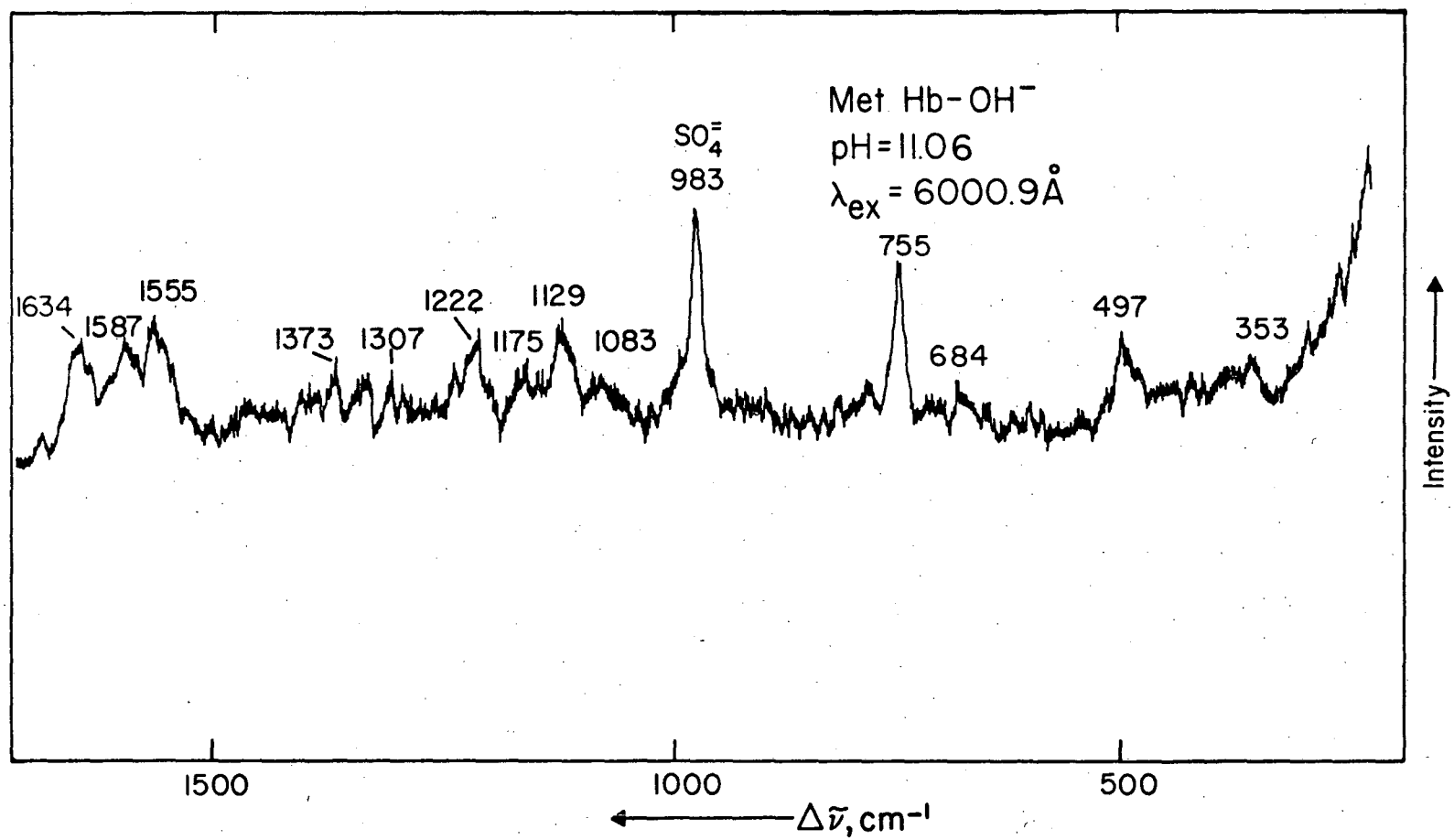

Fig. V-5. Resonance Raman spectrum of MetHb OH^- (0.76 mM heme). pH=11.06. Contains 0.2 M Na_2SO_4 as an internal standard. λ_{ex}=6000.9 Å. Energy= 4 X 10^{-3} joule/pulse. Pulse repetition rate= 30 Hz. Scan speed= 23 Å/min. Slitwidth= 2.5 Å.

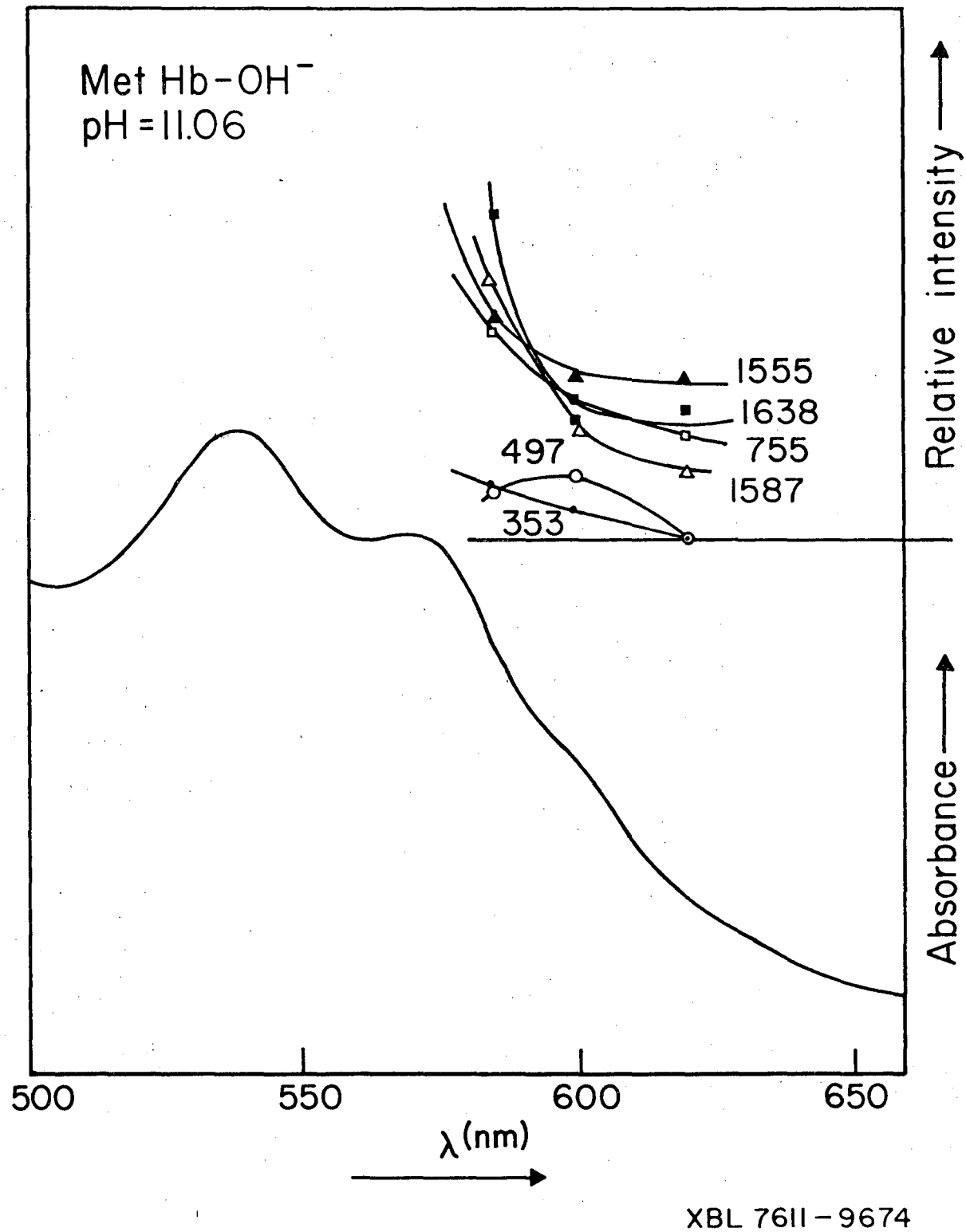

Fig. V-6. Absorption spectra and excitation profiles of Metlb OH^- Conditions same as in Fig. V-3.

the 497 cm^{-1} peak results from the Fe-O stretch, MetHb was freeze-dried and redissolved in $H_2{}^{16}O$ and $H_2{}^{18}O$ (95% enriched in ^{18}O, Bio-Rad Lab., Richmond, California, catalog number 7167451). Each of the resulting solutions was titrated at 0°C with a small amount of a 30% solution of $Na^{16}OH$ in $H_2{}^{16}O$. Fig. 7 shows the resonance Raman spectra of MetHb $^{18}OH^-$ and MetHb $^{16}OH^-$ excited at 6004.7 Å. The 497 cm^{-1} peak which appears in the spectrum of MetHb $^{16}OH^-$ shifts 20 cm^{-1} to lower energy following substitution of $^{18}OH^-$. The increased background in both of the spectra in Fig. 7 over that in Fig. 5, presumably is due to some denaturation of the MetHb during the freeze-drying process.

Using a harmonic oscillator model, the energy shift for the 497 cm^{-1} peak is 2 cm^{-1} less than the 22 cm^{-1} shift expected if this vibration were due to a pure Fe-O stretch. The enhancement of the Fe-O stretch at 6000 Å and the lack of observable excitation profile maxima for the other porphyrin macrocyclic modes in this region suggests that the shoulder of the absorption band at ca 6000 Å is a pure charge transfer transition which is not mixed with the $\pi \rightarrow \pi^*$ transition. In addition, the enhancement of the Fe-O stretch in MetHb OH^- lends further support to the assignment of the 413 cm^{-1} peak in MetHb N_3^- to the Fe-azide stretch. The similarity between the excitation profiles of MetHb N_3^- and MetHb OH^- suggests that the electronic transitions are similar charge transfer transitions, and predicts that the shoulder at ca 6000 Å in MetHb OH^- is z-polarized.

Another difference between the resonance Raman spectra of MetHb N_3^- and MetHb OH^- occurs between 1550-1640 cm^{-1}. The spectrum of MetHb N_3^- excited at 5590.8 Å shows intense peaks at 1640 and 1586 cm^{-1}, indicating

Fig. V-7. Resonance Raman spectra of MetHb $^{16}OH^-$ and MetHb $^{18}OH^-$ (ca. 0.9 mM heme). pH=10.2. λ_{ex}=6004.7 Å. Energy=2 X 10^{-3} joule/pulse. Pulse repetition rate=30 Hz. Scan speed= 16 Å/min. Slitwidth= 4.5 Å.

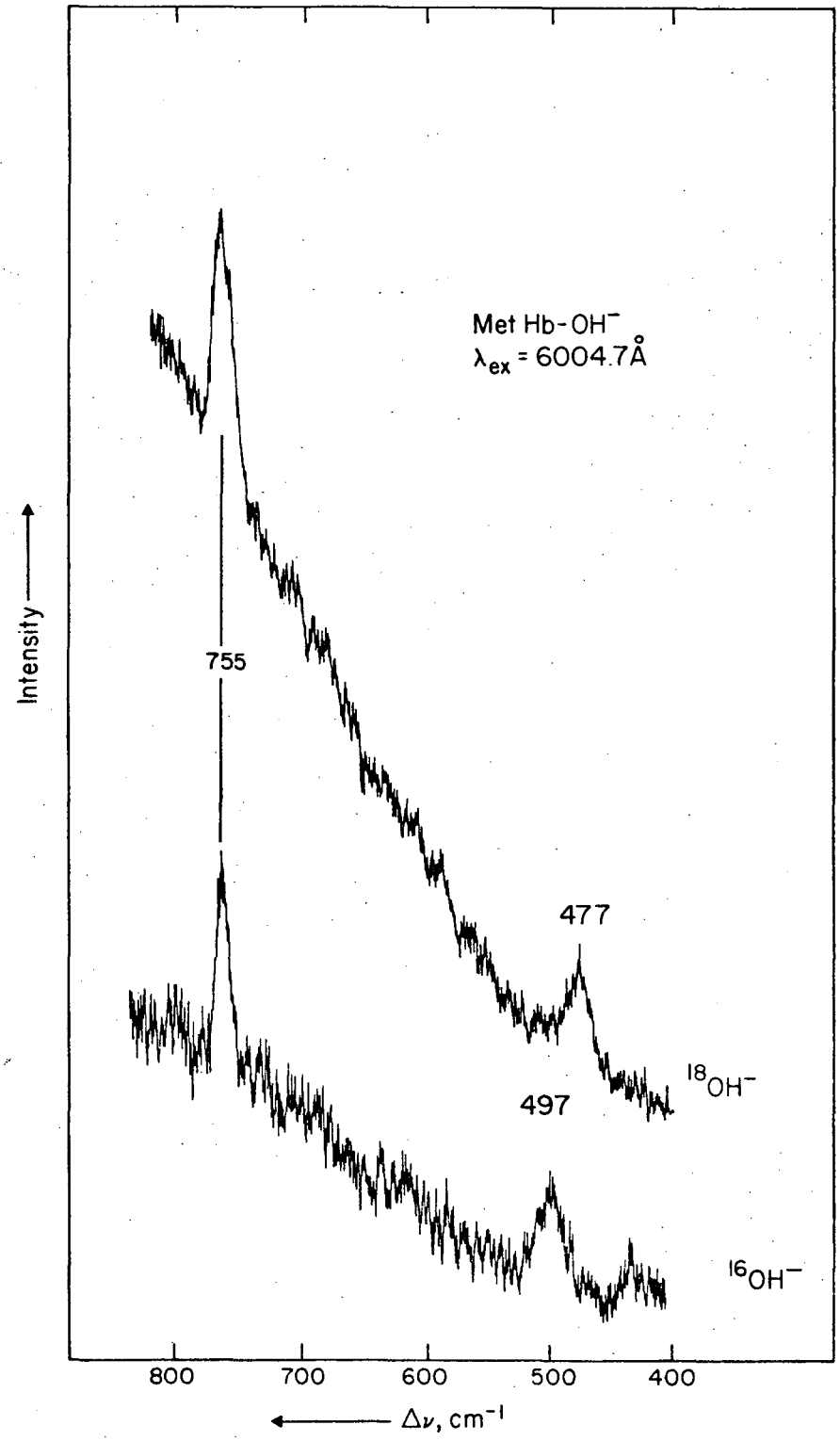
Met Hb-OH⁻
λex = 6004.7Å
Intensity
755
477
497
18OH⁻
16OH⁻
800
700
600
500
400
Δν, cm⁻¹
XBL 7611-9668

Fig. V-7.

that the iron is low-spin. The spectrum of MetHb OH^- shows peaks appearing at 1634, 1587 and 1555 cm^{-1}. In addition, a shoulder appears at ca 1605 cm^{-1}. The peak at 1587 cm^{-1} is indicative of the low-spin state of iron; while the shoulder at 1605 and the peak at 1555 cm^{-1} suggest not only the high-spin state of iron, but of a high-spin state similar to that of MetHb F^- and MetMb F^- (Spiro and Burke, 1976). The simultaneous appearance of peaks which are markers of the high and low-spin forms of hemoglobin suggests the existence of two forms of MetHb OH^- in solution.

Spectra similar to Fig. 5 between 1200-1700 cm^{-1} have been obtained by Ozaki et al. (Ozaki, et al., 1976) in their study of the pH dependence of the resonance Raman spectrum of MetMb. As the pH is increased from 7 to 11.6, the acid form of MetMb is converted to MetMb OH^-. At pH = 11.6, 99.8 % of the MetMb exists as the OH^- complex (Ozaki, et al., 1976). As the pH is raised from 7 to 11.6 the ratio of intensities of the 1581 cm^{-1} to the 1561 cm^{-1} band increases, indicating an increase in the concentration of the low-spin form. The presence of bands characteristic of the high and low-spin forms of iron at pH = 11.6 was interpreted by Ozaki, et al., as indicating that MetMb OH^- exists in two spin-states in solution (Ozaki, et al., 1976).

George, et al. (George, et al., 1961) studying the absorption spectra and magnetic susceptibilities of various axial ligand complexes of MetHb, suggested that a thermal equilibrium exists between the high and low-spin forms of MetHb OH^-. They estimated that between 50% and 55% of MetHb OH^- exists in the low-spin form at room temperature. By a comparison between the absorption spectra of various high and low-spin derivatives of MetHb and other heme proteins, George, et al., proposed

that the absorption spectrum of MetHb OH^- was due to the overlap of the absorption spectra of the individual high and low-spin forms, and that the high-spin form absorbed at longer wavelength than the low-spin form, contributing most of the intensity to the shoulder at 6000 Å in the absorption spectrum (Fig. 6).

The excitation profile measurements in Fig. 6 indicate that with excitation at 6196.0 Å, the ratio of intensities of the 1555 to 1587 cm^{-1} peak, R (R = I(1555)/I(1587)) is $\sim$ 2.1. As the excitation wavelength decreases R becomes smaller, equaling $\sim$ 1.5 at 6000.9 Å and $\sim$ 0.8 at 5849.9 Å (Fig. 6). Thus, the Raman data are consistent with the existence of two forms of MetHb OH^- in solution. Further, the increase of R at longer wavelength indicates that the high-spin form absorbs at longer wavelength than the low-spin, in agreement with George, et al. (George, et al., 1961). Yamamoto, et al., proposed that R reflects the relative concentrations of the low and high-spin forms of the heme iron (Yamamoto, et al., 1973). However, while R may be proportional to the concentrations of the high and low-spin forms, the excitation profiles (Fig. 6) indicate that the proportionality constant is a sensitive function of the excitation wavelength. Thus, a quantitative calculation of the relative concentrations of the high and low-spin forms is not possible in the absence of the absorption spectra and the excitation profiles of the individual high and low-spin forms.

Of all the bands shown in the excitation profiles in Fig. 6, only the 497 cm^{-1} peak shows an intensity maximum between 5849.9 and 6196.0 Å. Although the intensity of the 1555 cm^{-1} peak is greater than the intensity of the 1587 cm^{-1} peak for excitation wavelengths above 5900 Å, both the

1555 and 1587 cm^{-1} peaks appear to be in resonance with an electronic transition below 5850 Å.

The data support George et al. in their conclusions that two forms of MetHb OH^- exist in solution, with the high-spin form absorbing at longer wavelength. The selective enhancement of the 497 cm^{-1} feature and the lack of an intensity profile maximum for the 757, 1555, 1587 and 1638 cm^{-1} peaks at 6000 Å suggest that the electronic transition at 6000 Å is a charge transfer transition. The selective enhancement of only the Fe-axial ligand vibrations by both the 6000 Å and 6400 Å absorption bands of MetHb OH^- and MetHb N_3^- suggests a similarity between these electronic transitions.

MetHb F^-

In contrast to MetHb N_3^- which is predominantly low-spin and MetHb OH^- which is in a thermal spin-state equilibrium, MetHb F^- is high-spin (Antonini and Brunori, 1971). Fig. 8 shows the resonance Raman spectrum of MetHb F^- excited at 6175.1 Å. The dominant features in the Raman spectrum occur at 1610, 1550, 1217, 760, 471 and 443 cm^{-1}. The higher frequency region of the Raman spectrum shown in Fig. 8 (> 700 cm^{-1}) is qualitatively similar to previously reported spectra of MetHb F^- (Strekas, et al., 1973). In contrast to the Raman spectra of MetHb N_3^- and MetHb OH^-, which show peaks at 413 and 497 cm^{-1}, an intense doublet appears at 443 and 471 cm^{-1}. An examination of the excitation profiles and the absorption spectrum of MetHb F^- shown in Fig. 9 reveals a very complex behavior for many of the Raman peaks of MetHb F^-. The two peaks at 443 and 471 cm^{-1}, which are polarized, appear to be in resonance with the absorption peak at $\sim$ 6000 Å. However, it should be

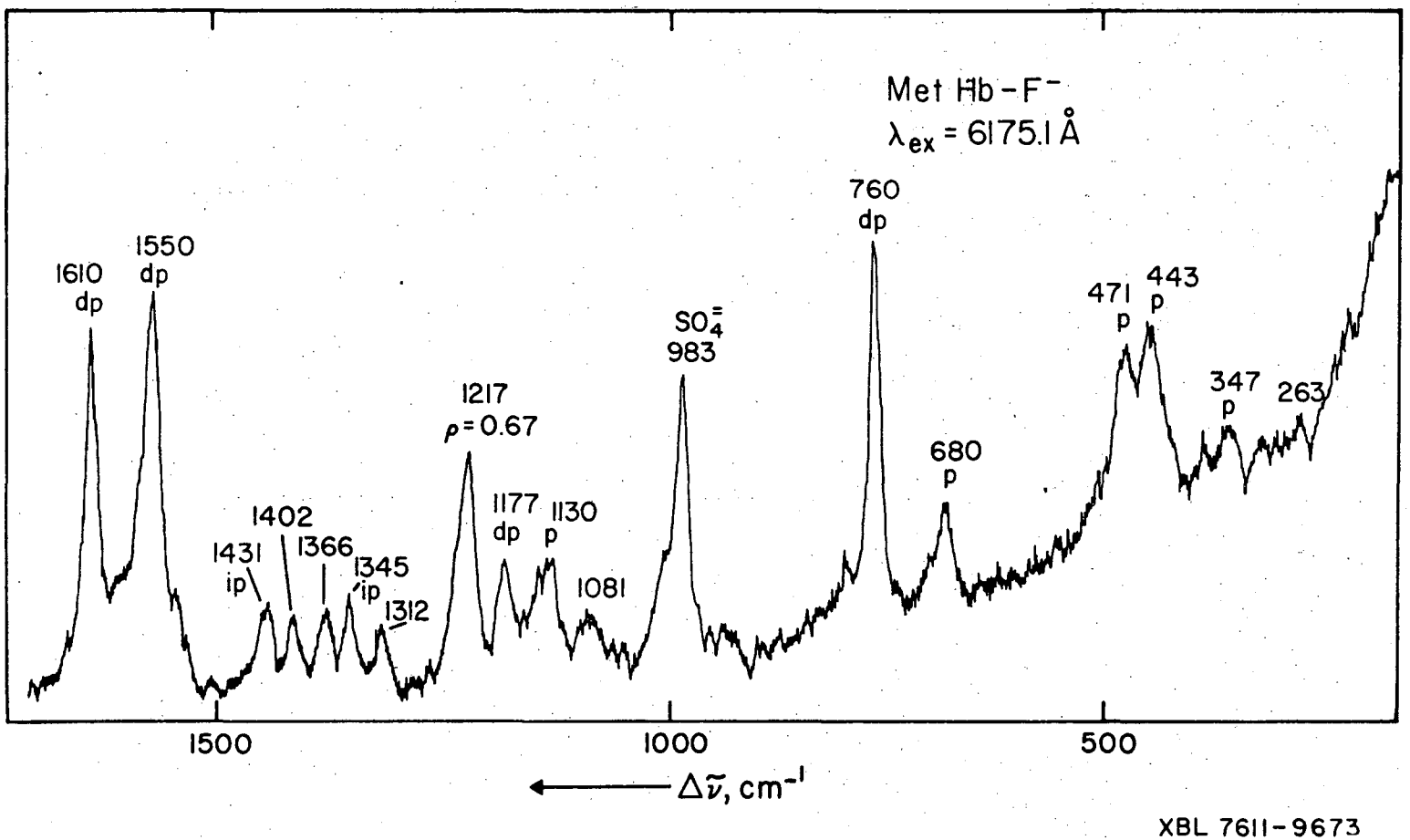

Fig. V-8. Resonance Raman spectrum of MetHb F^- (0.76 mM heme) containing 0.25 M Na_2SO_4 as an internal standard. λ_{ex} = 6175.1 Å. Energy= 2 X 10^{-3} joule/pulse. Pulse repetition rate= 30 Hz. Scan speed= 25 Å/min. Slitwidth = 3.7 Å. Position of SO_4 peak is shown in figure.

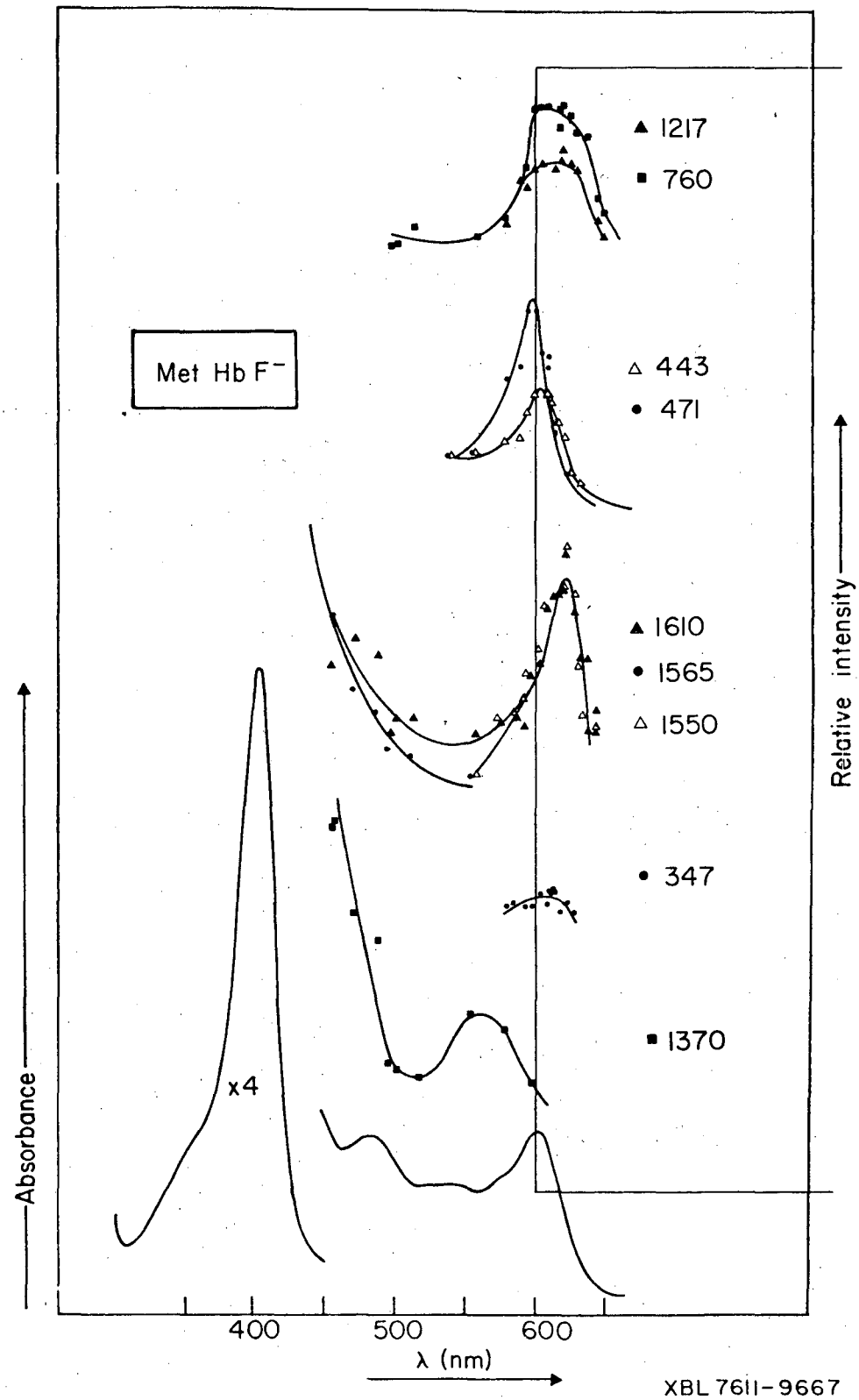

Fig. V-9. Absorption spectrum and excitation profiles of MetHb F^-. Conditions as in Fig. V-3. The points at wavelenghts below 5200 Å were obtained from previously reported spectra (Strekas, et al., 1973).

noted that the 443 cm^{-1} peak shows an intensity maximum at a somewhat higher wavelength than the 471 cm^{-1} peak; and at excitation wavelengths lower than 6080 Å, the 471 cm^{-1} peak is more intense than the 443 cm^{-1} peak. The appearance of the 443 and 471 cm^{-1} doublet is not unique to MetHb F^- and is not due to the quarternary structure of the Hb. Resonance Raman spectra of MetMb F^- and MetHb F^- are almost identical, with the doublets appearing at essentially the same frequency (± 3 cm^{-1}).

In view of the enhancement of Fe-axial ligand vibrations by the charge transfer bands of MetHb N_3^- and MetHb OH^-, and the fact that intense vibrations between 400-500 cm^{-1} have not been observed for any metalloporphyrins other than MnETP F^-, MetHb N_3^- and MetHb OH^-, it is tempting to assign the 443 and/or 471 cm^{-1} peaks to the Fe-F^- stretch. However, Ogashi et al. in their IR studies of metalloporphyrins, assigned an Fe-F^- stretch in ferric octaethylporphin F^- to a band at 602 cm^{-1} (Ogashi, et al., 1973). The evidence for this assignment was the selective appearance of this peak in the F^- complex and an isotope shift on substitution of ^{56}Fe for ^{54}Fe. Kincaid and Nakamoto observed the appearance of a 600 cm^{-1} peak in the resonance Raman spectrum of the F^- complex of ferric octaethylporphin. The 600 cm^{-1} peak shifted to 596 cm^{-1} following isotopic substitution of ^{56}Fe for ^{54}Fe (Kincaid and Nakamoto, 1976). Recently, Spiro and Burke (Spiro and Burke, 1976) observed the selective appearance of a 580 cm^{-1} peak in the resonance Raman spectrum of the fluoride complex of ferric mesoporphyrin IX dimethyl ester.

However, the environment of the iron in MetHb F^- is much different from that in fluoride complexes of non-protein bound metalloporphyrins.

In MetHb F^- the high-spin iron is constrained by the proximal histidine to lie out of the heme plane on the side opposite the fluoride (Deatherage, 1976). The steric non-bonding interactions between the charge cloud of the F^- and the porphyrin orbitals would be expected to cause the Fe-F^- bond length to increase compared to that of a non-protein bound ferric porphyrin fluoride complex, resulting in a decrease of both the bond strength and the vibrational frequency.

The existence of two polarized, closely lying peaks which have similar excitation profiles suggests a correlation between them. Although any assignment of these peaks is somewhat speculative in the absence of additional data, the observation by Deatherage et al., using X-ray difference Fourier diffraction, that the environment of the F^- ion in MetHb F^- is heterogeneous may account for the presence of two peaks assignable to the Fe-F^- stretch (Deatherage, 1976a). Deatherage observed the presence of an additional feature within the heme cavity which he proposed to be an H_2O molecule stabilized in the heme cavity by hydrogen bonding to the fluoride ion. The magnitude of the feature suggested that the water molecule is stabilized in the heme pocket only part of the time, leading to a heterogeneity in the fluoride environment. Hydrogen bonding with the fluoride ion would be expected to decrease the frequency of the Fe-F^- vibration.

Other alternative assignments of the 443 and 471 cm^{-1} doublet are possible. One of the peaks might result from the vibration of the imidazole of the proximal histidine against the iron. The doublet could result from a vibrational mode of the metalloporphyrin. However, no reports of intense porphyrin Raman bands between 400-500 cm^{-1} have

appeared in the literature. Additional experiments on model systems are necessary to assign the 443 and 471 cm^{-1} doublet conclusively.

Measurements of the resonance Raman spectrum of the fluoride complex of N-acetylated heme octapeptide from cytochrome c may help assign the doublet (Fraenkel-Conrat, 1957, Harbury and Loach, 1960). The heme group is covalently attached to the peptide with two thioether linkages and the iron of the heme is complexed to the peptide by the imidazole group of a histidine residue. Thus, the heme is in a coordination environment analogous to that in Hb and Mb. The major difference is the absence of a hydrophobic environment. Thus, if the doublet observed in MetHb F^- results from hydrogen bonding of the axial fluoride ligand to a water molecule trapped in some of the heme cavities, the resonance Raman spectrum of the octapeptide should show only one peak due to the axial fluoride ligand.

In addition to the 443 and 471 cm^{-1} peaks a weak, polarized Raman peak at 347 cm^{-1} appears to be in resonance with the 6000 Å absorption band. The vibrations which show their maximum intensity at 6250 Å occur at 1610 (dp) and 1550 (dp) cm^{-1} (Fig. 9). Since these peaks are depolarized they are either of B_{1g} or B_{2g} symmetry in the D_{4h} point group. However, the 760 cm^{-1} (dp) and 1217 cm^{-1} peaks each show a very broad excitation profile, suggesting that the excitation profiles (Fig. 9) may result from the overlap of two maxima at 6000 and 6250 Å. Weaker, anomalously polarized peaks at 1345 and 1431 cm^{-1} appear with excitation at ca 6000 and 6250 Å. However, these peaks are not observed with excitation between 6080.8 and 6150.0 Å. The 1217 cm^{-1} peaks show a depolarization ratio, ρ, of 0.62. For the D_{4h} point group theory predicts

(Chapter II) that vibrations of A_{1g} symmetry have $\rho = 0.125$, those of A_{2g} symmetry have $\rho = \infty$, and those of B_{1g} or B_{2g} have $\rho = 0.75$. Thus, a depolarization ratio intermediate between 0.125 and 0.75 suggests an overlap of an A_{1g} vibration with a vibration of B_{1g}, B_{2g} or A_{2g}. Thus, it appears that only depolarized or inversely polarized peaks show an intensity maximum at 6250 Å.

Measurements of the excitation profiles of MetHb F^- using the 5145, 5017, 4965, 4880, 4724 and 4579 Å lines of an Ar^+ ion laser show maxima appearing at ∿ 5080 Å for the 760 cm^{-1} peak, ∿ 4930 for the 1175 cm^{-1} peak and ∿ 4960 Å for the 1340 cm^{-1} peak (Strekas, et al. 1973). Assuming that the excitation profile maxima resulted from resonance with the β band, Strekas et al. subtracted the energies of the Raman bands from the energies of the excitation profile maxima and predicted that the α band occurs at ca 5260 Å. In their studies of the resonance Raman peaks of oxy Hb excited in the α band. Strekas and Spiro (Strekas and Spiro, 1973) noted that all of the observed Raman peaks displayed intensity profile maxima at the peak of the α band. Peaks at 1640 (dp), 1342 (ip), 1225 (dp) and 755 (dp) showed relatively narrow excitation profiles. Verma et al. showed that the 1640 (dp), 1313 (ap) and 1131 (ap) peaks of Cu(II) mesoporphyrin IX dimethyl ester, and the 1657 (dp), 1305 (dp), 1130 (ap?) and 342 (p) peaks of Ni-mesoporphyrin IX dimethyl ester were maximally enhanced at the α band maximum (Verma et al. 1974).

The excitation profiles of the resonance Raman peaks of MetHb F^- (Fig. 9) show a more complicated pattern, presumably because of the complexity of the visible absorption spectrum, which consists of at least four overlapping bands (Eaton and Hochstrasser, 1968). In

their measurements of the single crystal polarized absorption spectrum of MetMb F^-, Eaton and Hochstrasser observed that in contrast to MetMb N_3^-, which shows a z-polarized transition at ca 6400 Å, the entire visible absorption spectrum of MetMb F^- was x,y polarized. However, they noted that an inequivalency of x and y polarized electronic transitions occurred at ca 6250 Å, indicating a splitting of the degeneracy of the x and y directions. It has been proposed that the complexity of the visible absorption spectrum of MetHb F^- results from the mixing of charge transfer bands with porphyrin $\pi \rightarrow \pi^*$ transitions to the extent that none of the absorption bands in the visible region can be considered as pure transitions (Zerner et al. 1966; Eaton and Hochstrasser, 1968; Smith and Williams, 1970).

Caution is necessary in the interpretation of the excitation profile data of MetHb F^- because of the possible occurrence of interference effects between overlapping electronic transitions which are not resolved in the absorption spectrum (Friedman and Hochstrasser, 1973; Stein et al. 1976). One possible interpretation of the excitation profile measurements is that the absorption band at 6000 Å contains two electronic transitions occurring at 6000 and 6250 Å. The only independent evidence for the existence of an electronic transition at 6250 Å is the inequivalency of the x and y directions of the single crystal absorption spectra. Since, an inequivalency of the x and y directions occurs at 6250 Å, a description of the electronic transitions in the D_{2h} point group is appropriate. In the D_{2h} point group the symmetry of the vibrations which would mix x and y electronic transitions is: $\Gamma_x \times \Gamma_y = \Gamma_{B_{2u}} \times \Gamma_{B_{3u}} = \Gamma_{B_{1g}}$. Thus, vibrations of B_{1g} symmetry are

expected to be enhanced at 6250 Å. However, B_{1g} vibrations in the D_{2h} point group correlate to B_{2g} and A_{2g} vibrations in the D_{4h} point group (Kitagawa, et al. 1975); and depolarized and inversely polarized vibrations are expected to be enhanced at 6250 Å, in agreement with the excitation profile data. None of the polarized vibrations shows an excitation profile maximum at 6250 Å. Instead, the polarized 347, 443, and 471 cm^{-1} peaks show excitation profile maxima at ∿ 6000 Å. The 471 cm^{-1} peak is the most intense feature in the Raman spectrum with excitation at 6000 Å.

Eaton and Hochstrasser suggested that the inequivalency of the x and y directions results from the splitting of the d_{xz}, d_{yz} orbitals of the iron. However, the enhancement at 6250 Å of porphyrin macrocyclic modes exclusively suggests that the origin of the degeneracy splitting occurs mainly in the porphyrin macrocycle and is not a result of an axial ligand induced inequivalency of the d_{xz} or d_{yz} orbitals. If the inequivalency resulted from the metal orbitals, vibrations of A_{2g} and B_{2g} symmetry about the metal would be enhanced by terms such as $\langle d_{xz}|\frac{\partial H}{\partial Q_a}|d_{yz}\rangle$ in the polarizability expression (Chapter IV). Thus, the inequivalency in the x and y directions may result from an interaction not through the iron but directly on the porphyrin plane by the heme environment. This could result from a steric influence of the proximal histidine, which might bind to the iron in one particular orientation with respect to the x and y directions of the porphyrin macrocycle. Alternatively, the splitting might result from the interaction of the heme with another species in the heme cavity.

Effect of Inositol Hexaphosphate

Inositol hexaphosphate (IHP), which is known to alter the spin-state equilibrium of MetHb OH^- and MetHb N_3^-, appears to convert MetHb F^- from the R to the T form (Perutz, et al. 1974b and c). Perutz proposes that in the T form that iron lies further out of the porphyrin plane. Because of the steric interactions of the sixth ligand with the heme plane, the frequency of the vibration of the sixth ligand to the iron should be a sensitive function of the out-of-plane distance of the metal. Since the F^- axial ligand is constrained to interact with the porphyrin π orbitals, the Fe-F^- bond is like a stretched sping. Any movement of the iron would either shorten or lengthen the bond distance.

In 5-coordinate, high-spin complexes of ferric porphyrins the iron lies $\sim$ 0.45 Å out of the plane towards the 5th axial ligand (Hoard, 1975). However, in MetHb F^- the iron lies out of the plane on the opposite side from which the F^- must bind. The out-of-plane distance of the iron from the heme in MetHb F^- is 0.3 Å (Deatherage, et al. 1976a; Perutz, et al. 1974b). Thus, the iron is displaced a total 0.75 Å behind the porphyrin plane in MetHb F^- compared to ferric porphyrin fluoride. The $\sim$ 100 cm^{-1} difference between the Fe-F^- vibrations in MetHb F^- and ferric porphyrin fluorides suggests that the frequency of this vibration should be a sensitive measure of any movement of the iron with respect to the porphyrin plane. Thus, IHP was added to solutions of MetHb X^- ($X = F^-$, OH^-, N_3^-) and resonance Raman spectra were excited at wavelengths which maximally enhanced the Fe-X vibrations. The addition of IHP to solutions of MetHb X^- had no effect on the resonance Raman spectra within the signal-to-noise ratio of the spectra. The fact that IHP has no effect on the

energy of the Fe-O vibration in MetHb OH^- may not be surprising in view of the fact that IHP does not bind well to MetHb at pH greater than 7 (Perutz, et al., 1974c). However, the lack of a shift in the energy of the vibrations which are assigned to Fe-N_3^- and Fe-F^- stretching suggests that no movement of the iron occurs on the addition of IHP. The addition of IHP to MetHb F^- results in changes in the CD spectra, the absorption spectra and the sulfhydryl reactivities, which is consistent with a transition of the R to the T quarternary form (Perutz, et al., 1974b). Perutz's model predicts a change in the out-of-plane distance of the iron from the porphyrin upon the R → T transition. If the 443 and/or 471 peaks result from an Fe-F^- vibrations, then any change in the out-of-planarity of the iron should result in a significant shift in the energy of the Fe-F^- vibration. Thus, it appears that no movement of the iron occurs on the addition of IHP, suggesting that either IHP does not induce the R → T transition or that Perutz's model is incorrect. However, the basis for these conclusions rests on the assignment of the 443 and/or 471 cm^{-1} peaks to the Fe-F^- stretch.

The arguments in favor of this assignment are: 1. The 443 and 471 cm^{-1} peaks are the dominant features in the resonance Raman spectrum of MetHb F^- excited at the maximum of the charge transfer band at 6000 Å. 2. Intense, polarized Raman peaks between 410-500 cm^{-1} have been observed only in the resonance Raman spectra of MnETP F^-, MetHb OH^-, MetHb N_3^- and MetHb F^-, and only with excitation in the charge transfer bands. 3. The 495 cm^{-1} peak in MnETP F^- is assigned to an Mn-F stretch (Chapter IV). The 497 cm^{-1} peak in MetHb OH^- has been shown by isotopic substitution to be an Fe-O vibration. The assignment of the 413 cm^{-1} peak in MetHb N_3^-

to a Fe-N_3 stretch is supported by the IR assignment of an Fe-N_3 vibration at 421 cm^{-1} (Ogashi, et al., 1973). 4. No feature corresponding to the 600 cm^{-1} Fe-F^- stretch observed in the IR, and resonance Raman spectra of fluoride complexes of ferric porphyrins is observed upon excitation in the charge transfer band of MetHb F^- (Ogashi, et al., 1973; Kincaid and Nakamoto, 1976; Spiro and Burke, 1976).

Conclusions

The excitation profiles for the 413 and 495 cm^{-1} peaks of MetHb N_3^- and MetHb OH^- are similar, indicating a similarity between the electronic transitions. The Fe-O vibration in MetHb OH^- occurs at 497 cm^{-1}, while the Fe-azide vibration occurs at 413 cm^{-1}.

It is suggested that the 443 and 471 cm^{-1} peaks enhanced by the 6000 Å charge transfer bond of MetHb F^- result from a heterogeneity in the heme cavity caused by the presence of an H_2O molecule in some of the heme cavities. The H_2O hydrogen bonds to the fluoride ligand, lowering the frequency of the Fe-F^- vibration. The enhancement of porphyrin macrocyclic vibrations in the 6000 Å absorption band suggests a substantial $\pi \rightarrow \pi^*$ contribution. The lack of an effect of IHP on the resonance Raman spectrum of the OH^-, N_3^- and F^- complexes of MetHb suggests that there is no movement of the iron with respect to the porphyrin plane. Either, IHP does not induce the R → T transition or the trigger mechanism proposed by Perutz is incorrect.

A comparison of the extended x-ray absorption fine structure spectrum (EXAFS) of deoxyHb A with that of DeoxyHb Kempsey led Eisenberger et al. to conclude that there was no substantial movement (> 0.02 Å) of

the iron between the high (R) and low affinity (T) quarternary forms (Eisenberger, et al., 1976). Hb Kempsey has a mutation which eliminates a hydrogen bond across one of the α and β subunit interfaces in the deoxy quarternary structure, causing deoxyHb Kempsey to exist solely in the high affinity quarternary form. The EXAFS spectrum of deoxyHb Kempsey is almost identical to that of deoxyHb A indicating that no significant structural changes occur about the iron atom. Thus, both EXAFS studies of deoxyHb and resonance Raman studies of the OH^-, F^- and N_3^- complexes of MetHb suggest that no movement of the iron occurs between the R and T forms.

What causes the differences between the ligand affinities of the R and T quarternary forms? Possibly a steric effect of the protein on the heme is involved which decreases the accessibility of the heme binding site in the T form (Perutz, et al., 1976; Deatherage, et al., 1976b). Another possibility is that a change occurs in the π interactions between the porphyrin macrocycle and the surrounding protein matrix (Maxwell and Caughey, 1976), leading to changes in the electronic structure of the porphyrin, concommitant changes in the iron d orbitals and changes in the ligand affinities of the heme.

The energy of the Fe-axial ligand vibrations may not be a good monitor of these effects. However, it is possible that the excitation profiles may contain some information on steric and π non-bonding interactions between the protein and the heme or both. Polarized single crystal absorption spectra and the excitation profile data (Fig. 9) both indicate an inequivalency of the x and y directions of MetHb F^- at 6250 Å.

If the inequivalency of the x and y directions results from non-bonding interactions between the heme and the protein, changes in the excitation profiles upon the addition of IHP may monitor changes in the interactions between the R and T quarternary forms.

Resonance Raman spectroscopy has potential for probing the intermolecular interactions of complex systems. However, the selectivity of the technique also implies a limitation, because only vibrations which are coupled to the resonant electronic transition are enhanced. Thus, to obtain information on a particular region of a molecule, excitation must occur within an electronic transition coupled to the vibrations of the atoms in that region. Resonance Raman spectroscopy is a relatively new technique. As the availability of tunable lasers increases, the value of the technique will increase. This spectroscopic technique has potential to help solve many of the outstanding problems in biology. The potential ability to study molecules in situ makes the technique even more valuable.

References I

Antonini, E. and Brunori, M., Hemoglobin and Myoglobin in Their Reactions with Ligands, North-Holland Publishing Co., 1971.

Deatherage, J. F., Loe, R. S., and Moffat, K., J. Mol. Biol. 104, 723 (1976a).

Deatherage, J. F., Loe, R. S., Anderson, C. M., and Moffat, K., J. Mol. Biol. 104, 687 (1976b).

Eaton, W. A. and Hochstrasser, R. M., J. Chem. Phys. 49, 985 (1968).

Eisenberger, P., Shulman, R. G., Brown, G. S., and Ogawa, S., Proc. Nat'l. Acad. Sci. USA 73, 491 (1976).

Fermi, G., J. Mol. Biol. 97, 237 (1975).

Fraenkel-Conrat, H., Methods Enzymol. 4, 247 (1957).

Friedman, J. and Hochstrasser, R. M., Chem. Phys. Lett. 32, 414 (1975).

George, P., Beetlestone, J., and Griffith, J. S., Haematin Enzymes, Vol. I., Ed. J. Falk, R. Lemburg and R. K. Morton, Pergamon Press, New York, 1961.

Harbury, H. A. and Loach, P. A., J. Biol. Chem. 235, 3640 (1960).

Hoard, J. L., in Porphyrins and Metalloporphyrins, ed. K. M. Smith, Elsevier Scientific Publishing Co., New York, (1975).

Kabat, K., Biochem. 6, 3443 (1967).

Kincaid, J. and Nakamoto, K., Spectrosc. Lett. 9, 19 (1976).

Kitagawa, T., Kyogoku, Y., Iizuka, T., and Saito, M. I., J. Am. Chem. Soc. 98, 5169 (1976).

Kitagawa, T., Ogashi, H., Watanabe, E., and Yoshida, Z-I., J. Phys. Chem. 79, 2629 (1975).

Maxwell, J. C. and Caughey, W. S., Biochem. 15, 388 (1976).

Monod, J., Wyman, J. and Changeux, J. P., J. Mol. Biol. 12, 88 (1965).

Ogashi, H., Watanabe, E., Yoshida, Z., Kincaid, J. and Nakamoto, K., J. Am. Chem. Soc. 95, 2845 (1973).

Ozaki, Y., Kitagawa, T., and Kyoguku, FEBS Lett. 62, 369 (1976).

Perutz, M. F., Muirhead, H., Cox, J. M. and Goaman, L.C.G. Nature 219, 131 (1968).

Perutz, M. F., Nature 228, 726 (1970).

Perutz, M. F., Nature 237, 495 (1972).

Perutz, M. F., Ladner, J. E. Simon, S. R., Ho, C., Biochem. 13, 2163 (1974).

Perutz, M. F., Fersht, A. R., Simon, S. R., and Roberts, G. C. K., Biochem. 13, 2174 (1974).

Perutz, M. F., Heidner, E. J., Ladner, J. E., Beetlestone, J. G., Ho, C., and Slader, E. F., Biochem. 13, 2187 (1974).

Perutz, M. F., Kilmartin, J. V., Nagai, K., Szabo, A., Simon, S. R., Biochem. 15, 378 (1976).

Perutz, M. F. and Teneyck, L. F., Cold Spring Harbor Symp. Quant. Biol. 36, 295 (1972).

Smith, D. W. and Williams, R. J. P., Structure and Bonding 7, 1 (1970).

Spiro, T. G., and Strekas, T. C., J. Am. Chem. Soc. 96, 338 (1974).

Spiro, T. G., Biochim. Biophys. Acta 416, 169 (1975).

Spiro, T. G., and Burke, J. M., J. Am. Chem. Soc. 98, 5482 (1976).

Stein, P., Miskowski, V., Woodruff, W. H., Griffin, J. P., Werner, K. G., Gaber, B. P., and Spiro, T. G., J. Chem. Phys. 64, 2159 (1976).

Strekas, T. C., and Spiro, T. G., Biochim. Biophys. Acta. 263, 830 (1972).

Strekas, T. C., and Spiro, T. G., J. Raman Spectrosc. 1, 387 (1973).

Strekas, T. C., Packer, A. J., and Spiro, T. G., J. Raman Spectrosc. 1, 197 (1973).

Stryer, L., Biochemistry, W. H. Freeman and Co., San Francisco, (1975).

Stryer, L., Kendrew, J. C., and Watson, H. C., J. Mol. Biol. 8, 96 (1964).

Verma, A. L., Mendelsohn, R., and Bernstein, H. J., J. Chem. Phys. 61, 383 (1974).

Vickery, L., Nozawa, T., and Sauer, K., J. Am. Chem. Soc. 98, 343 (1976).

Yamamoto, T., Palmer, G., Gill, D., Salmeen, I. T., and Rimai, L., J. Biol. Chem. 248, 5211 (1973).

Zerner, M., Gouterman, M., and Kobayashi, H., Theor. Chim. Acta. 6, 363 (1966).

TECHNICAL INFORMATION DIVISION
LAWRENCE BERKELEY LABORATORY
UNIVERSITY OF CALIFORNIA
BERKELEY, CALIFORNIA 94720